# APJES

# Journal of Engineering and Science

## *Academic Platform Journal of Engineering and Science*

## Contact

# APJES

# Journal of Engineering and Science

## Contents Volume 9 / Issue 3

# Kopula Yöntemi ile Osmaniye Bölgesinin İki Değişkenli Kuraklık Frekans Analizi

[1,2]Musa Eşit, [2]Mehmet İshak Yüce

[1]Gaziantep Üniversitesi İnşaat Mühendisliği Bölümü, Gaziantep, yuce@gantep.edu.tr, (iD)

[2]Adıyaman Üniversitesi İnşaat Mühendisliği Bölümü, Adıyaman, mesit@adiyaman.edu.tr, (iD)

**Öz**

İklim değişikliğinin dünyanın birçok bölgesinde ekstrem doğa olaylarını tetiklediği gerçeği, birçok bilim insanı tarafından ciddi bir vaka olarak kabul edilmektedir. Çok değişkenli frekans dağılımları, hidrolojik tasarım ve risk yönetimi için giderek daha fazla önem kazanmaktadır. Geleneksel çok değişkenli dağılımlar, tüm bileşen marjinallerinin aynı dağılım ailesinden olması gerektiği için ciddi şekilde sınırlamalara sahiptir. Kopula yöntemi, bu sınırlamanın üstesinden gelen çok değişkenli dağılımların türetilmesi için yeni ortaya çıkan bir yaklaşımdır. Bu çalışmada, Osmaniye ilinin yağış istasyonu uzun dönem veriler ile kuraklık analizi kopula fonksiyonu kullanılarak hesaplanmıştır. İlk olarak, kuraklık parametreleri olan kuraklık süresi ve şiddeti SPI metodu kullanılarak elde edilmiştir. Gözlemlenen kuraklık süresi için Lognormal, kuraklık şiddeti için ise Weibull en uygun marjinal dağılım olarak bulunmuştur. Her bir kuraklık parametresi için tek değişkenli dağılım fonksiyonu elde edildikten sonra, Gumbel kopulası belirlenen 10 kopula fonksiyonu arasında Akaike Bilgi Kriteri (AIC), Bayes Bilgi Kriteri (BIC), Maksimum olabilirlik (MLE) yöntemleri ve kuyruk bağımlılığı da dikkate alınarak seçilmiştir. En son olarak Osmaniye ili kuraklık olaylarının süre ve şiddet parametrelerinin ortak dönüş periyotları hesaplanmıştır. Bu analiz sonucunda, karar vericilere Osmaniye ilinin gelecekteki kuraklıklara daha duyarlı olması konusunda bilgi verebilir. Bu bilgiler ışığında, muhtemel yapılması düşünülen su temini sistemi, hidrolik tasarım ve su yönetimi gibi konularda yararlı bilgiler sağlamaktadır.

*Anahtar Kelimeler:* SPI, Kopula, Osmaniye, Yağış, Dönüş periyodu

# Bivariate Drought Frequency Analysis based on Copula Theory for Osmaniye Region

**Abstract**

Multivariate frequency distributions are becoming increasingly important for hydrological design and risk management. Traditional multivariate distributions have serious limitations as all component margins should be from the same distribution family. The Copula function is a newly approach to deriving multivariate distributions that overcome this limitation. In this study, drought analysis was calculated using the copula function for Osmaniye province with long-term precipitation data. Firstly, drought parameters including drought duration and severity were obtained by using SPI method. Lognormal and Weibull was observed to be the most suitable marginal distribution for drought duration and drought severity, respectively. After obtaining the univariate distribution function for each drought parameter, the Gumbel copula was selected among the 10 copula functions considering Akaike Information Criterion (AIC), Bayes Information Criterion (BIC), Maximum likelihood (MLE) methods and tail dependency. Finally, the drought return period for Osmaniye province has been calculated. It provides useful information on topics such as the possible water supply system, hydraulic design and water management.

**Keywords:** SPI, Copula, Osmaniye, Precipitation, Return Period

*Sorumlu Yazar: Gaziantep Üniversitesi İnşaat Mühendisliği Bölümü, Gaziantep, yuce@gantep.edu.tr

## 1. GİRİŞ

Kuraklık, önemli çevresel ve ekonomik etkileri olan büyük doğa tahribatlarından biri olarak görülmektedir. Çöllerden veya ormanlardan bağımsız olarak dünyanın her yerinde herhangi bir iklimde ortaya çıkabilir. Aynı zamanda en pahalı ama en az anlaşılmış doğal tehlikelerden biri olarak algılanmış olup [1], tarımsal, ekonomik ve çevresel zararlar üzerinde büyük olumsuz etkilere neden olabilir [2,3]. Son yıllarda, dikkate değer nüfus artışı ve iklim değişikliğinin neden olduğu yağışlardaki düzensizlik nedeniyle kuraklık sıklığı önemli ölçüde artmıştır [4]. Örneğin, eski dönemdeki kuraklıklar büyük nüfusları etkilemiş olup (doğal afetlerle kıyasla %35'ini temsil etmektedir), bu da genellikle önemli ölçüde ölümler ile sonuçlanmıştır [5].

Kuraklık temel olarak dört bileşenle karakterize edilir: Süre, şiddet, yoğunluk ve zaman aralığı. Kuraklıklar karmaşık olgular olduğundan, tek bir değişken tek başına kuraklıkların kapsamlı bir değerlendirmesini sağlamamaktadır [7]. Bu nedenle, tek değişkenli kuraklık özelliklerine dayanan bir analiz, kuraklık bileşenleri arasında anlamlı bir ilişki yakalayamaz. Kuraklıkları tespit etmek ve izlemek için çeşitli endeksler geliştirilmiş olup, yaygın olarak Palmer Kuraklık Şiddet İndeksi (PDSI) ve Standart Yağış İndeksi (SPI) kuraklık sınıflandırılması için daha sık kullanılan indekslerdir [8]. Su dengesi kavramına dayanan Palmer Kuraklık Endeksi, yağış, buharlaşma, su akışı ve toprak nemi gibi parametreleri kalibre etmeyi içermektedir. Bu indeks Amerika Birleşik Devletleri'nde uygulanmakta olup, ancak başka yerlerde çok az kabul görmektedir [9]. Guttman [10,11], Ray ve Shewale [12]'in yaptıkları çalışma sonuçlarına göre, nemli bölgelerde bu indeksin tarımsal kuraklığı, yarı kurak ve kurak alanlarda ise hidrolojik kuraklığı temsil ettiğini öne sürmüşlerdir.

Standart Yağış İndeksi, olasılık kavramına dayanan ve yaygın olarak kabul edilen bir başka indekstir. Yağış anomalileri, küresel iklimin doğal olarak yinelenen bir özelliği olup ve kuraklık, hidrolojik döngünün çeşitli bileşenlerini etkiler [13]. Sadece yağış verisini girdi olarak hesaplayan bu indeks, kuruluk ve nemlilik sınıflandırmasında PDSI' dan daha iyi temsil ettiği incelenmiştir [10]. SPI, yağıştan ortalama farkın standart sapmaya bölünmesiyle elde edilen farkı göstermektedir; bu iki istatistiksel parametre, en az 30 yıl önce geçmiş sürekli kayıtlardan belirlenmektedir [14,15]. Bu indeksin standartlaştırılmış olmasından dolayı, dünyadaki kuraklık etkisini değerlendirmek için kullanılabilir. Belirli bir konum için SPI, seçilen zaman ölçeği için olasılık dağılım fonksiyonunu tahmin ederek kısa, orta veya uzun vadeli zaman ölçeği için de hesaplanabilir. Bu, daha önce bahsedilen farklı kuraklık kategorilerinin etkisini ele almak için yararlı bir indeks olarak değerlendirilmektedir [16,17,18].

Kuraklık genellikle süre, şiddet, pik değer ve benzeri gibi ilişkili birkaç değişkenle karakterize edilebilen karmaşık bir olgudur [19]. Kuraklık özelliklerini (örn. frekans, risk,

tehlike vb.), nicel olarak değerlendirmek için en uygun yol olasılık teorisi ve stokastik yöntemini kullanmaktır [20]. Kuraklıkların olasılıksal karakterizasyonu hakkında önemli ölçüde araştırma yapılmıştır. Bununla birlikte, bu çalışmaların çoğunluğu tek değişkenli analizle uğraşmış olup, kuraklık birkaç rastgele ilişkili değişkenle karakterize edilen karmaşık bir olgu olduğundan, kuraklık özelliklerinin tek değişkenli analizi, değişkenler arasındaki önemli korelasyonu açıklayamamaktadır [21]. Çok değişkenli analizler, kuraklıkların daha kusursuz bir karakterizasyonu sağlamaktadır. Bununla birlikte kuraklık durumlarında, kuralık parametrelerinin (şiddet ve süre vb.) farklı dağılım fonksiyonlarına uyması sebebiyle, çok değişkenli modellerin oluşturulması zordur. Bu nedenle, geleneksel çok değişkenli frekans analizi yöntemlerini uygulayarak, kuraklık özelliklerini tam olarak tanımlamak mümkün değildir [22]. Son on yılda, kopulalar çeşitli disiplinlerde çok değişkenli problemleri ele alma yöntemi olarak ortaya çıkmıştır [23]. Bununla birlikte, kopulaları kullanan çok değişkenli dağılımlar bu tür zorlukların üstesinden gelebilir. Son yıllarda, kopulalar çok değişkenli hidrolojik analiz için kullanılmıştır. Örneğin, yağmur sıklığı analizi [24], taşkın frekans analizi, kuraklık frekans analizi [20] yapılmıştır. Kopula fonksiyonlarının teorik altyapısı hakkında detaylı bilgi Nelson [25] ve Salvadori ve ark. [23] tarafından araştırılmıştır. Kuraklık frekans analizi için Shiau [20], kuraklık süresi ve şiddetinin ortak dağılımını iki boyutlu kopulalar kullanarak modellemiştir. Mirakbari ve ark. [26] bölgesel kuraklık analizi için iki değişkenli kopula fonksiyonlarını kullanmışlardır. Çok değişkenli kopulaların (iki değişkenden fazla) kullanımı da son zamanlarda ortaya çıkmıştır. Song ve Singh [22] kuraklık süresi, şiddeti ve zaman aralığı arasındaki ortak olasılık dağılımını üç değişkenli Plackett kopula fonksiyonunu kullanarak modellemiştir. Geniş bir bağımlılığı karakterize edebilen çeşitli kopulalar bulunduğundan, farklı hidrolojik uygulamalar için uygun kopulaların seçimi kolay olmamaktadır.

Literatürde çok sayıda kopula temelli kuraklık çalışması bulunabilse de sadece birkaç araştırmacı Türkiye'de çok değişkenli kuraklık modellemesi için kopula fonksiyonlarını değerlendirmiştir. Tosunoğlu ve Can [27], 1 aylık Standart Yağış Endeksi'nde (SPI) Arşimet kopulası kullanarak meteorolojik kuraklıkların Türkiye üzerindeki ortak olasılık dağılımlarını modellemek için uygulamışlardır. Bu çalışmanın amacı, Osmaniye bölgesinin çift değişkenli kopula fonksiyonu kullanılarak, meteorolojik kuraklığın ortak olasılık dağılımlarını elde etmektir.

## 2. MATERYAL VE METOT

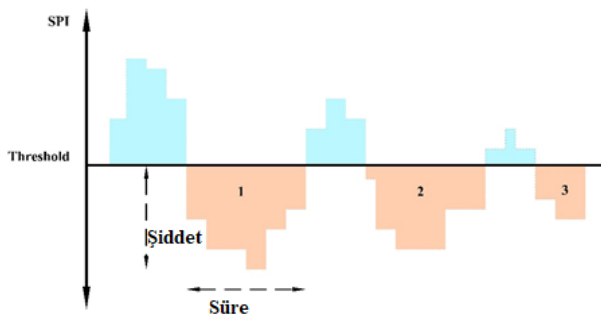### 2.1. Kuraklık Parametrelerinin Hesaplanması

Bir SPI serisine dayanan kuraklık tanımlama, kuraklık döneminin, SPI değerlerinin 0'dan küçük olduğu ardışık sayıda zaman aralığı olarak kabul edilmesi ile gerçekleştirilebilir. Şekil 1.'de SPI ve kuraklık

parametrelerinin zaman serilerini göstermektedir. Her kuraklık olayı kuraklık süresi D, kuraklık şiddeti S olmak üzere iki ana özellik ile karakterize edilir. Bu değişkenlerin tanımları aşağıda açıklanmıştır:

Kuraklık süresi, D, SPI sıfır eşik değerinin altında kaldığı ardışık aralıkların (ay) sayısı olarak tanımlanır. Kuraklık şiddeti S, kuraklık dönemi boyunca kümülatif bir SPI değeri olarak tanımlanır. Kuraklık şiddeti aşağıdaki formülle hesaplanmaktadır.

$$S = -\sum_{i=1}^{D} SPI_i \qquad (1)$$

Kuraklık zaman aralığı L, bir kuraklığın başlamasından bir sonraki kuraklığın başlangıcına kadar geçen süre olarak tanımlanır [8]. Standartlaştırılmış SPI değerlerine dayanarak, kuraklık sınıflandırılması Tablo 1.'de gösterilmiştir.



Şekil 1. Kuraklık parametrelerinin grafiksel olarak gösterimi

Tablo 1. SPI metoduna göre indeks değerleri ve sınıflandırma

| SPI | Kategori |
|---|---|
| $\geq 2$ | Olağanüstü Nemli |
| 1.50 ~ 1.99 | Çok Nemli |
| 1.00 ~ 1.49 | Orta Nemli |
| 0.99 ~ 0 | Normal |
| 0 ~ -0.99 | Normal Kurak |
| -1.00 ~ -1.49 | Orta Kurak |
| -1.50 ~ -1.99 | Şiddetli Kurak |
| $\leq -2$ | Olağanüstü Kurak |

### 2.2. Tek Değişkenli Kuraklık Parametrelerinin Dağılımı

İki değişkenli kuraklık frekans analizini yapmadan önce, öncelikle her bir kuraklık parametresi için (süre ve şiddet) en uygun dağılımın bulunması gereklidir. Önceki yapılan birçok çalışmada kuraklık süresi üstel dağılım [20,28] ile, kuraklık şiddeti Gama dağılımı [20,29] ile daha iyi modellendiği gösterilmiştir. Ancak, Yusof ve ark., [30] en çok kullanılan iki olasılık dağılımının her durumda iyi olmadığını ileri sürmektedir. Bu nedenle, bu çalışmada kuraklık şiddetine ve kuraklık süresine en iyi dağılımı bulmak için, literatürde en çok kullanılan Lognormal, Lojistik, Gama, Üstel, Weibull ve Normal dağılımlar gibi çeşitli dağılımlar kullanılmıştır. Her kuraklık parametresi için kullanılan dağılımların performansı Anderson-Darling (AD), Kolmogorov Smirnov (KS), Cramers-von Mises (CvM), Akaike Bilgi Kriteri (AIC), Bayes Bilgi Kriteri (BIC) ve Maksimum olabilirlik yöntemleri (MLE) ile test edilmiştir.

### 2.3. Kopula Teorisi

Kopula, rastgele değişkenler arasındaki bağımlılık yapısını modelleyen kullanışlı bir fonksiyondur. Yani, bir kopula, rastgele değişkenlerin ortak olasılık dağılımlarını, rastgele değişkenlerin marjinal dağılımlarını birleştirerek oluşturmaktadır [31,32]. Birçok kopula fonksiyonu olmasına karşın, Arşimet kopula fonksiyonları genel olarak hidrolojik ve meteorolojik alanlarda kullanılmaktadır. Sklar teoremine göre, iki rasgele değişken x ve y sırasıyla marjinal dağılım fonksiyonu FX(x) ve FY(y) olarak düşünülürse, bu iki farklı marjinali birbirine bağlamak için modellenen FX,Y (x, y) benzersiz bir kopula C vardır. C aşağıdaki formülle matematiksel olarak ifade edilir;

$$F_{X,Y}(x, y) = C(F_X(x), F_Y(y)) \qquad (2)$$

Denklem 1'de görüldüğü gibi, bir kopula tek değişkenli bir dağılıma göre çok değişkenli bir dağılım ile tanımlanabilmektedir. İlaveten, FX (x) ve FY (y) sürekli ise, C tamamen benzersiz olup [7], ortak olasılık yoğunluğu fonksiyonu aşağıdaki gibi tanımlanmaktadır;

$$f_{X,Y}(x, y) = c(F_X(x), F_Y(y)) f_X(x) f_Y(y) \qquad (3)$$

Burada, fX (x) ve fY (y), sırasıyla FX (x) ve FY (y) ile ilişkili yoğunluk fonksiyonlarıdır ve c, C'nin yoğunluk fonksiyonu olarak ifade edilir.

$$c(u, v) = \frac{\partial^2 C(u, v)}{\partial u\, \partial v} \qquad (4)$$

Bu kopula fonksiyonlarının yapısı ve parametreleri detaylı olarak Tablo 2'de kısaca verilmiştir.

**Tablo 2.** Kopula fonksiyonlarının genel tanımı

| Copula | Function | Support |
|---|---|---|
| Gaussian copula | $C(u_1,u_2) = \int_{-\infty}^{\phi-1}(u_2) \int_{-\infty}^{\phi-1}(u_1) \frac{1}{2\pi(1-p^2)^{\frac{1}{2}}} exp\left\{-\frac{x_1^2+x_2^2-2px_1x_2}{2(1-p^2)}\right\} dx_1x_2$ | $x_1, x_2 \in R$ |
| Student t copula (t-copula) | $C(u_1,u_2) = \int_{-\infty}^{t_v^{-1}}(u_2) \int_{-\infty}^{t_v^{-1}}(u_1) \frac{1}{2\pi(1-p^2)^{\frac{1}{2}}} exp\left\{1+\frac{x_1^2+x_2^2-2px_1x_2}{v(1-p^2)}\right\}^{-\frac{(v+2)}{2}} dx_1x_2$ | $x_1, x_2 \in R$ |
| Clayton copula | $C(u_1,u_2) = \left(u_1^{-\theta}+u_2^{-\theta}-1\right)^{-\frac{1}{\theta}}$ | $\theta \in [0,\theta)$ |
| Gumbel copula | $C(u_1,u_2) = exp\left\{-\left[(-lnu_1)^{\theta}+(-lnu_2)^{\theta}\right]^{\frac{1}{\theta}}\right\}$ | $\theta \in [1,\infty)$ |
| Frank copula | $C(u_1,u_2) = -\frac{1}{\theta}ln\left[1+\frac{(e^{-\theta u_1}-1)(e^{-\theta u_2}-1)}{e^{-\theta}-1}\right]$ | $\theta \in R$ |
| Joe copula | $C(u_1,u_2) = 1-\left[(1-u_1)^{\theta}+(1-u_2)^{\theta}-(1-u_1)^{\theta}(1-u_2)^{\theta}\right]^{\frac{1}{\theta}}$ | $\theta \in [0,\theta)$ |
| BB1 copula | $C(u_1,u_2) = \left\{1+\left[\left(u_1^{-\theta}-1\right)^{\delta}+\left(u_2^{-\theta}-1\right)^{\delta}\right]^{-\frac{1}{\theta}}\right\}$ | $\theta > 0, \delta \geq 1$ |
| BB6 copula | $C(u_1,u_2) = 1-\left(1-exp\left\{-\left[\left(-log(1-(1-u_1)^{\theta})\right)^{\delta}+\left(1-log(1-(1-u_2)^{\theta})\right)^{\delta}\right]^{\frac{1}{\delta}}\right\}\right)^{\frac{1}{\theta}}$ | $\theta \geq 1, \delta \geq 1$ |
| BB7 copula | $C(u_1,u_2) = 1-\left(1-\left[(1-(1-u_1)^{\theta})^{-\delta}+(1-(1-u_2)^{\theta})^{-\delta}-1\right]^{-\frac{1}{\delta}}\right)^{\frac{1}{\theta}}$ | $\theta \geq 1, \delta > 0$ |
| BB8 copula | $C(u_1,u_2) = \delta^{-1}\left(1-\left\{1-\frac{[1-(1-\delta u_1)^{\theta}][1-(1-\delta u_2)^{\theta}]}{1-(1-\delta)^{\theta}}\right\}^{\frac{1}{\theta}}\right)$ | $\theta \geq 1, \delta \in (0,1]$ |

### 2.4. Kuyruk Bağımlılığı Parametrelerinin Tahmini

Kuyruk bağımlılığı değişkenlerin sağ üst kuyruğundaki aşırı değerler ve / veya sol alt kuyruğu arasındaki uyumla ilgilidir [34]. Çünkü uzun süreli ve büyük şiddette kuraklık olayı insan toplumu ve ekolojik sistemler üzerinde muazzam bir etkiye sahip olabilir. Üst kuyruk bağımlılığının aşırı kuraklık olayının analizinde alt kuyruk bağımlılığından daha fazla ilgisi olduğu görülmüştür [29]. Hidrolojide, kuyruk bağımlılıklarını göz ardı etmek aşırı kuraklık olayları tahminlerde yüksek belirsizliğe neden olup, bu da hidrolojik tasarım için istenmeyen bulgular ile sonuçlanabilir. Üst (alt) kuyruk bağımlılığı, kopula fonksiyonu olarak şu şekilde ifade edilebilir:

$$\lambda_u = \lim_{t\to 1^-} \frac{1-2t+C(t,t)}{1-t} \qquad (5)$$

$$\lambda_L = \lim_{t\to 1^-} \frac{C(t,t)}{t} \qquad (6)$$

Parametrik olmayan üst kuyruk bağımlılığı aşağıdaki formülle hesaplanabilir.

### 2.5. Dönüş Aralığı Metodu

Su kaynakları sistemi, hidrolojik ve hidrolik sistemlerin yönetimine genel bir yaklaşım kuraklık özelliklerinin dönüş aralıklarının tahmin edilmesidir. Özellikle kuraklık koşullarında önemli bilgiler vermektedir. Belirli bir değere eşit veya bu değerden büyük olan tek değişkenlikteki kuraklık süresinin dönüş periyodu şu şekilde hesaplanabilir:

$$\lambda_u^{CFG} = 2-2exp\left\{\frac{1}{n}\sum_{i=1}^{n} log\left[\frac{\sqrt{log\left(\frac{1}{u_1}\right)log\left(\frac{1}{v_1}\right)}}{log\left(\frac{1}{max(u_1,v_1)^2}\right)}\right]\right\} \qquad (7)$$

$$T_D = \frac{E(L)}{1-F_{D(d)}} \qquad (8)$$

Burada, L kuraklık zaman aralığını göstermektedir. Kuraklık şiddetinin belirli bir değere eşit veya bu değerden büyük dönüş periyodu, aşağıdaki gibi tanımlanan formül kullanılarak elde edilebilir.

$$T_S = \frac{E(L)}{1-F_{S(s)}} \qquad (9)$$

Ortak dönüş periyodu kuraklık süresi ve şiddeti için iki koşul için tahmin edilebilmektedir;

$$T_{DS} = \frac{E(L)}{P(D \geq d,\ S \geq s)} = \frac{E(L)}{1 - F_D(d) - F_S(s) + C(F_D(d), F_S(s))} = \frac{E(L)}{1 - F_D(d) - F_S(s) + F_{DS}(d, s)} \quad (10)$$

$$T'_{DS} = \frac{E(L)}{P(D \geq d\ or\ S \geq s)} = \frac{E(L)}{1 - F_{DS}(d, s)} = \frac{E(L)}{1 - C(F_D(d), F_S(s))} \quad (11)$$

Bu eşitliklerde, $T_{DS}$, hem kuraklık sürenin hem de şiddetinin belirli bir değere eşit veya büyük olması durumunu gösterirken (D ≥ d ve S ≥ s), $T'_{DS}$ dönüş periyodu ise ya kuraklık süresinin ya da kuraklık şiddetinin belirli bir değere eşit veya yüksek olma durumunu ifade etmektedir (D ≥ d ya da S ≥ s).

## 3. SONUÇLAR VE TARTIŞMA

### 3.1. Kuraklık Parametrelerinin Marjinal Dağılımı

İlk olarak, Osmaniye ilinin 1986-2016 yılları arasındaki yağış verilerini kullanarak kuraklık süresi ve şiddeti SPI-3 aylık zaman ölçeğinde metodu ile belirlenmiştir. SPI-3 zaman serisi Şekil 2'de gösterilmiştir.
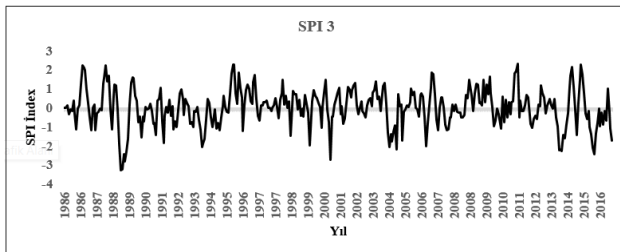


**Şekil 2.** Osmaniye ilinin SPI-3 aylık zaman serisi

SPI-3 zaman serisinden kuraklık süresi (D), şiddeti (S) ve her bir kuraklığın zaman aralığı (bölüm 2.1'de kuraklık süresinin ve şiddetinin nasıl hesaplanacağı detaylı olarak anlatılmıştır.) belirlendikten sonra,

kuraklık parametrelerinin tek değişkenli en uygun marjinal dağılımı Tablo 3 ve 4'teki performans test sonuçlarına hesaplanmıştır. Marjinal dağılımların parametreleri, oluşturulan teorik kümülatif olasılık dağılımlarının, gözlemlenen süre ve şiddetlerin aşılmama ihtimallerine karşı çizilmesiyle ortaya çıkan değerler arasında, en uygun dağılım elde edilmiştir. Seyhan Havzası'nda yer alan meteorolojik istasyonlarda 1986-2016 yılları arası gözlemlenen kuraklık olaylarının süre ve şiddet parametrelerine en uygun teorik dağılımlar Lognormal, Gama, Lojistik, Lojistik, Üstel, Weibull ve Normal dağılımları arasından seçilmiştir. Her kuraklık parametresi için kullanılan dağılımların performansı Anderson-Darling (AD), Kolmogorov Smirnov (KS), Cramers-von Mises (CvM), Akaike Bilgi Kriteri (AIC), Bayes Bilgi Kriteri (BIC) ve Maksimum olabilirlik yöntemleri (MLE) ile test edilmiştir. Performans testleri ile belirlenen en küçük değer, hem kuraklık süresi hem de kuraklık şiddeti için en uygun dağılım bulunmaktadır. Test sonuçlarına göre, Kuraklık süresi için en uygun Lognormal dağılımı, α = 0,855, β = 0,758 olarak hesaplanırken, kuraklık şiddeti için en uygun dağılım Weibull, η = 1,320 β = 3,470 olarak belirlenmiştir. Gözlemlenen veri ve belirlenen en uygun dağılımların kümülatif dağılım fonksiyonları arasındaki ilişki kuraklık süresi ve şiddeti için sırasıyla Şekil 3'te gösterilmiştir.

**Tablo 3.** Kuraklık süresi için kullanılan dağılımların performans testleri ile ölçülmesi

| Kuraklık Süresi | Lognormal | Lojistik | Gama | Üstel | Weibull | Normal |
|---|---|---|---|---|---|---|
| **Kolmogorov-Smirnov** | **0,1723** | 0,2143 | 0,2040 | 0,2707 | 0,2259 | 0,2285 |
| **Cramer-von Mises** | 0,3163 | 0,3965 | 0,3234 | 0,4370 | **0,3023** | 0,5817 |
| **Anderson-Darling** | 2,2704 | 2,7322 | 2,1797 | 2,8326 | **2,0242** | 3,3583 |
| **Akaike Bilgi Kriteri (AIC)** | **219,8280** | 255,0369 | 226,5729 | 234,4894 | 229,8280 | 263,6649 |
| **Bayes Bilgi Kriteri (BIC)** | **223,8060** | 259,0149 | 230,5508 | 236,4784 | 233,7851 | 267,6428 |
| **Maksimum Ol. Yöntemi (MLE)** | **-107,9140** | -125,5184 | -111,2864 | -116,2447 | -112,9036 | -129,8324 |

**Tablo 4.** Kuraklık şiddeti için kullanılan dağılımların performans testleri ile ölçülmesi

| Kuraklık Şiddeti | Lognormal | Lojistik | Gama | Üstel | Weibull | Normal |
|---|---|---|---|---|---|---|
| **Kolmogorov-Smirnov** | 0,0922 | 0,2394 | 0,1111 | 0,1907 | **0,0675** | 0,2433 |
| **Cramer-von Mises** | 0,0607 | 0,5119 | 0,1206 | 0,4391 | **0,03411** | 1,1165 |
| **Anderson-Darling** | 0,4654 | 3,9670 | 0,7725 | 2,5868 | **0,20630** | 6,2317 |
| **Akaike Bilgi Kriteri (AIC)** | 203,4746 | 275,0349 | 205,608 | 208,5667 | **200,8678** | 294,1332 |
| **Bayes Bilgi Kriteri (BIC)** | 207,4526 | 279,0128 | 209,586 | 210,5557 | **204,8458** | 298,1111 |
| **Maksimum Ol. Yöntemi (MLE)** | -99,7372 | -135,5174 | -100,804 | -103,2833 | **-98,43391** | -145,0666 |
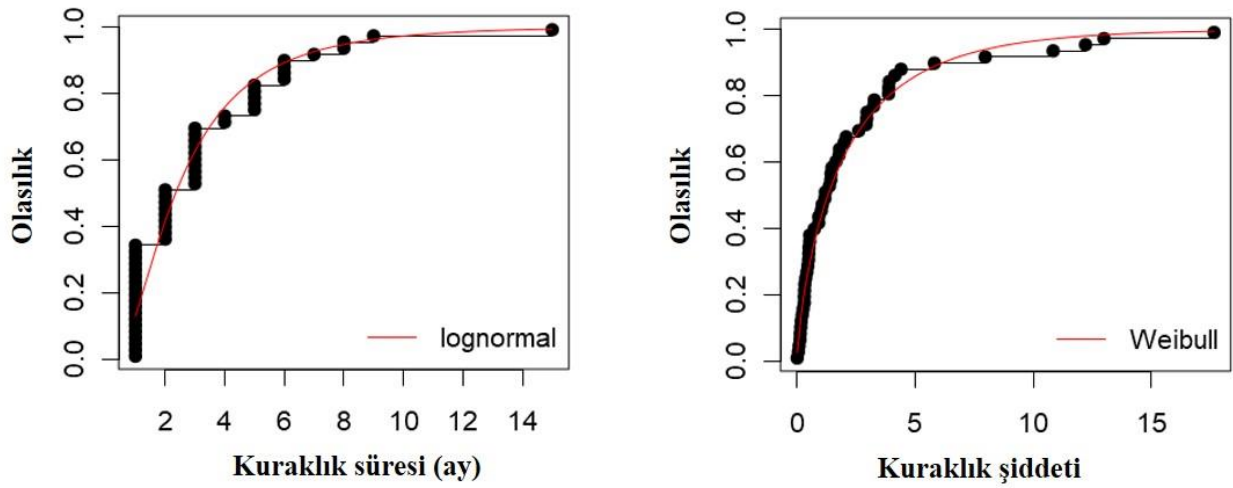
**Şekil 3.** Kuraklık süresi ve şiddeti için belirlenen en uygun marjinal dağılımların kümülatif dağılım fonksiyonu

### 3.2. Ortak Dağılım Fonksiyonun Belirlenmesi

Gözlemlenen kuraklık süresi ve şiddeti için sırasıyla Lognormal ve Weibull en uygun marjinal dağılım olarak hesaplandığı için, genel olarak yaygın kullanılan iki değişkenli dağılımlar kullanılmaz. Bu çalışmada kuraklık süresi ve şiddeti için kopula temelli iki değişkenli dağılım elde edilmiştir. Kuraklık süresi ve şiddeti arasındaki bağımlılığı modellemek için Gaussian, Student't, Clayton, Gumbel, Frank, Joe, BB1, BB6, BB7 ve BB8 kopula dahil olmak üzere 10 kopula test edilmiştir. Gözlemlenen veriler için en uygun kopula; performans testleri, üst kuyruk bağımlılığı dikkate alınmıştır. Bu sonuçlar ışığında, Gumbel kopulası diğer kopula fonksiyonlarına kıyasla en uygun dağılım olarak belirlenmiştir. En düşük AIC ve BIC

değerlerinin en uygun kopulayı belirlemede yardımcı olurken, kuraklık süresi ve şiddeti arasındaki bağlılığın, üst kuyruk bağlılığı arasında yakın bir ilişki olması gerekmektedir. Tablo 5'te görüldüğü gibi, gözlemlenen veriler arasındaki veri bağımlılığı Kendall Tau sonucuna göre 0,726 değeri hesaplanırken, bu değere en yakın üst kuyruk bağımlılığı sadece Gumbel, Joe, BB6 ve BB7 kopulalarında görülmektedir. Bu üç kopula arasında en uygun Gumbel kopulası en düşük AIC ve BIC değerine göre hesaplanmıştır. Gumbel kopulası ile üretilen 1000 veri *(u, v)* ile gözlemlenen veriler arasında iyi bir ilişki Şekil 4'te görülmektedir.

**Tablo 5.** Kullanılan kopula fonksiyonlarının performans test sonuçları

| | | | | | | | Kuyruk Bağımlılığı | | Kendal Tau |
| Numara | Kopula | MLE | AIC | BIC | Par 1 | Par 2 | Alt kuyruk | Üst Kuyruk | 0.727 |
|---|---|---|---|---|---|---|---|---|---|
| 1 | Gaussian Kopula | 36,34 | -70,67 | -68,68 | 0,87 | | 0 | 0 | |
| 2 | Student t Kopula | 36,18 | -68,35 | -64,38 | 0,86 | 30 | 0,142 | 0,142 | |
| 3 | Clayton Kopula | 24,1 | -46,21 | -44,22 | 2,2 | | 0,73 | 0 | |
| 4 | Gumbel Kopula | 35,25 | -68,5 | -66,51 | 2,75 | | | 0,713 | |
| 5 | Frank Kopula | 33,72 | -65,45 | -63,46 | 9,69 | | 0 | 0 | |
| 6 | Joe Kopula | 32 | -62,01 | -60,02 | 3,38 | | 0 | 0,772 | |
| 7 | BB1 Kopula | 35,53 | -67,07 | -63,09 | 0,24 | 2,52 | 0,313 | 0,683 | |
| 8 | BB6 Kopula | 35,25 | -66,5 | -62,52 | 1 | 2,75 | 0 | 0,714 | |
| 9 | BB7 Kopula | 34,09 | -64,18 | -60,21 | 2,95 | 1,39 | 0,606 | 0,735 | |
| 10 | BB8 Kopula | 37,96 | -71,92 | -67,94 | 6 | 0,89 | 0 | 0 | |

MLE: Maksimum olabilirlik yöntemleri, AIC: Akaike Bilgi Kriteri, BIC: Bayes Bilgi Kriteri, Par: Parametre
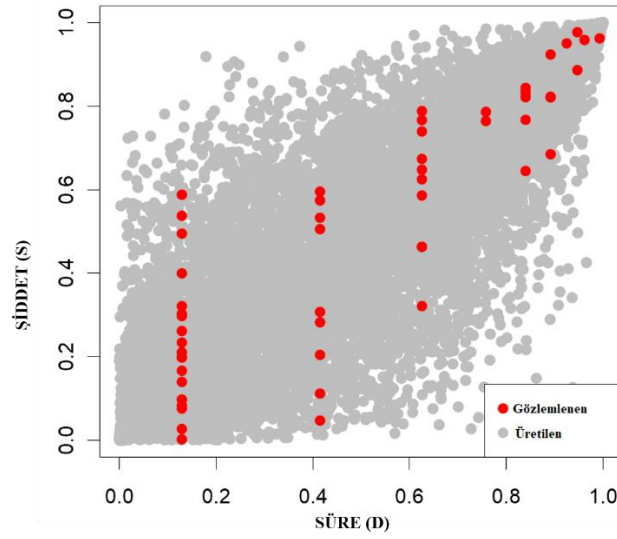
**Şekil 4.** Gözlemlenen verilerin (kırmızı) Gumbel kopulası ile üretilen rastgele veriler (gri) ile karşılaştırılması

### 3.3. Tek ve İki Değişkenli Dönüş Periyodu Belirlenmesi

Tek değişkenli kuraklık süresi ve şiddeti için belirlenen marjinal dağılımlar için eşitlik 7 ve 8'deki denklemlere göre belirlenmiştir. $T_{D/S}$ herhangi bir kuraklık parametresinin belirli bir değere eşit veya büyük olması durumundaki dönüş periyodunu (10, 20, 50, 100, 200 ve 500 yıllık) temsil ederken E(L) ise kurak geçen ortalama süre aralığını göstermektedir. E(L) Osmaniye ili için 6.77 ay olarak hesaplanmıştır. Kuraklık süresi ve şiddeti için kendi marjinal dağılımları dikkate alınarak hesaplanan dönüş periyodu Tablo 6'da gösterilmiştir. Bu sonuçlara göre kuraklık süresi değerlendirildiğinde, kuraklık süresinin 16.07 aya eşit veya yüksek olması durumundaki hesaplanan dönüş periyodu 100 yıl olarak belirlenmiş olup, bu dönüş periyoduna karşılık gelen kuraklık şiddeti ise 17.57 olarak bulunmuştur. Kuraklık süresi ve şiddeti birbirleri arasında yüksek bir bağımlılığa sahip olduklarından, bu parametrelerin tek tek incelenmesinin aksine, ortak değerlendirilmeleri sonucu dönüş periyotlarının hesaplanması, dikkate alınan bölgenin kuraklığının daha iyi irdelenmesine ve su yönetimi gibi problemlerinin çözümüne fayda sağlayacaktır.

Kopula, kuraklık parametrelerinin ortak dönüş periyotlarını 9. ve 10. eşitliğe göre hesaplamaya imkân sağlamaktadır. $T_{DS}$, hem kuraklık süresinin hem de kuraklık şiddetinin belirli bir değere eşit veya büyük olması durumundaki dönüş periyodunu hesaplarken, $T'_{DS}$ ise kuraklık süresinin ya da kuraklık şiddetinin belirli bir değere eşit veya yüksek olması durumundaki dönüş periyodunu dikkate almaktadır. Kopula temelli ortak dönüş periyotları Tablo 6'da gösterilmiştir. Örneğin, kuraklık süresinin 16.07 ay ve kuraklık

şiddetinin 17.57 eşit veya yüksek olması durumunda, ortak dönüş periyodu ($T_{DS}$) 139 yıl olarak hesaplanmıştır. Oysaki tek tek kuraklık parametreleri değerlendirildiğinde bu dönüş periyodu ($T_{D/S}$) 100 yıl olarak bulunmuştur. Kuraklık süresinin 16.07 ay ya da kuraklık şiddetinin 17.57 eşit veya yüksek olması durumunda ($T'_{DS}$), ortak dönüş periyodu 77.79 yıl olarak hesaplanmıştır.

**Tablo 6.** Kuraklık süresi ve şiddetinin ortak dönüş periyotları

| Dönüş Periyodu | D (Süre) | S (Şiddet) | $T_{DS}$ (ortak dönüş periyodu) | $T'_{DS}$ (ortak dönüş periyodu) |
|---|---|---|---|---|
| 10 | 7,83 | 8,23 | 13,81 | 7,84 |
| 20 | 10,00 | 10,87 | 27,83 | 15,61 |
| 50 | 13,27 | 14,60 | 69,88 | 38,93 |
| 100 | 16,08 | 17,57 | 139,96 | 77,79 |
| 200 | 19,20 | 20,66 | 280,12 | 155,52 |
| 500 | 23,86 | 24,91 | 700,60 | 388,71 |

Kuraklık parametrelerinin ortak dönüş periyotları farklı değerler için hesaplanmış olup, Şekil 5'te verilmiştir. Bu izohips eğrileri sayesinde, kuraklık parametrelerinin alacağı farklı değerler hesaplanması için olanak sağlamakta olup, ayrıca tek değişkenli frekans analizleri ile kolay bir şekilde kıyaslanabilmektedir. Türetilmiş ortak kuraklık süresi ve şiddeti dönüş periyodu, belirli bir su kaynakları sisteminin kestirilemeyen riskini değerlendirmek için kullanılabilir. Örneğin, su temini sisteminde, kuraklık süresinin 2 ayı kuraklık şiddetinin ise 4'ü aştığı durumlarda yeterli düzeyde su ihtiyacı karşılayamaz. Böylesi bir durumda ortak dönüş periyodu büyük önem kazanmaktadır.
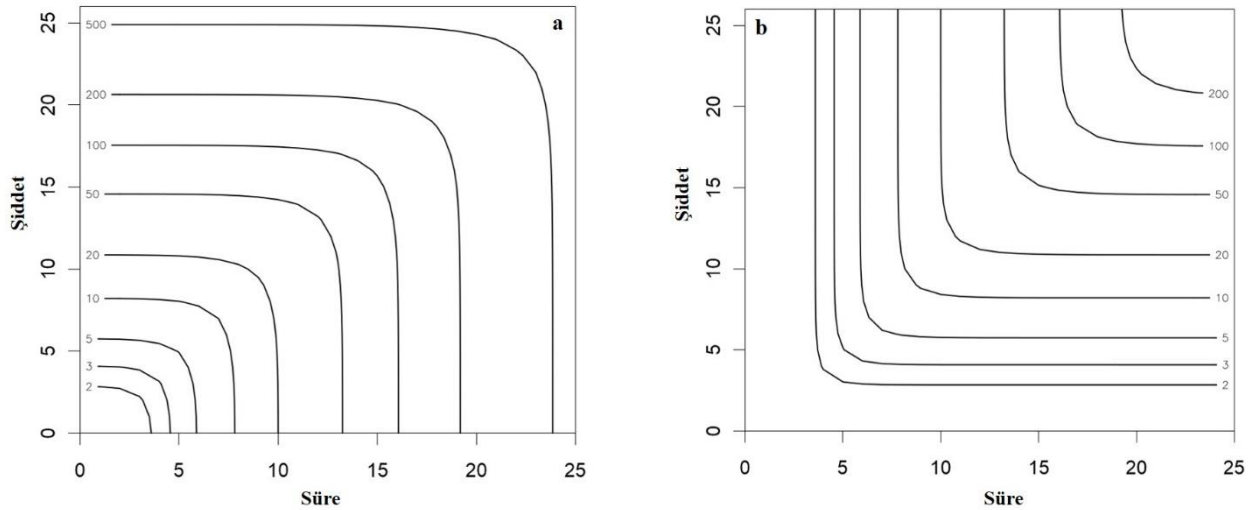
**Şekil 5.** Kuraklık parametresinin her iki koşul için (a) $T_{Ds}$ (b) $T'_{DS}$ ortak dönüş periyotları

# KAYNAKLAR

[1]     Kao, S. C., & Govindaraju, R. S. A copula-based joint deficit index for droughts. Journal of Hydrology, 380(1-2), 121-134, 2010

[2]     Heim Jr, R. R. A review of twentieth-century drought indices used in the United States. Bulletin of the American Meteorological Society, 83(8), 1149-1166, 2002

[3]     Sheffield, J., Wood, E. F., & Roderick, M. L. Little change in global drought over the past 60 years. Nature, 491(7424), 435-438, 2012

[4]     McKee, T. B., Doesken, N. J., & Kleist, J. The relationship of drought frequency and duration to time scales. In Proceedings of the 8th Conference on Applied Climatology (Vol. 17, No. 22, pp. 179-183), January 1993

[5]     Below, R., Grover-Kopec, E., & Dilley, M. Documenting drought-related disasters: A global reassessment. The Journal of Environment & Development, 16(3), 328-344, 2007

[6]     Wilhite, D. A. Drought as a natural hazard: concepts and definitions, 2000

[7]     Shiau, J. T., Feng, S., & Nadarajah, S. Assessment of hydrological droughts for the Yellow River, China, using copulas. Hydrological Processes: An International Journal, 21(16), 2157-2163, 2007

[8]     Mishra, A. K., & Singh, V. P. A review of drought concepts. Journal of hydrology, 391(1-2), 202-216, 2010

[9]     Kogan, F. N. Droughts of the late 1980s in the United States as derived from NOAA polar-orbiting satellite data. Bulletin of the American Meteorological Society, 76(5), 655-668, 1995

[10]     Guttman, N. B. Accepting the standardized precipitation index: a calculation algorithm 1. JAWRA Journal of the American Water Resources Association, 35(2), 311-322, 1999

[11]     Guttman, N. B. Comparing the palmer drought index and the standardized precipitation index 1. JAWRA Journal of the American Water Resources Association, 34(1), 113-121, 1998

[12]     Ray, K. S., & Shewale, M. P. Probability of occurrence of drought in various sub-divisions of India. Mausam, 52(3), 541-546, 2001

[13]     Efstathiou, M. N., & Varotsos, C. A. Intrinsic properties of Sahel precipitation anomalies and rainfall. Theoretical and applied climatology, 109(3-4), 627-633, 2012

[14]     McKee, T. B. Drought monitoring with multiple time scales. In Proceedings of 9th Conference on Applied Climatology, Boston, 1995, 1995

[15]     Eris, E., Aksoy, H., Onoz, B., Cetin, M., Yuce, M. I., Selek, B., ... & Karakus, E. U. Frequency analysis of low flows in intermittent and non-intermittent rivers from hydrological basins in Turkey. Water Supply, 19(1), 30-39, 2019

[16]     Du, J., Fang, J., Xu, W., & Shi, P. Analysis of dry/wet conditions using the standardized precipitation index and its potential usefulness for drought/flood monitoring in Hunan Province, China. Stochastic environmental research and risk assessment, 27(2), 377-387, 2013

[17]     Çetin, M., Aksoy, H., Önöz, B., Eriş, E., İshak, M., Yüce, B. S., ... & Orta, S. Deriving Accumulated Precipitation Deficits from Drought Severity-Duration-Frequency Curves: A Case Study in Adana Province, Turkey. SCIENTIFIC COMMITTEE-BİLİM KURULU, 39, 2018

[18]     Aksoy, H., Onoz, B., Cetin, M., Yuce, M. I., Eris, E., Selek, B., ... & Cavus, Y. SPI-based drought severity-duration-frequency analysis. In Proceedings of the 13th International Congress on Advances in Civil Engineering, Izmir, Turkey (pp. 12-14), September 2018

[19]     Tsakiris, G., Kordalis, N., Tigkas, D., Tsakiris, V., & Vangelis, H. Analysing drought severity and areal extent by 2D Archimedean copulas. Water Resources Management, 30(15), 5723-5735, 2016

[20]     Shiau, J. T. Fitting drought duration and severity with two-dimensional copulas. Water resources management, 20(5), 795-815, 2006

[21]     Cancelliere, A., & Salas, J. D. Drought length properties for periodic-stochastic hydrologic data. Water resources research, 40(2), 2004

[22]    Song, S., & Singh, V. P. Frequency analysis of droughts using the Plackett copula and parameter estimation by genetic algorithm. Stochastic Environmental Research and Risk Assessment, 24(5), 783-805, 2010

[23]    Salvadori, G., De Michele, C., Kottegoda, N. T., & Rosso, R. Extremes in nature: an approach using copulas (Vol. 56). Springer Science & Business Media, 2007

[24]    Kuhn, G., Khan, S., Ganguly, A. R., & Branstetter, M. L. Geospatial–temporal dependence among weekly precipitation extremes with applications to observations and climate model simulations in South America. Advances in Water Resources, 30(12), 2401-2423, 2007

[25]    Nelsen, R. B. An introduction to copulas. Springer Science & Business Media, 2007

[26]    Mirakbari, M., Ganji, A., & Fallah, S. R. Regional bivariate frequency analysis of meteorological droughts. Journal of Hydrologic Engineering, 15(12), 985-1000, 2010

[27]    Tosunoglu, F., & Can, I. Application of copulas for regional bivariate frequency analysis of meteorological droughts in Turkey. Natural Hazards, 82(3), 1457-1477, 2016

[28]    Shiau, J. T., & Modarres, R. Copula-based drought severity-duration-frequency analysis in Iran. Meteorological Applications: A journal of forecasting, practical applications, training techniques and modelling, 16(4), 481-489, 2009

[29]    Lee, T., Modarres, R., & Ouarda, T. B. Data-based analysis of bivariate copula tail dependence for drought duration and severity. Hydrological Processes, 27(10), 1454-1463, 2013

[30]    Yusof, F., Hui-Mean, F., Suhaila, J., & Yusof, Z. Characterization of drought properties with bivariate copula analysis. Water resources management, 27(12), 4183-4207, 2013

[31]    Sklar, A., SKLAR, A., & Sklar, C. A. Fonctions de reprtition an dimensions et leursmarges, 1959

[32]    Salvadori, G., & De Michele, C. Frequency analysis via copulas: Theoretical aspects and applications to hydrological events. Water resources research, 40(12), 2004

[33]    Poulin, A., Huard, D., Favre, A. C., & Pugin, S. Importance of tail dependence in bivariate frequency analysis. Journal of Hydrologic Engineering, 12(4), 394-403, 2007

# Expert Modelling and Prediction of Von Mises Stresses in High Speed Steel Cutting Tool Using FEM (ANSYS)

[1]Cyril Aliyegbenoma, [2]Mercy Ozakpolor
[1]Department of Production Engineering, Faculty of Engineering, University Of Benin, Benin City, Edo State, Nigeria
*[1]cyril.aliyegbenoma@eng.uniben.edu, 
[2]othuke2477@gmail.com,

**Abstract**

In the machining world, development of predictive models is one remedy to reducing tool failure and its associated challenges like reduction in integrity of machined parts, production shutdown and idle time for machine operators.
In this research, we want to show how robust the Finite Element (ANSYS) method is, by comparing its predictive capacity to the experimental machining operation.

To achieve the scope of the study, Seventeen (17) varying set of experiments were conducted for the cutting tool using the three levels Box-Behnken's design (BBD) of experiment at varying process parameters of 200-600 rpm spindle speed, 0.05-0.15mm/rev feed rate and 0.5 - 1.5mm depth of cut. During, the orthogonal cutting of AISI 1010 mild steel measuring 200mm length by 44mm diameter, the electrical strain gauge connected to the Electronic strain meter E10 was used to measure the tools' induced strains from where the equivalent von mises stresses were generated for the research. The finite element software was then used to model the HSS tool for prediction of the concerned response based on the designed matrix generated by the Design Expert. The experimental values were compared with the ANSYS simulated values using the absolute mean percentage error and the reliability plot.

At the end, both the experimental and FEM (ANSYS) readings were in close agreements with a mean absolute percentage error of 0.544%. Therefore, this research has clearly shown that ANSYS is a very robust expert tool that can be used to model and predict von mises stresses in HSS cutting tool.

**Keywords:** BBD, FEM, HSS, ANSYS, Cutting tool, ENC, Von-mises stress.

## 1. INTRODUCTION

The metal cutting process is a deformation process that uses a cutting tool to remove unwanted material from a work piece produce designed specifications. It is the oldest and most vital form of machining in the manufacturing world. Technically, it has advanced from the traditional and manual cutting method to the newest manufacturing technique that has many processes with automated tools design for high quantities and precisions. These modern heavy machine tools like the computer numerically controlled (CNC) lathes have be found to generate more heat than the simple manual tools due to the sliding friction of the chip on the rake face. The heat produced during the operation brings about abnormal thermal gradient in the form of von mises stresses due to high strains. The produced von mises stress is the major cause of tool fracture, fatigue and

failure at last. A situation resulting from loses of bindings within the crystals in the tool materials [1]. Besides, literature has shown that the major cause of increasing cutting temperature and von mises stress is uncontrolled process parameters, since cutting tools have specific geometry. Experimental investigations carried out on the process parameter of a cutting tool and its influence on cutting forces and surface roughness for finished Hard Turning operation using MDN250 steel, the experimental operation involved cutting speed, depth of cut and feed rate as control variables, while feed force, surface roughness and the thrust force were taken as response parameters [2]. During the experiment, the flank wear was measured with tool maker's microscope. And at the end, the work prove that good surface appearance in material can be attained when cutting speed, depth of cut are set close to their high level (93m/min and 0.2mm respectively)

*Corresponding Author: Department of Production Engineering, Faculty of Engineering, University Of Benin, Benin City, Edo State, Nigeria
cyril.aliyegbenoma@eng.uniben.edu

with feed rate at low level of 0.04mm/rev. A methodology for the determination of work piece flow stress and the friction at the chip-tool interface during the high-speed cutting at high deformation rates due to the high cutting temperatures of the cutting zone. Their results were used to stimulate the high-speed machining using the finite element analysis based program. The flow stress model based on process dependent parameters like the stain, strain-rate and temperature were used together with the friction model so as to enable them to determine the unknown parameters of the flow stress and the friction model [3]. Most commonly used method for the determination of flow stresses are the tension, uniform and torsion tests was postulated [4].

They analyzed the role of flow stresses and friction coefficient on machining using finite element analysis. In their work, the coulomb friction model was cited as the commonly used technique in most finite element method while the Jonson-cook constitutive law was presented as a prerequisite predictive model [5].

They also analyzed the residual stresses induced by dry turning on difficult- to- machined materials. Their focus was on the effects of cutting process parameters on the residual stresses and surface integrity while turning Inconel 718 and Austentic stainless steel AISI 318L under dry condition with coated and uncoated carbide tools. A three- dimensional predictive finite element model was developed and on comparing both the predicted and experimental result, a new knowledge on surface integrity in terms of residual stresses was developed [6].

The quantitative analysis of the flow stress constitutes one of the most important inputs to the simulation of a metal forming process. The authors also stated that the flow stress of a metal may be quantified in terms of its dependence on strain, strain-rate and temperature. They further stressed that the flow stress can also be based on the internal state variables such as dislocation, density, grain size, phase formation, as well strain-rate and temperature [7].

The investigation on the influence of tool wear on surface roughness using differently shaped ceramic tools in a hard turning operation was carried out [8]. The surface roughness was determined by the macroscopic tool geometry at certain levels of feed rates. Others that also studied on similar research issue [9][10].

## 2. MATERIALS AND METHODS

### 2.1 Experimental Method

The experimental cutting test in this work, involved the dry cutting of a cylindrical mild steel bar of 200mm length by 44mm diameter using the industrial 2060 ENC model Lathe machine. The high speed steel single point cutting tool was

employed for the machining operation. The Box-Behnken Design (BBD) of experiment was adopted for this work, table 1 shows the cutting parameters which are the spindle speed, depth of cut and feed rate. From table 1, seventeen (17) experimental test were generated for the research. While, Table 2 shows the generated BBD matrix for the three process parameters as well as the response obtained after the experiment.

**Table 1: Cutting parameters and their corresponding levels**

| Tools Types | | High speed steel (HSS) | | |
|---|---|---|---|---|
| Work piece materials | | Mild Steel | | |
| Cutting parameters | Symbols/ units | Low (-1) | Medium (0) | High (+1) |
| Spindle speed | n, rpm | 200 | 400 | 600 |
| Feed rate | f,mm/rev | 0.05 | 0.1 | 0.15 |
| Depthof cut | ap, mm | 0.5 | 1.0 | 1.5 |

**Table 2: Experimental data for high speed steel cutting tool while machining mild steel**

| Test No | Spindle speed, n (rpm) | Feed rate ,f (mm/ rev) | Depth of cut, ap (mm) | Von mises stresses N/mm$^2$ |
|---|---|---|---|---|
| 1 | 200 | 0.15 | 1.00 | 275.50 |
| 2 | 400 | 0.05 | 1.50 | 755.80 |
| 3 | 600 | 0.10 | 1.50 | 1353.0 |
| 4 | 200 | 0.10 | 0.50 | 461.50 |
| 5 | 600 | 0.05 | 1.00 | 510.50 |
| 6 | 400 | 0.05 | 0.50 | 260.10 |
| 7 | 600 | 0.10 | 0.50 | 462.50 |
| 8 | 600 | 0.15 | 1.00 | 1290.1 |
| 9 | 400 | 0.10 | 1.00 | 907.45 |
| 10 | 200 | 0.05 | 1.00 | 518.56 |
| 11 | 400 | 0.15 | 1.50 | 1915.9 |
| 12 | 400 | 0.10 | 1.00 | 907.51 |
| 13 | 400 | 0.10 | 1.00 | 907.50 |
| 14 | 400 | 0.10 | 1.00 | 907.50 |
| 15 | 400 | 0.10 | 1.00 | 907.51 |
| 16 | 400 | 0.15 | 0.50 | 650.00 |
| 17 | 200 | 0.10 | 1.50 | 1363.9 |

Figure 1 shows the experimental set-up, where a strain meter connected to a single electrical strain guage was used to take readings from which the induced equivalent stresses were generated.
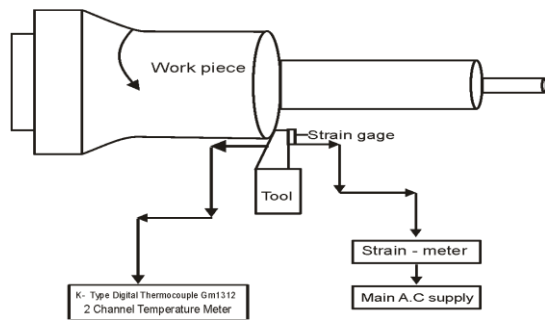
**Figure 1:** Experimental set-up

### 2.1.1 FEM Simulation

Finite element software such as ANSYS is a tool used for simulating the behavior of cutting tool during machining. It analyzes finite element problem in three steps, namely: preprocessing, solution and post processing [11] as explained below.

### 2.1.2 Preprocessing:

This includes defining the geometrical properties of the problem, the element types to be used, the material properties of the elements, the geometrical properties of the elements loadings. Thirdly, is to analysis the setting where the boundary conditions such as fixed support, applied force, pressure etc. are specified. However, to find the induced stresses on the cutting tool, the cutting force should be known.

In this study, AutoCAD Inventor was used for the model design.
(length, area etc.), the element connectivity (mesh the model), the physical constraints (boundary conditions) and the

After the geometry modeling, we exported the geometry to ANSYS for nodes and elements generation for the meshed cutting tool. The fixed support for the cutting tool was movement restricted in the top and bottom part. The various applied forces are determined from the spindle speed, feed rate and depth of cut values using equation (1) as given in table 3. The force is the force reaction coming from the work piece which is equal and opposite to the actual cutting force applied. These values were inputted to ANSYS.

For turning operation using high speed steel tipped tool with $\alpha = +10^0, \lambda = 45^0, R = 2mm, i = 0^0, C = 10^0,$ without lubrication, the relation is:

$$F_c = Cd^x f^y V^n, kgf \qquad (1)$$

Where
$F_c$ = cutting force, N
$f$ = feed, mm/rev

$d$ = depth of cut, mm
$V$ = cutting speed, m/min

For work material such as steel and steel castings, with tensile strength of $75\,kgf/mm^2$ and feed less than or equal to $0.75\,mm/rev$   take   $C = 300, x = 1.0, y = 0.75, n = -0.15$ [12].

**Table 3:** Summary of cutting tool force

| Test No | Spindle Speed (rpm) | Feed rate (mm/rev) | Depth of cut (mm) | Forces (N) |
|---|---|---|---|---|
| 1 | 200 | 0.15 | 1.00 | 43.94772225 |
| 2 | 400 | 0.05 | 1.50 | 26.06346724 |
| 3 | 600 | 0.10 | 1.50 | 41.24686998 |
| 4 | 400 | 0.10 | 0.50 | 16.21204987 |
| 5 | 600 | 0.05 | 1.00 | 16.35035708 |
| 6 | 400 | 0.05 | 0.50 | 8.687822414 |
| 7 | 600 | 0.10 | 0.50 | 13.74895666 |
| 8 | 600 | 0.15 | 1.00 | 37.27075435 |
| 9 | 400 | 0.10 | 1.00 | 29.2222349 |
| 10 | 200 | 0.05 | 1.00 | 19.27948506 |
| 11 | 400 | 0.15 | 1.50 | 59.41185751 |
| 12 | 400 | 0.10 | 1.00 | 29.2222349 |
| 13 | 400 | 0.10 | 1.00 | 29.2222349 |
| 14 | 400 | 0.10 | 1.00 | 29.2222349 |
| 15 | 400 | 0.10 | 1.00 | 29.2222349 |
| 16 | 400 | 0.15 | 0.50 | 19.8039525 |
| 17 | 200 | 0.10 | 1.50 | 48.63614962 |
| 17 | 200 | 0.10 | 1.50 | 48.63614962 |

**Solution**: The features in this step such as matrix manipulation, numerical integration, and equation solving are carried out automatically by the software. The governing algebraic equation in matrix form, computation of the unknown values of the primary field and assembling is done automatically.

## 3 FINDINGS

In this section is the evaluation and interpretation of the various von mises stresses will be presented.

### 3.1 RESULTS

**Post processing**: Interpretation and evaluation of results is expressed this stage.

For a turning operation with spindle speed of 200 rpm, feed rate of 0.15 mm/rev and a depth of cut of 1 mm, the stress of $1278.20 N/mm^2$ was generated on the cutting tool. Figure 2 shows the stress buildup from minimum to maximum during the turning process, when a cutting force of 43.9477 N was applied.
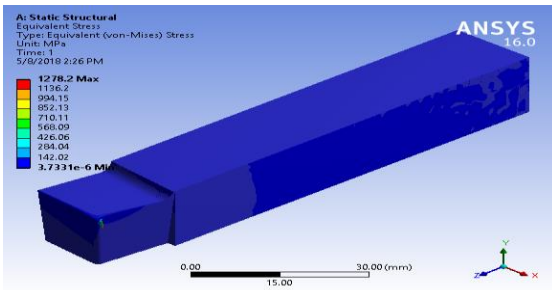
**Figure 2:** von-mises stress for cutting force
Of 43.9477N using FEM

For a turning operation with spindle speed of 400 rpm, feed rate of 0.05 mm/rev and a depth of cut of 1.50 mm, the stress of 764.44 N/mm² was generated on the cutting tool. Figure 3 shows the stress buildup from minimum to maximum during the turning process, when a cutting force of 26.0635 N was applied.,
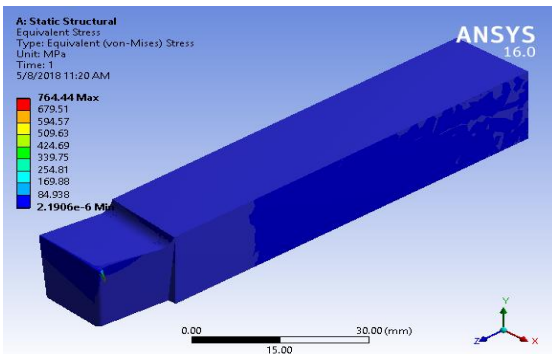


**Figure 3** von-mises stress for cutting force
Of 26.0635N using FEM

For a turning operation with spindle speed of 600 rpm, feed rate of 0.10 mm/rev and a depth of cut of 1.50 mm, the stress of 1365.90 N/mm² was generated on the cutting tool. Fig. 4 shows the stress buildup from minimum to maximum during the turning process, when a cutting force of 41.2469 N was applied
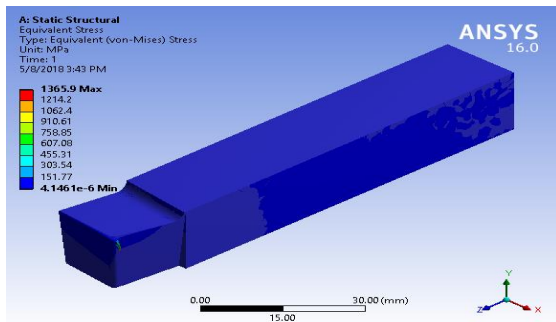


**Figure 4** von-mises stress for cutting force
of 41.2469N using FEM

For a turning operation with spindle speed of 400 rpm, feed rate of 0.10 mm/rev and a depth of cut of 0.50 mm, the stress of 464.25 N/mm² was generated on the cutting tool. Figure 5 shows the stress buildup from minimum to maximum during the turning process, when a cutting force of 16.2120 N was applied
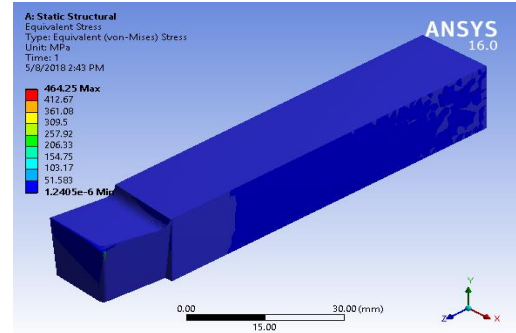


**Figure 5** von-mises stress for cutting force
of 16.2120N using FEM

The same predictive approach was used for experiment numbers 5-17. See the summary of the maximum ANSYS predicted response values obtained for the BBD design of experiment in Table 4 below

**Table 4:** Summary of ANSYS generated Von-mises Stresses for HSS cutting tool

| Test No | Spindle Speed (rpm) | Feed rate (mm/rev) | Depth of cut (mm) | Von mises Stress (N/mm²) |
|---|---|---|---|---|
| 1 | 200 | 0.15 | 1.00 | 1278.20 |
| 2 | 400 | 0.05 | 1.50 | 764.44 |
| 3 | 600 | 0.10 | 1.50 | 1365.90 |
| 4 | 400 | 0.10 | 0.50 | 464.25 |
| 5 | 600 | 0.05 | 1.00 | 511.10 |
| 6 | 400 | 0.05 | 0.50 | 262.63 |
| 7 | 600 | 0.10 | 0.50 | 464.25 |
| 8 | 600 | 0.15 | 1.00 | 1278.20 |
| 9 | 400 | 0.10 | 1.00 | 910.56 |
| 10 | 200 | 0.05 | 1.00 | 511.10 |
| 11 | 400 | 0.15 | 1.50 | 1920.00 |
| 12 | 400 | 0.10 | 1.00 | 910.56 |
| 13 | 400 | 0.10 | 1.00 | 910.56 |
| 14 | 400 | 0.10 | 1.00 | 910.56 |
| 15 | 400 | 0.10 | 1.00 | 910.56 |
| 16 | 400 | 0.15 | 0.50 | 649.24 |
| 17 | 200 | 0.10 | 1.50 | 1365.90 |

## 4. DISCUSSION

The prediction of high speed steel cutting tool von mises stresses when machining mild steel using dry orthogonal cutting process was carried out, using both experimental methods and the finite element method. This is to know how

accurate the FEM could predict the stresses generated on the tool. The Box-Behnken's experimental design with the aid of the Design Expert 7.00 version was used to generate the design of experiment (DOE) as shown in table 6. The von-mises stresses obtained in table 2 is the experimental values. To get the FEM stress values, the forces gotten from table 3 using equation (1), were employed to generate the von-mises stresses in table 4. At the end, a comparative study between the experimental and FEM using the absolute mean percentage error was given in table 5.

**Table 5:** FEM comperitave prediction of von-mises stresses and experimental reading

| Test No | Von mises stress N/mm$^2$ Experimental | Von mises stress N/mm$^2$ FEM predicted | Absolute percentage error (%) |
|---|---|---|---|
| 1 | 1275.50 | 1278.20 | 0.21 |
| 2 | 755.80 | 764.44 | 1.14 |
| 3 | 1353.00 | 1365.90 | 0.95 |
| 4 | 461.50 | 464.25 | 0.96 |
| 5 | 510.50 | 511.10 | 0.12 |
| 6 | 260.10 | 262.63 | 0.97 |
| 7 | 462.50 | 464.25 | 0.38 |
| 8 | 1290.10 | 1278.20 | 0.92 |
| 9 | 907.45 | 910.56 | 0.34 |
| 10 | 518.56 | 511.10 | 1.44 |
| 11 | 1915.95 | 1920.00 | 0.21 |
| 12 | 907.51 | 910.56 | 0.33 |
| 13 | 907.50 | 910.56 | 0.34 |
| 14 | 907.50 | 910.56 | 0.34 |
| 15 | 907.51 | 910.56 | 0.33 |
| 16 | 650.00 | 649.24 | 0.12 |
| 17 | 1363.90 | 1365.90 | 0.15 |

The Mean Absolute Error is 0.544%

To assess the accuracy of the predictions as well as the suitability of the Expert model, a reliability plot of the experimental and the finite element was carried out, as shown in Figure 6
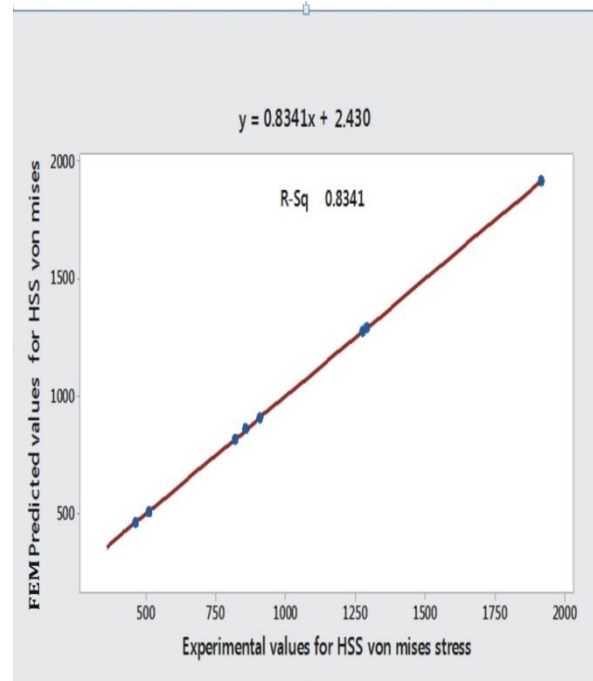


**Figure 6** Reliability plots of Experimental and Finite element

From table 5, it can be seen that both experimental and FEM (ANSYS) reading were in close agreements, with a mean absolute percentage error of 0.544%. To assess the accuracy of the predictions as well as the suitability of the finite element model, a reliability plot of the experimental and the predicted values was carried out, as shown in Figure 6. The clustered points along the line in Figure 6 show the closeness between the experimental and the predicted values. This research therefore has clearly shows that ANSYS is a very robust predictive tool, which can be used to model and predict stresses in cutting tools.

**5. CONCLUSION**

The present research study focused on predicting high speed steel cutting tool at various cutting parameters while machining mild steel under dry condition. The experimental design was conducted by the three factors Box-Behnken design. During, the cutting tool tests, the strain gauge was connected to an A.C supply strain meter, which was used to measure the induced strain from which the stress was generated. The FEM software was used to verify the test results. In all, the following conclusions have been drawn;

1. The FEA result shows that the von mises stress are found at the tip of the cutting tool.
2. The experimental test shows that the chip formations were found to be a continuous type at lower spindle speed and feed rate. According to findings [13].

3. As depth of cut increases from 0.5 to 1.5mm there is a sudden rise in tools' von mises stresses. This is the major reasons of tools' wears and failures, due to increased deformations

From the obtained results, it has been showed that the predictions of the von mises stress of a cutting tool can improve the service life of the cutting tool as well as the integrity of the machined components. It is therefore recommended that the metal cutting industries should adopt FEM Expert means such as the ANSYS, to determine the right process parameter for a specified cutting process, in order to prolong the service life of the cutting tools and avoid exceeding the yield point; the cause of tool wear and failure when machining mild steel with high speed steel cutting tools.

## 4. ACKNOWLEDGEMENT

## REFERENCES

[1]. Lazoglu, L. and Altintas, Y. (2002) Prediction of tool chip temperature in continuous and interrupted machining. Int. J. Mach. Tools Manufacture. Vol. 42, PP. 1011-1022.

[2]. Lawani, D. I., Mehta, N. K and Jain, P. K (2008) Experimental Investigations of Cutting Parameters Influence on Cutting Forces and Surface Roughness in Finish Hard Turning of 250 Steel. Journal of Materials Processing and Technology, Vol. 206, PP. 167-179.

[3]. Ozel, T. and Zeren, E. (2004) "Determination of Work Material Flow Stress and Friction For FEA Of Machining Using Orthogonal Tests". Journal of Material Processing Technology, PP. 153-154, & 1019-1025.

[4]. Yen, Y. C., Sohner J., Weule H., Schmidt J. and Altan T. (2003)Estimation of Tool Wear of Carbide Tool in Orthogonal Cutting using Finite Element Method Simulation, Machining Science and Technology, Vol. 6, PP. 467-486.

[5].Maranhao C. and Davim J. P. (2011). "The Role Of Flow Stress And Friction Coefficient In Fem Analysis Of Machining: A Review". Rev.Adv. Mater. Sci. 30 (2012) 184-188

[6]. Outeiro, J. C., Pina, J. C., M'saoubi, R., Pusauec, .F and Jawahir, I.S. (2008) Analysis Of Residual Stresses Induced by Dry Turning of Difficult-To-Machine Materials. CIRP Annals – Manufacturing Technology, Vol. 57, Pp. 77-80.

[7]. Altan, T. and Semiatim (2012) Measurement and Interpretation of Flow Stress Data for the Simulation of Metal-Forming Processes. Air Force Research Laboratory, Materials and Manufacturing Directorate, Ohio. The Ohio State University Columbus, Oh.

[8]. Grzesik and Wanat (2006) Influence of Tool Wear on Surface Roughness in Hard Turning using different Shaped Ceramic Tools Wear, Vol. 265, PP. 327-335.

[9]. Chou, K. Y., Evans, J. C. and Barash, M. M. (2002) Experimental Investigation on CBN Turning of Hardened AISI 52100 Steel. Journal of Materials Processing Technology, Vol.124, PP. 274-283.

[10]. Benga, G. C and Abrao, A. M. (2013)Turning of Hardened 100 Cr 6 Bearing Steel with Ceramic and PCBN Cutting Tools. Journal of Materials Processing Technology, Vol.143-144, PP. 237-241.

[11]. Collins Eruogun Etin-osa and Joseph Ifeanyi Achebo. (2017). Analysis of Optimum Butt Welded Joint for Mild Steel Components Using FEM (ANSYS). American Journal of Naval Architecture and Marine Engineering DOI: 10.11648/j.aas.20170206.12

[12]. Sharma, A.V.N.I., Raji, Satyanarayana, Gopichand, A. and Subbaiah, K.V (2012) Optimization of cutting parameters on mild steel with HSS and Cemented Carbide tipped tools using ANN. International journal of Research in Engineering and Technology. ISSN2319-1163, Vol. 1, PP.1-4.

[13]. Ozel, Trugrul, And Taylan, Altan. (2000) Determination of Work Piece Flow Stress and Friction at the Chip-Tool Contact for High-Speed Cutting. International Journal of Machine Tools and Manufacture, Vol. 40, PP. 133-152.

# Design Equation for Operating Frequency of Patch Antenna with a Rectangular Tuning Stub at Early Phase 5G Bands

*[1]Barış Gürcan Hakanoğlu, [2]Şekip Esat Hayber, [3]Mustafa Türkmen
[1]Kırşehir Ahi Evran University, Department of Electronics and Automation, 40300, Kaman, Kırşehir,
bghakanoglu@ahievran.edu.tr, 🆔
[2]Kırşehir Ahi Evran University, Department of Electrical and Electronics Engineering, 40100, Bağbaşı, Kırşehir,
sehayber@ahievran.edu.tr, 🆔
[3]Erciyes University, Department of Electrical and Electronics Engineering, 38039, Talas, Kayseri,
turkmen@erciyes.edu.tr, 🆔

**Abstract**

In this paper, microstrip patch antennas with rectangular tuning stubs are analyzed, and variations of the resonant frequency depending on the dimensions of the stub have been studied. According to these variations, a design equation has also been proposed for the antennas. The operating frequencies are selected from the early phase 5G bands (700, 2300, 3500, and 4700 MHz), but the equation validity is tested for additional frequencies as 6500 MHz and 8500 MHz which are randomly selected. To identify the material effects, analyses are conducted for two different dielectrics, FR4 and Rogers RT/Duroid 5880. The calculations have been performed for twelve different reference antennas and twelve stub-placed modified antennas. It has been shown that the patch antennas with rectangular tuning stubs pave the way to tune the antenna resonance up to 7.5%-27.6% of its reference design frequency. For example, the proposed structure designed for 700 MHz can shift the resonant frequency up to 511.5 MHz for FR4 and 507 MHz for Rogers RT/Duroid 5880. Moreover, the shifting in frequency at 8500 MHz can reach 7950 MHz for FR4 and 7865 MHz for Rogers RT/Duroid 5880 with reasonable $S_{11}$ levels.

***Keywords:*** Microstrip Antenna, Rectangular Patch Antenna, Early 5G, Tuning Stub, Design Equation.

## 1. INTRODUCTION

Microstrip patch antennas have many advantages, such as being lightweight, cost-effective, and having compatible dimensions with various surfaces, circuits, and devices. However, the major shortcoming of such antennas is their limited bandwidth which makes the input impedance very fragile to fabrication errors and dielectric material tolerances. So, causing changes in the effective length of the patch, manual tuning can adjust the operating frequency. It has been shown that the resonant frequency of a patch antenna can be fine-tuned by placing a tuning stub on one edge of the antenna with the tuning range dependent on the length and the width of the stub [1]. Tunable frequency microstrip antennas can also be realized using RF microelectromechanical systems (MEMS) technology [2]. Tuning and miniaturizing can be performed simultaneously by etching slots in the patch and using thin posts placed near the edge [3]. Besides, it has been demonstrated that a microstrip patch antenna can be tuned on a liquid crystal substrate using a DC bias. The simulated and measured tuning ranges have been found at 8% and 4%, respectively [4]. A microstrip patch antenna on a tunable electromagnetic

band-gap (EBG) structure is proposed with the feature of performing the tuning through a diode-loaded EBG substrate [5]. Another application area for tuning stubs is to obtain triple frequency operation and circular polarization [6, 7]. Moreover, stubs are proposed to enhance the patch's bandwidth and make the whole structure more compact [8, 9].

The motivation for the design frequencies of the antennas in this paper is the early phase 5G bands. Three regions, such as the low range up to 3 GHz, mid-range between 3 GHz-6 GHz, and the high range above 6 GHz, are studied [10]. These bands are still under consideration for some countries, but some have already completed the frequency assignments. Many countries in Europe decided to utilize the 3400-3800 MHz range for the early phase of 5G. The United States launches out 3550-3700 MHz band for a new Citizens Broadband Radio Service to accommodate various commercial services on a shared basis. As a different part of the spectrum, the 4400-5000 MHz band is concerned by Japan and China. Japan has assigned 4400-4900 MHz band for 5G trials, and China defined 4800-5000 MHz band for 5G [11]. Besides, the 2300 MHz band is also released to be

*[1]Corresponding author: Kırşehir Ahi Evran University, Department of Electronics and Automation, 40300, Kırşehir, Turkey
bghakanoglu@ahievran.edu.tr

a candidate for 5G communication in Sweden and United Kingdom [12]. Moreover, the Radio Spectrum Policy Group of the European Commission reveals that the 700 MHz band also needs to be operated in practice to make possible nationwide and indoor 5G coverage [13].

This study performs a detailed parametric analysis of the rectangular tuning stub (RTS) effect on the resonant frequency of microstrip patch antenna (MPA) and formulates a design equation. Microstrip patch antenna with rectangular tuning stub will be called MPA-RTS throughout the paper. RTS is placed on the top edge of the patch. The variations of stub edge dimensions result in different ways on the resonant frequencies and reflection coefficient levels. While the width of the stub variation causes a slight shift in resonant frequency and not so much change in reflection coefficient levels, the length of the stub variation produces a significant change in frequency shifting and reflection coefficient levels.

Moreover, the amount of frequency shifting varies according to the operating band. While an MPA-RTS is operating at 700 MHz shifts the resonant frequency up to 511.5 MHz for FR4 and 507 MHz for Rogers RT/Duroid 5880, an 8500 MHz operating MPA-RTS shifts the resonant frequency up to 7950 MHz for FR4 and 7865 MHz for Rogers RT/Duroid 5880 with reasonable return loss levels.
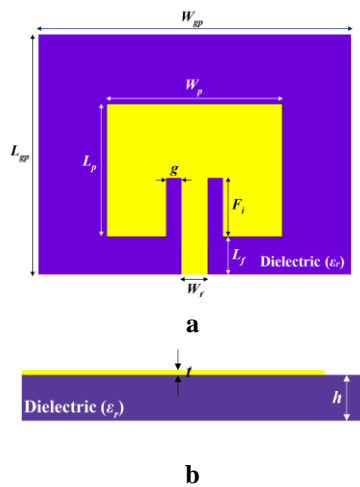
## 2. DESIGN



**Figure 1. a.** Top view of MPA **b.** Side view of MPA.

The reference antennas are designed for early phase 5G and frequencies outside the 5G bands using the proposed Equations 1-4 derived from the patch antenna's transmission line model [14]. Also, to observe the material effects, two different dielectrics with different heights are used for the

substrates, FR4 and Rogers RT/Duroid 5880, with the permittivity, $\varepsilon_r$ of 4.4 and 2.2, respectively. The heights of the substrates are 1.5 mm for FR4 and 0.787 mm for RT5880. Figure 1a shows the top view of an example design for the antenna, and Figure 1b shows the side view of the structure. All antennas are designed with the same procedure. First, with Equation 1, the width of the patch, $W_p$ is calculated based on the following parameters: $f_r$, $\varepsilon_r$, and $h$, where $f_r$ is the resonant frequency, $\varepsilon_r$ is the relative permittivity, and $h$ is the substrate height. After that, Equation 2 enables us to obtain the effective permittivity, $\varepsilon_{reff,}$ which should be known to calculate the length extension, $\Delta L_p$ due to the fringing field with the condition of $W_p/h{>}1$ (Equation 3). Finally, with Equation 4, the patch length, $L_{p,}$ can be calculated.

$$W_p = \frac{v_0}{2f_r}\sqrt{\frac{2}{\varepsilon_r + 1}} \qquad (1)$$

$$\varepsilon_{eff} = \frac{\varepsilon_r + 1}{2} + \frac{\varepsilon_r - 1}{2}\left(1 + 12\frac{h}{W_p}\right)^{-\frac{1}{2}} \qquad (2)$$

$$\frac{\Delta L_p}{h} = 0.412\frac{\left(\varepsilon_{eff} + 0.3\right)\left(\frac{W_p}{h} + 0.264\right)}{\left(\varepsilon_{eff} - 0.258\right)\left(\frac{W_p}{h} + 0.8\right)} \qquad (3)$$

$$L_p = \frac{v_0}{2f_r\sqrt{\varepsilon_{eff}}} - 2\Delta L_p \qquad (4)$$

There are no specific rules for the dielectric substrate dimensions. It is recommended that the length of the substrate, $L_{gp,}$ and the width of the substrate, $W_{gp,}$ should be greater than $6h+L_p$ and $6h+W_p$, respectively [15]. We performed a parametric analysis and an optimization about the edge dimensions of the substrate and took the values at which we obtain the reasonable $S_{11}$ levels. The radiating part is modeled as a lossy conductor, and its thickness, $t$, is set to 0.035 mm (Figure 1b). The feeding is performed through a microstrip feed line with a width of $W_f$ and the length of $L_f$ together with an inset feeding part with the dimensions of the length $F_i$ and the width $g$. For each design, $W_f$ is taken as 3 mm for fabrication and impedance matching conditions for 50 ohms SMA (SubMiniature version A) connector. Due to the same reason, the width of the inset feeding, $g$, is calculated together with $W_f$, $h$, and $\varepsilon_r$ to match 50 ohms. The length of inset feeding, $F_i$, is obtained through parametric analyses until we have the lowest $S_{11}$ levels. The optimized parameters of the MPAs are summarized in Tables 1 and 2.

**Table 1.** The optimized parameters of the MPAs for FR4 ($\varepsilon_r$=4.4), $h$=1.5 mm.

| Parameters (mm) | Frequency (GHz) | | | | | |
|---|---|---|---|---|---|---|
| | 0.7 | 2.3 | 3.5 | 4.7 | 6.5 | 8.5 |
| $W_{gp}$ | 233.66 | 71.81 | 47.46 | 34.81 | 25.83 | 19.85 |
| $L_{gp}$ | 182.90 | 55.75 | 36.57 | 26.80 | 19.49 | 14.75 |
| $W_p$ | 130.32 | 39.66 | 26.06 | 19.41 | 14.03 | 10.73 |
| $L_p$ | 101.95 | 30.76 | 20.02 | 14.74 | 10.44 | 7.78 |
| $F_i$ | 35.30 | 11.70 | 8.20 | 6.40 | 4.60 | 3.50 |
| $g$ | 0.68 | 0.21 | 0.14 | 0.11 | 0.08 | 0.06 |
| $L_f$ | 38.89 | 11.84 | 7.78 | 5.79 | 4.19 | 3.20 |
| $W_f$ | 3.00 | 3.00 | 3.00 | 3.00 | 3.00 | 3.00 |

**Table 2.** The optimized parameters of the MPAs for Rogers RT/Duroid 5880 ($\varepsilon_r$=2.2), $h$=0.787 mm.

| Parameters (mm) | Frequency (GHz) | | | | | |
|---|---|---|---|---|---|---|
| | 0.7 | 2.3 | 3.5 | 4.7 | 6.5 | 8.5 |
| $W_{gp}$ | 314.19 | 95.95 | 63.20 | 47.16 | 34.19 | 26.22 |
| $L_{gp}$ | 255.41 | 77.65 | 50.96 | 37.88 | 27.31 | 20.79 |
| $W_p$ | 169.05 | 51.52 | 33.86 | 25.21 | 18.23 | 13.94 |
| $L_p$ | 144.07 | 43.60 | 28.51 | 21.12 | 15.14 | 11.45 |
| $F_i$ | 35.30 | 16.20 | 11.10 | 8.60 | 6.20 | 4.80 |
| $g$ | 0.95 | 0.29 | 0.19 | 0.14 | 0.11 | 0.08 |
| $L_f$ | 38.89 | 11.83 | 7.78 | 5.79 | 4.19 | 3.20 |
| $W_f$ | 3.00 | 3.00 | 3.00 | 3.00 | 3.00 | 3.00 |

According to the above results, reference antennas are modeled using Computer Simulation Technology Microwave Studio (CST MWS) [16]. To tune the resonant frequency, an RTS has been placed on the top edge of the patch with the dimensions of $L_{RTS}$ for the length and $W_{RTS}$ for the width. Figure 2 shows an example model for MPA-RTS. This figure shows that with the help of the RTS, it is possible to design antennas occupying less room. The dimensions of the RTS affect the resonant frequency and reflection

coefficient levels of the antennas. So, a detailed parametric analysis should be performed about $L_{RTS}$ and $W_{RTS}$.
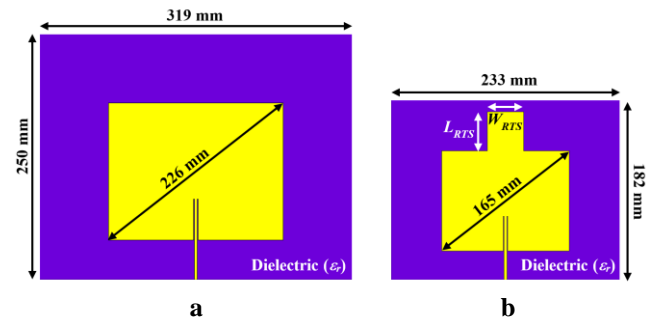


**Figure 2.** MPAs operating at 511.5 MHz **a.** without RTS b. with RTS.

## 3. RESULTS AND DISCUSSIONS

The effects of the variation of the stub parameters on the resonance frequency, $f_r$, and reflection coefficient parameters, $S_{11}$, are investigated using time-domain analysis for wideband or multiband antennas in CST MWS based on finite integration technique (FIT). For the study, FR4 material is preferred for dielectric substrate, and the results are also confirmed for a different dielectric material such as Rogers RT/Duroid5880. Other sized antennas are selected at quite different frequency values in addition to 5G frequencies. Thus, the obtained approximate model is valid for a wide range.

### 3.1. Effect of RTS parameters

MPA-RTS structures are obtained by adding RTSs to MPAs operating at early phase 5G frequencies such as 700, 2300, 3500, 4700 MHz. In addition to these frequencies, antennas are also analyzed at 6500 and 8500 MHz to confirm the validity of the obtained equation. In each case, the parametric analysis starts with $W_{RTS} \times L_{RTS} = 0.5$ mm×0.5 mm until they reach at the near endpoints of the patch for $W_{RTS}$ and of the substrate for the $L_{RTS}$. The variation path along the $L_{RTS}$ can be called dielectric substrate distance (DSD). 0.5 mm is chosen as the step size for both parameters of RTS. The results of the FIT-based time-domain analysis for wideband or multiband antennas in CST MWS obtained from 4700 MHz are shown in Figure 3 as an example. All of the results obtained for the other frequencies examined in this study have similar characteristics to those for 4700 MHz which will be shown in the next section as an approach for the MPA-RTS.
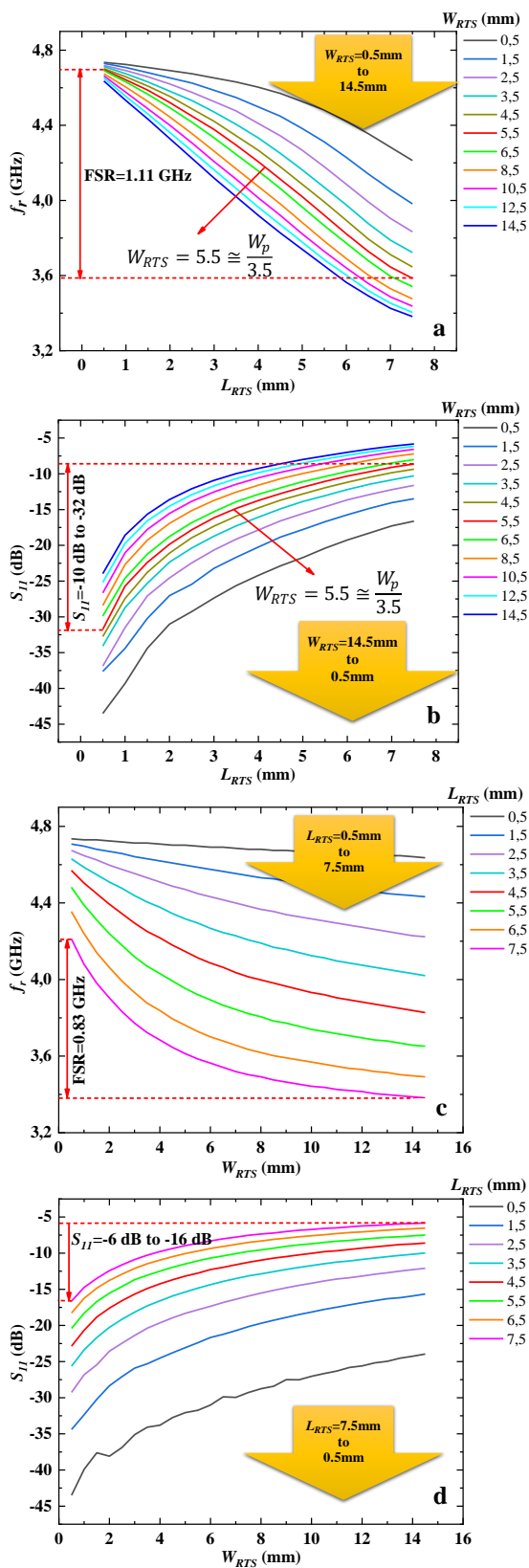
**Figure 3.** The effect of RTS parameters on the operating frequency and $S_{11}$ of the MPA-RTS **a.** fr versus $L_{RTS}$ **b.** $S_{11}$ versus $L_{RTS}$ **c.** $f_r$ versus $W_{RTS}$ **d.** $S_{11}$ versus $W_{RTS}$

Figure 3a-3d shows the variation of resonance frequencies and related $S_{11}$ parameters when $L_{RTS}$ and $W_{RTS}$ change simultaneously along the dielectric and the width of the patch, respectively. It can be seen from Figure 3a that the increase of $L_{RTS}$ and $W_{RTS}$ result in shifting the resonances downwards, beginning from 4700 MHz at which the antenna was initially designed. The frequency shifting range called FSR is 1110 MHz from 4700 MHz to 3590 MHz in Figure 3a, where the $S_{11}$ levels are acceptable. Figure 3b shows that when $W_{RTS}$ decreases, $S_{11}$ levels increase in a negative direction up to -32 dB, which is desirable for these parameters. However, $S_{11}$ levels are not at desired levels for all $W_{RTS}$ values. From Figure 3a and Figure 3b, we should find a particular value for $W_{RTS}$ at which we get a wide shifting range of frequencies and reasonable $S_{11}$ levels at the same time. From the plots, this optimal value is reached at the point when $W_{RTS}$=5.5mm or 1/3.5 of $W_p$, which can also be expressed as follows,

$$W_{RTS} = W_p/3.5 \qquad (5)$$

Figure 3c and Figure 3d show that the effect of $W_{RTS}$ on the frequency and $S_{11}$ parameters for different $L_{RTS}$ values. However, both the amount of change in FSR and the values of $S_{11}$ are not at desired levels. Hence, we can say that the main effect on resonance is due to $L_{RTS}$. As a result, by placing RTS, microstrip antennas will operate at different frequencies according to variations of the length of the stub.

The effects of the variation of $L_{RTS}$ on the frequency are given in Figure 4 by taking the $W_{RTS}$ as constant for the antenna at each frequency as in Equation 5. Here, the limit value of $L_{RTS}$ is the size of the dielectric substrate. Analyzes were performed for more values by decreasing the operating frequency and thus increasing the antenna dimensions. In Figure 4, while the solid purple line shows the $L_{RTS}$ - frequency change for the FR4 substrate, the light blue solid line shows the $L_{RTS}$ - frequency change for the RT5880 substrate. The change of the reflection coefficient parameters of the antenna with the increase of $L_{RTS}$ is given in the graphs as inset figures. Thus, it can be seen in which values the reflection coefficient parameters fall below -10dB due to the frequency effect of $L_{RTS}$. Then, an equation is formed with these parametric analysis results, which is explained in Section 3.2.

### 3.2. An Approach for Patch Antenna with RTS

A mathematical approach that does not require multiple simulation processes is developed in this section. When the condition of $W_{RTS}=W_p/3.5$ is met, $f_{RTS} \, \alpha \, \exp(-0.7L_{RTS}/W_p)$ can be derived. So, design simplicity is established. Equation 6 shows the expressions for the operating frequency of the regression analysis ($R^2$=0.98) on the time domain analysis for wideband or multiband antennas in CST MWS. It can also be calculated with this equation the results with different $W_p$, $L_{RTS}$, and $\varepsilon_r$ values from the MPA-RTS structures satisfying the condition $W_{RTS}=W_p/3.5$.

$$f_{RTS} = \frac{v_0}{2W_p}\sqrt{\frac{2}{\varepsilon_r + 1}} \times e^{-\left(\frac{0.7L_{RTS}}{W_p}\right)}$$

$$= f_r \times e^{-\left(\frac{0.7L_{RTS}}{W_p}\right)} \tag{6}$$

The lower limit of Equation 6 approaches Equation 1, which is valid for conventional MPAs. The lower limit is expressed as follows:

$$\lim_{L_{RTS}\to 0} f_{RTS} = f_r \tag{7}$$

Similarly, the upper boundary condition of Equation 6 tends to reduce the resonance frequency of the antenna by about 24%.

$$\lim_{L_{RTS}\to(\text{DSD})} f_{RTS} \cong 0.76 \times f_r \tag{8}$$

Moreover, percentage error values are shown in Figure 5. Percentage error values differ according to the frequency values and substrate material. In this context, according to the graphs for $f_r$=700 MHz, 2300 MHz, 3500 MHz, and 4700 MHz, the percentage error values for RT5880 are slightly higher than for FR4 in general. Similarly, according to the graphs for 6500 MHz and 8500 MHz, it was seen that the percentage error value in FR4 is higher than in RT5880. In other words, the performance of Equation 6 is better for antennas built with RT5880 at high frequencies. It can be concluded that the error values average is 2% for the first

four frequency values, and the highest value rises to 4.5% in a very narrow region. Moreover, the average error value for 6500 MHz is 2.87%, which is 3.76% for 8500 MHz. Considering all frequencies and two types of substrate materials, the most common percentage error average was calculated as 2.44%.

**Table 3.** Comparison of similar studies in the literature with the current study.

|  | Structure | Frequency GHz | Tuning Range | Formed Equation |
|---|---|---|---|---|
| [1] | Rectangular patch antenna with rectangular tuning stubs | 2.95 | 3.33% | No |
| [17] | Circular patch antenna with rectangular tuning stubs | 1.695 | 9% | No |
| [18] | Tunable stacked patch PIFA | 0.745 | 10% | No |
| This work | Rectangular patch antenna with a rectangular tuning stub | 0.7 | 27% | Yes |
|  | Rectangular patch antenna with a rectangular tuning stub | 3.5 | 17% | Yes |
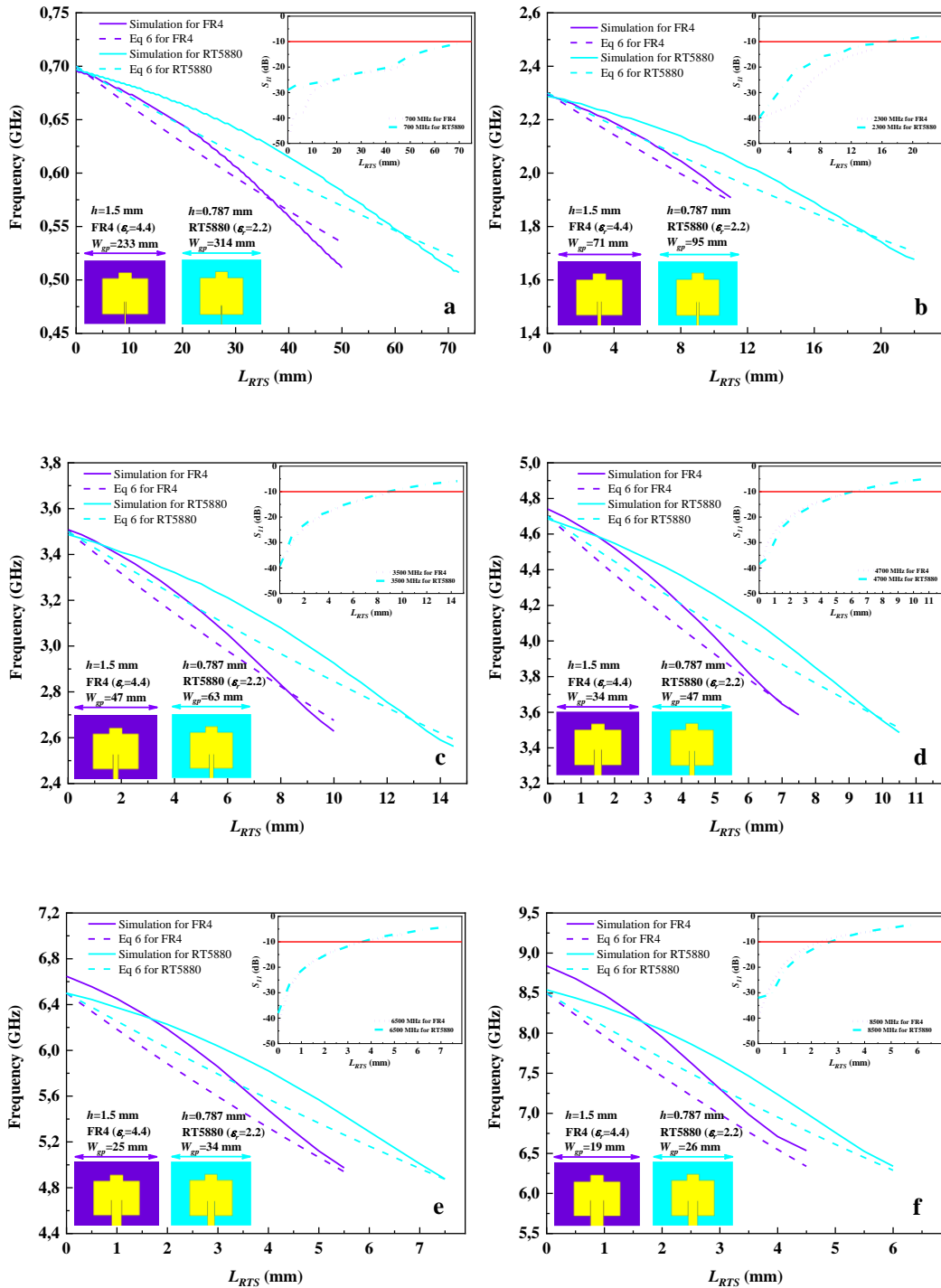
**Figure 4.** Comparisons of operating frequencies of MPA-RTSs with simulation and Equation 6 (Eq 6) for FR4 and Rogers RT/Duroid 5880 **a.** $f_r$=700 MHz **b.** $f_r$=2300 MHz **c.** $f_r$=3500 MHz **d.** $f_r$=4700 MHz **e.** $f_r$=6500 MHz **f.** $f_r$=8500 MHz effect of RTS parameters on the operating frequency and $S_{11}$ of the MPA-RTS **a.** $f_r$ versus $L_{RTS}$ **b.** $S_{11}$ versus $L_{RTS}$ **c.** $f_r$ versus $W_{RTS}$ **d.** $S_{11}$ versus $W_{RTS}$.
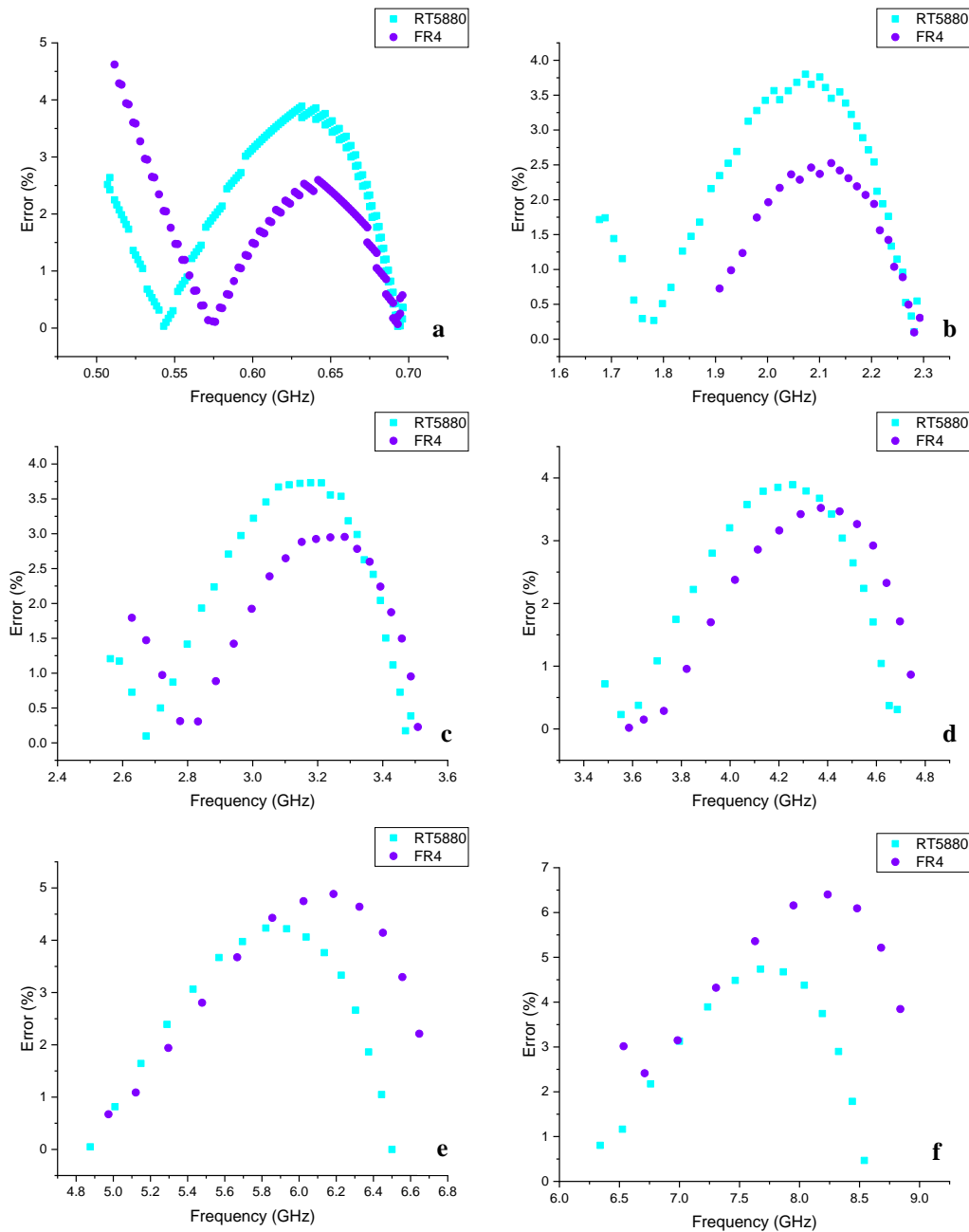
**Figure 5.** Percentage error values according to the simulation results of the developed formula for different frequencies, **a.** $f_r$=700 MHz **b.** $f_r$=2300 MHz **c.** $f_r$=3500 MHz **d.** $f_r$=4700 MHz **e.** $f_r$=6500 MHz **f.** $f_r$=8500 MHz.

There are microstrip antennas with tuning stubs in the literature. The comparison of some of these with our study is given in Table 3. The general purpose of adding tuning stubs, as is known, is to adjust the antenna around a specific operating frequency. The typical features of the compared studies are that they have more complex geometries and require time-consuming simulations for each size variation. However, in this study, both the adjustment range has been extended, and an analytical model has been developed that gives approximately 2% accurate results. Thus, there is no

need for repeated long simulation processes for each geometric value.

## 4. CONCLUSIONS

Patch antennas with rectangular tuning stubs operating at early phase 5G bands are designed and simulated. The effects on the radiation characteristics are analyzed by performing a multi-parameter analysis. It has been shown that the edge dimension variations of the stub directly affect the resonant frequency of the antenna and reflection coefficient levels. Also, for an optimal value of the stub width, the frequency shift amount and reflection coefficient levels are reasonable,

1/3.5 of the patch width. After performing a detailed parametric analysis for the stub length, a design equation is proposed. This equation relates the antenna's resonant frequency to the stub length, with the condition of stub width having a definite optimal value.

## REFERENCES

[1]. Du Plessis, M., and John Cloete. "Tuning stubs for microstrip-patch antennas." IEEE Antennas and Propagation magazine 36.6 (1994): 52-56.

[2]. Erdil, Emre, et al. "Frequency tunable microstrip patch antenna using RF MEMS technology." IEEE transactions on antennas and propagation 55.4 (2007): 1193-1196.

[3]. Sheta, Abdel-Fattah, and Samir F. Mahmoud. "A widely tunable compact patch antenna." IEEE Antennas and Wireless Propagation Letters 7 (2008): 40-42.

[4]. Liu, L., and R. J. Langley. "Liquid crystal tunable microstrip patch antenna." Electronics Letters 44.20 (2008): 1179-1180.

[5]. Liang, Jing, and HY David Yang. "Microstrip patch antennas on tunable electromagnetic band-gap substrates." IEEE transactions on antennas and propagation 57.6 (2009): 1612-1617.

[6]. Sung, Y. "Axial Ratio-Tuned Circularly Polarized Square Patch Antenna with Long Stubs." International Journal of Antennas and Propagation 2018 (2018).

[7]. Hasan, Wanis Alfitouri, et al. "Design and fabrication of triple frequency microstrip patch antenna by attaching tuning stub element." 2016 10th International Conference on Telecommunication Systems Services and Applications (TSSA). IEEE, 2016.

[8]. Arya, Ashwini K., Rao Shahid Aziz, and Seong-Ook Park. "Planar ultra-wideband printed wide-slot antenna using fork-like tuning stub." Electronics Letters 51.7 (2015): 550-551.

[9]. Bokhari, S. A., et al. "A small microstrip patch antenna with a convenient tuning option." IEEE Transactions on antennas and Propagation 44.11 (1996): 1521-1528.

[10]. 5G Americas, (2017). 5G Spectrum Recommendations. https://www.5gamericas.org/wp-content/uploads/2019/07/5 GA_5G_Spectrum_Recommendations_2017_FINAL.pdf (Accessed: 02.01.2020).

[11]. Lee, Juho, et al. "Spectrum for 5G: Global status, challenges, and enabling technologies." IEEE Communications Magazine 56.3 (2018): 12-18.

[12]. Global Mobile Suppliers Association, (2018). Spectrum for Terrestrial 5G Networks: Licensing Developments Worldwide. https://gsacom.com/paper/5g-spectrum-terrestrial-networks/ (Accessed:02.01.2020).

[13]. RSPG19-036 FINAL, Strategic Roadmap Towards 5G For Europe, Radio Spectrum Policy Group of European Commission, Brussels, 2019.

[14]. Balanis, Constantine A. "Antenna Theory Analysis And Design', New Jersey John Willey & Sons." Inc, Publication (2005).

[15]. Joler, Miroslav, and Josko Kucan. "Impact of Slot Parameters on the Three Resonant Frequencies of a Rectangular Microstrip Antenna: Study of the impact of the slot length, width, and position." IEEE Antennas and Propagation Magazine 57.4 (2015): 48-63.

[16]. Computer Simulation Technology (CST) Microwave Studio, Framingham, MA, USA, 2017.

[17]. Ray, K. P., and Kumar, G. "Tuneable and dual-band circular microstrip antenna with stubs." IEEE transactions on antennas and propagation, 48(7), 1036-1039, (2000).

[18]. Karmakar, N. C., "Shorting strap tunable stacked patch PIFA." IEEE Transactions on Antennas and Propagation, 52(11), 2877-2884, (2004).

**Academic Platform Journal of Engineering and Science**

# Gasification of Forest Residues for Sustainable Development in the Mediterranean Region of Turkey

*[1]Zuhal Akyürek, [2]Afşin Güngör

[1]Burdur Mehmet Akif Ersoy University, Faculty of Engineering and Architecture, Department of Energy Systems Engineering, Istiklal Campus,15030, Burdur, Turkey, drzuhalakyurek@gmail.com, (iD)
[2]Akdeniz University, Faculty of Engineering, Department of Mechanical Engineering, 07070, Antalya, Turkey, afsingungor@hotmail.com, (iD)

## Abstract

In this study, the energy generation potential of forest residues in the Mediterranean Region of Turkey are determined by using different gasifier technologies. Gasification is one of the conventional waste to energy conversion technologies for energy production. Syngas, the end product of gasification process, is generally used in internal combustion engines, turbines and boilers as a renewable fuel. Energy potential of forest residues in Mediterranean Region of Turkey was estimated in up-draft fixed bed gasifier, down-draft fixed bed gasifier and circulating fluidized bed gasification systems. The theoretical results revealed that, among the alternatives, down-draft gasifier has shown the highest annual energy production potential of 1125 GWh. The results revealed that forest residues can be utilized as significant renewable energy source in Turkey.

*Keywords:* Gasification; Forest Residues; Renewable Energy; Waste Management; Turkey

## 1. INTRODUCTION

Energy is the key driver of sustainable development. The rapid growth in population, technology and industrial development have triggered the global energy demand in the past decades. This continuously increasing energy demand have resulted in environmental pollution due to emission of greenhouse gases from fossil resources [1]. Renewable energy is a vital instrument to mitigate climate change [2,3]. Biomass is considered as one of the viable options for renewable energy production to reduce the adverse effects of fossil fuel combustion and for overcoming the severe environmental damage [3-6].

Biomass is a readily available, affordable and clean energy supply that can be derived from a variety of waste materials including forestry residues, agricultural crops, agro-industrial and Municipal Solid Waste (MSW) with different moisture content and chemical composition [7]. Energy from biomass has a major advantage of being stored and transformed into heat and electricity, unlike the other renewable sources. Utilization of biomass provides recovering energy from waste materials and protecting environment from anthropogenic emissions [8]. In the view of these issues, valorization of bio-waste by means of renewable energy production gains more importance for a sustainable environment.

Combustion, pyrolysis and gasification are three main thermochemical conversion technologies for production of energy from solid fuels. The gasification process plays an important role in terms of the opportunity to convert waste into a clean and usable form of energy under thermal conditions. In gasification, thermal oxidation of biomass is carried out in a medium with lower amount of oxygen than what is required for stoichiometric combustion, in the temperature range of 800-1000 °C to produce highly flammable gas composed mainly of methane, hydrogen, oxygen, carbon dioxide and nitrogen [9-13]. Compared to other conventional technologies such as combustion and pyrolysis, gasification can provide greater energy recovery, heat capacity and better conversion efficiency, etc. [14].

Operational parameters and biomass characteristics such as moisture content of fuel, gasifying agent, equivalence ratio, gasifier temperature, particle size and shape of biomass, etc. have strong influence on the gasification efficiency [15]. Air, oxygen and/or steam are used as gasifying agents in gasification process. Several studies have carried out on biomass gasification with different gasifying agents, temperatures and gasifiers [16-19]. Air is more widely used as gasifying agent compared to other alternative agents such as steam, air/steam, oxygen hence due to its economical and operationally advantageous feature [20]. Syngas quality depends on its heating value and tar content. Higher the

heating value and lower the tar content results in higher quality [21].

Gasification is a practical route for energy production from woody fuels. Hanaoka et al. [22] studied the effect of woody biomass components on air-steam gasification using the downdraft fixed-bed gasifier and suggest that data obtained in gasification process could possibly be used to predict the composition of product gas generated in air-steam gasification of woody biomass. Kim et al. [23] investigated air-blown gasification of woody biomass in a pilot-scale bubbling fluidized bed gasifier. The composition of the syngas was significantly affected by equivalence ratio. They obtained syngas with adequate heating value for power generation using a syngas engine. Safarian et al. [24] developed an equilibrium simulation model was to evaluate the performance of 28 wood and woody biomass gasification in a downdraft gasifier.

High amount of forestry residues in Turkey signify their availability for energy production. In this study, gasification energy potential of forestry residue inventory in Mediterranean Region has been evaluated with different types of gasifiers by using the previously published syngas composition data [15, 19].

## 2. MATERIALS AND METHODS

The Mediterranean Region occupies the southern coast of Turkey, including Antalya, Burdur, Isparta, Mersin, Adana, Hatay, Osmaniye and Kahramanmaraş provinces. The climate of the region is characterized by rainy and cool winters, and dry and hot summers at the coastal parts and cold, snowy winters and dry and hot summers in the interior parts. The region has total land area of 8,943,734 ha where forestry land occupies 4,181,174 ha [25]. The distribution of forestry areas in the region is demonstrated in Figure 1.
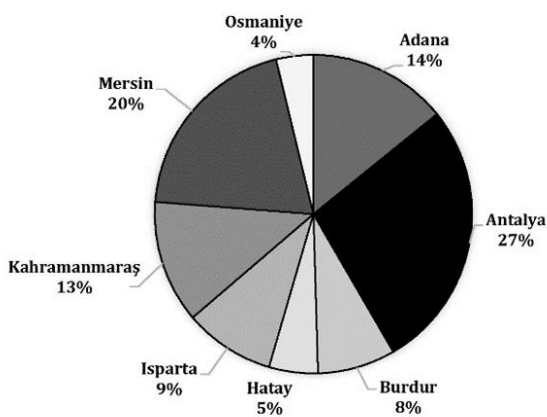


**Figure 1.** Distribution of total forestry areas in the Mediterranean Region

Forest residues generally consist of logging residues and dead wood. High availability of forestry residues in the

Region offers great potential for renewable energy production. Forestry residue production rates in the Region are shown in Table 1. The data has collected from Biomass Map of Turkey (BEPA) [21].

**Table 1.** Forestry residue amount and their tons of oil equivalence in the Mediterranean Region.

| Forest Managing Directorate | Waste Potential (ton/year) | Energy Equivalence (TOE) |
|---|---|---|
| Adana | 315,200.00 | 175,995 |
| Antalya | 88,196.40 | 49,370 |
| Isparta | 2,720 | 1,508 |
| Mersin | 98,520.00 | 54,349 |
| Kahramanmaraş | 15,192.40 | 8,421 |
| **Total** | **519,828.8** | **289,643** |

Biomass gasifiers convert organic solid materials into a gaseous fuel. The specific gas production rate is calculated from the ratio of the syngas flow-rate (in $Nm^3/h$) and the biomass fed to the gasifier (in kg/h) [15]:

$$PR_{Syngas}\left(\frac{Nm^3}{kg}\right) = \frac{Q_{Syngas}}{M_{Biomass}} \qquad (1)$$

The energy value of the syngas can be expressed:

$$E_{Syngas}\left(\frac{MJ}{Nm^3}\right) = \frac{Q_{Syngas}LHV_{Syngas}}{M_{Biomass}LHV_{Biomass}} \qquad (2)$$

Different types of gasifiers have been developed for partial oxidation of the solid waste such as fixed bed downdraft, fixed bed updraft, fluidized bed. Schematic description of the gasifier types used in this study is demonstrated in Figure 2.

As can be seen from the figure, in the updraft gasifiers, the gasifying agents such as air, oxygen and steam enter the system from the bottom part of the gasifier and leaves from the top. This configuration provides counter current interaction of biomass and combustible gases. In updraft gasifier high thermal efficiency can be achieved however, syngas can be contaminated with tar particles when leaving the system, which restricts its application in turbine and engines [26]. Solid fuel enters the system from the top of gasifier and move toward the bottom where it gets oxidized and generate flue gases. In downdraft gasifiers co-current flow of solid fuel and gasifying agent enters from the top of the gasifier and move in downward direction which reduces the tar contamination of syngas. Fluidized bed gasifiers have highly fuel flexible configuration. In circulating fluidized beds, biomass circulates within the gasifier and the cyclone separator. In Table 2, typical syngas compositions for different air-gasifiers using wood biomass are presented.
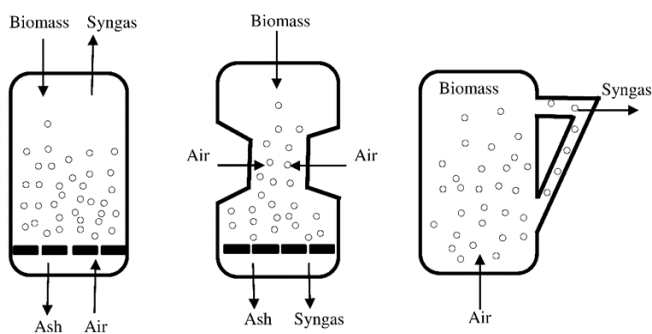
**Figure 2.** Different gasifier configurations (a) updraft, (b) downdraft, (c) circulating fluidized bed (CFB) [7].

**Table 2.** Syngas composition from experimental results of woody biomass gasification using different types of gasifiers [15, 19]

| Gasifier Type | Gas composition (% vol, dry basis) | | | | |
|---|---|---|---|---|---|
| | $H_2$ | CO | $CO_2$ | $CH_4$ | $N_2$ |
| Updraft | 11 | 24 | 9 | 3 | 53 |
| Downdraft | 17 | 21 | 13 | 1 | 48 |
| CFB | 14.1 | 18.7 | 14.7 | 3.5 | 47.7 |

## 3. RESULTS AND DISCUSSION

Biomass gasification systems are used to convert solid biomass into producer gas, which has high calorific value. The efficiency of gasifiers and the composition of the syngas depends on many factors such as operating parameters, gasifying agents and gasifier types. In this study the energy content of the produced syngas from forestry residues are calculated by using the results of experimental studies that are performed in different gasifier configurations such as updraft fixed bed, downdraft fixed bed and circulating fluidized bed gasifiers [7]. The estimated syngas composition of the biomass residues is shown in Figure 3.
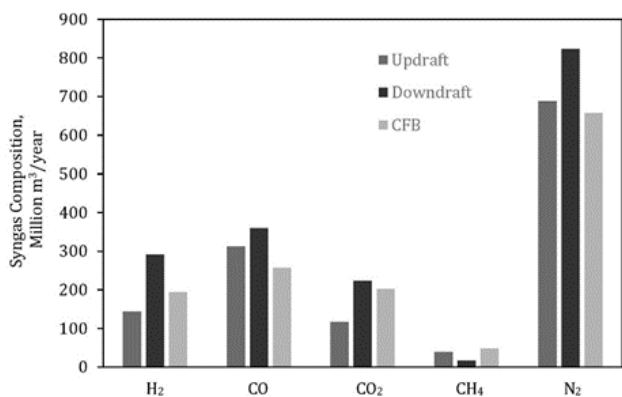


**Figure 3.** Production rate of syngas components from updraft, downdraft and CFB systems

As can be seen from the figure downdraft gasifier has shown to have higher hydrogen, carbon monoxide, carbon dioxide

and nitrogen emission indicating higher energy production performance compared to updraft and circulating fluidized bed systems.

Energy generation potential of forestry residues is illustrated in Figure 4.
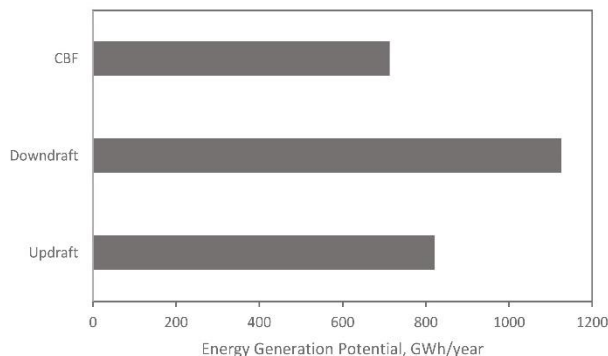


**Figure 4.** Energy potential of forest residues in the Mediterranean Region from updraft, downdraft and CFB systems.

Annual energy generational potential from downdraft gasifier system is obtained as 1125 GWh. Downdraft gasification technology can provide higher potential of energy generation.

## 4. CONCLUSION

Gasification is a proven technology route for conversion of biomass into hydrogen and other combustible products. The gasifier configurations have high influence on the product gas composition. This study evaluated the impact of different gasifiers on energy generation from forestry residues in Mediterranean Region of Turkey based on the previously published experimental data. Comparisons have proved that downdraft gasifier has higher energy production capacity than those of updraft and circulating fluidized bed systems. Mediterranean Region has shown to have 1125 GWh annual thermal energy production potential from downdraft air-gasification of forestry residues.

## REFERENCES

[1]     T.M.L. Winley, "The Paris warming targets: emissions requirements and sea level consequences", Climatic Change, vol. 147, 31-45, 2018.
[2]     M. Richter, "Utilities' Business Models for Renewable Energy: A Review", Renewable and Sustainable Energy Reviews, vol. 16, no. 5, 2483-493, 2012.

[3]     Z. Akyürek, A.Ö. Akyüz, A. Güngör, "Optimizing the Tilt Angle of Solar Panels to Reduce Carbon Footprint: Case for the West Mediterranean Region of Turkey", International Journal of Engineering, Design and Technology, vol. 1, no. 1, 10-15, 2019.

[4]     A. Hegazy, A.O. Ghallab, F.H. Ashour, "Integrated gasification combined cycle using Egyptian Maghara coal–rice straw feedstock", Waste Management and Research, vol. 35, 656–68, 2017.

[5]     A. Vakais, A. Sotiropoulos, K. Moustakas, D. Malamis, M. Baratieri, "Utilisation of biomass gasification by-products for onsite energy production", Waste Management & Research, vol. 34, 564–71, 2017.

[6]     G. Wielgosiński, P. Łechtańska, O. Namiecińska, O. "Emission of some pollutants from biomass combustion in comparison to hard coal combustion", Journal of the Energy Institute, vol. 90, 787-96, 2017.

[7]     Z. Akyürek, A.Ö. Akyüz, A. Güngör, "Energy potential from gasification of agricultural residues in Burdur, Turkey", Techno-Science, vol. 2, no. 1, 15-19, 2019.

[8]     Z. Akyürek, "Potential of biogas energy from animal waste in the Mediterranean Region of Turkey", Journal of Energy Systems, vol. 2, no. 4, 159-167, 2018.

[9]     O. Gohlke, "Efficiency of energy recovery from municipal solid waste and the resultant effect on the greenhouse gas balance", Waste Management and Research, vol. 27, 894- 906, 2009.

[10]     E.J. Lopes, , N. Queiroz, C.I.. Yamamoto, P.R.C. Neto, "Evaluating the emissions from the gasification processing of municipal solid waste followed by combustion", Waste Management, vol. 73, 504-10, 2018.

[11]     K.G. Burra, M.S. Hussein, R.S., Amano, A.K. Gupta, "Syngas evolutionary behavior during chicken manure pyrolysis and air gasification", Applied Energy, vol. 181, 408-15, 2016.

[12]     A. Gungor, M., Ozbayoglu, C. Kasnakoglu, A. Biyikoglu, B.Z. Uysal, "A parametric study on coal gasification for the production of syngas", Chemical Papers, vol 66, 677-683, 2012.

[13]     A. Gungor, U. Yildirim, "Two dimensional numerical computation of a circulating fluidized bed biomass gasifier", Computers & Chemical Engineering, vol 48, 234-50, 2013.

[14]     S.K., Sansaniwal, K. Pal, M.A.. Rosen, S.K. Tyagi, "Recent advances in the development of biomass gasification technology: A comprehensive review", Renewable and Sustainable Energy Reviews, vol. 72, 363-84, 2017.

[15]     M. La Villetta, M., Costa, N. Massarotti, "Modelling approaches to biomass gasification: A review with emphasis on the stoichiometric method", Renewable and Sustainable Energy Reviews, vol 74, 71-88, 2017.

[16]     R.C. Saxena, D. Seal, S Kumar, H.B. Goyal, "Thermo-chemical routes for hydrogen rich gas from biomass: a review", Renewable Sustainable Energy Reviews, vol 12, 1909–27, 2008.

[17]     D. Sutton, B. Kelleher, J.R.H. Ross, "Review of literature on catalysts for biomass gasification", Fuel Process Technology, vol 73, 155–73, 2001.

[18]     Y. Chhiti, M. Kemiha, "Thermal conversion of biomass, pyrolysis and gasification: a review", International Journal of Engineering Science, vol 2, 75–85, 2013.

[19]     N. Couto, A. Rouba, V. Silva, E. Monteiro, K. Bouziane, "Influence of the biomass gasification processes on the final composition of syngas", Energy Procedia, vol 36, 596-606, 2013.

[20]     N. Salami, Z. Skála, "Use of the Steam as Gasifying Agent in Fluidized Bed Gasifier", Chemical and Biochemical Engineering Quarterly, vol. 29, 13-18, 2015.

[21]     BEPA, Biomass Atlas of Turkey, 2019. http://bepa.yegm.gov.tr/ (Accessed 22.07.2020)

[22]     Hanaoka, T., Seiichi, I.S., Ogi, T., Uno, S., Minowa, T. "Effect of woody biomass components on air-steam gasification", Biomass and Bioenergy, vol. 28, 69-76, 2005.

[23]     Kim, Y.D., Yang, C.W., Kim, B.J., Kim, K.S., Lee, J.W., Moon, J.H., Yang, W., Yu, T.U., Lee, U.D., "Air-blown gasification of woody biomass in a bubbling fluidized bed gasifier", Applied Energy, vol. 112, 414-420, 2013.

[24]     Safarian, S., Unnthorsson R., Richter, C., Performance analysis of power generation by wood and woody biomass gasification in a downdraft gasifier, International Journal of Applied Power Engineering, vol. 10(1), 80-88, 2021.

[25]     Republic of Turkey, Ministry of Agriculture and Forestry, General Directorate of Forestry. https://www.ogm.gov.tr/Sayfalar/Ormanlarimiz/Illere-Gore-Orman-Varligi.aspx (Accessed 22.07.2020)

[26]     S.K. Sansaniwala, M.A. Rosen, S.K. Tyagi, "Global challenges in the sustainable development of biomass gasification: An overview", Renewable and Sustainable Energy Reviews, vol 80, 23–43, 2017.

**Academic Platform Journal of Engineering and Science**

*journal homepage: http://apjes.com/*

# Numerical Study on Suspended Sediment Transport under the Effect of Water Temperature in Reservoirs and Lakes

*[1]Redvan Ghasemlounia, [2]Mehmet Sedat Kabdaşlı

*[1]Dept of Civil Eng., Faculty of Engineering, Istanbul Gedik University, Turkey, redvan.ghasemlounia@gedik.edu.tr, (iD)
[2] Faculty of Civil Engineering, Istanbul Technical University, Turkey, kabdaslis@itu.edu.tr, (iD)

## Abstract

Water resources management is one of the most important issues and challenges in the world. This management may be in the form of quality management or quantitative management of water resources. Quality management of water resources is of great importance. A major problem in this case is how the input flow (for example a river) will behave when water flows to a dam reservoir or lake. Distribution of the input stream to the reservoir/lake depends on important parameters such as inflow discharge, input depth, situation and type of the reservoir outlet, type of inlet sediment , sediment concentration of inflow current and reservoir/lake , and etc. Therefore, this effect of each of the mentioned parameters on the distribution in the reservoir or lake should be examined. An important parameter that has not yet been studied is the effect of temperature of the inflow current's and the reservoir/lake's water on the distribution. For this purpose, the FLOW3D computational fluid dynamics code was selected in this study. The effect of water temperature and concentration of suspended sediment on distribution in reservoirs/lakes is considered. Several simulations with different water temperature and suspended sediment concentration values were done. Results are shown and compared each other. The results indicate the high effect of water temperature on distribution of sediments. The rising in water temperature value leads to settling the suspended sediments faster. Therefore, the temperatures of inflow and reservoir water affect the depositing and settling of suspended sediments.

*Keywords:* Reservoirs and lakes, Sediment transport, FLOW3D, Suspended sediment, Water Temperature

## 1. INTRODUCTION

Nowadays, aridness is the main problem for the arid and semi-arid regions. On this basis, the preservation of the water resources has high attention and particular importance. For this reason, policies and patterns of water use have major role. One of these policies is construction of dams. The importance of dam construction in these regions has increased in recent years. Therefore, in these regions, dams are important manmade structures, because they are the only source of water during water shortage seasons. In arid and semi-arid countries, dams are mostly constructed for supplying the drinking water and irrigation. Here, management of these resources plays a major role than the construction of them. So, water resources need a good management in the present century because of these limitations of water resources, especially. For better management of water resources, investigation of all parameters of the hydrologic cycle and climatic characteristics including precipitation, wind, temperature, runoff, evaporation and etc. is required. These natural and climatic characteristics affect the water quality of the water resources, dam reservoirs and lakes. In this study, dam reservoirs and lakes are considered. There are several factors and phenomena that affect the quality of water in

lakes and reservoirs. One of the most important problems that occur in dam reservoirs is sedimentation. There are some problems caused by sedimentation in dam reservoirs such as decreasing of storage volume of the reservoirs after operation. Sedimentation is the main phenomena that lead to dam death. This phenomenon is endangering the life of dams, insensibly and during the time, gradually. Beyond that sedimentation makes project uneconomical; in arid and semi-arid regions, it is important especially due to water shortage. Evaluation of sedimentation and the distribution of sediments in dam reservoir is necessary to increase the efficiency of hydro facilities. One of the other phenomena that affect water quality in reservoirs is named as stratification [1].This phenomenon is a result of the available differences between the input river and lake water's density in terms of temperatures and suspended sediments. In addition to research on stratification and its impacts on water quality, it is important to examine how these layers are formed. Study of stratification phenomena has special significance because of the importance of water quality. Stratification in lakes and dam reservoirs has two forms as: thermal stratification and the stratification that caused by concentration of suspended particles. Each of these phenomena could affect the water quality of reservoirs or lakes, extremely. So, study on these

phenomena is one of the important subjects that should be done in water resources management in reservoirs and lakes, especially. Stratification has important implications for fisheries management, phytoplankton (algae) populations, and water supply quality, generally. Currents have different distribution behavior, when reach to the reservoir/lake based on their density, which is extremely influenced by their water temperature, discharge and suspended sediment concentration. Types of flows according to differences between density of river flow and density of water in reservoir or lake are defined here. When a river flow with the density equal to $\rho_{river}$ comes into the reservoir or lake with density of $\rho_{reservoir/lake}$, it can has one of the following behaviors shown in Figure 1, totally [2, 3].
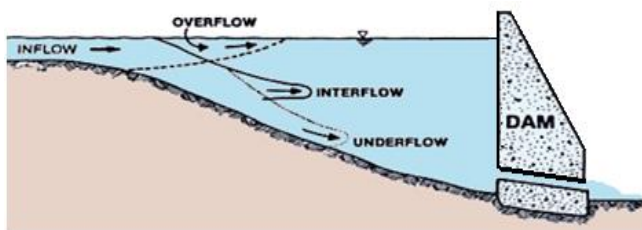


**Figure 1.** Behavior of river water meets reservoir/lake [3].

Over flow, inter flow and under flow also could be named as Hyperpycnal, Hypopycnal, Homopycnal and Hyperpycnal flow, respectively. Numerous studies are available in the case of sediments motion and sediment distribution in reservoirs and lakes due to changes in conditions of inflowing river and reservoir/lake. Several experimental and numerical studies related to the sediment transport are done by many researcher and scientists. But there isn't any study about the effect of the water temperature on distribution and transport of the suspended sediment particles. For example, Milliman (1981) studied on the transfer of river-born particular material to the ocean river inputs to ocean systems [4]. Van Rijn (1984) studied on the suspended sediment transport, and investigated the parameters controlling the suspended load transport [5]. In another research, Williams (1989) studied on the topic titled as sediment concentration versus water discharge during single hydrological events in rivers and investigated the relation between sediment concentration and water discharge [6]. Kostic and Parker (2003) have developed a moving boundary model of deltaic sedimentation in lakes and reservoirs [7]. Salant et al. (2008) concluded the directly relation between suspended sediment concentrations and discharge [8]. Algan et al. (2000) investigated the sediment and freshwater discharges of the Anatolian river into the Black sea [9]. Fang & Wang (2000) worked on a topic entitled three-dimensional mathematical model of suspended-sediment transport [10]. They predicted the deposition of suspended sediment in Yangtze River. United States Sociecty of Dams, Committee on Hydraulics of Dams, Subcommittee on Reservoir Sedimentation (USSD) studied and prepared a report under titled the modeling sediment movement in reservoirs (2015) [11].

Many other researchers found the significance of the effects of thermal stratification on the hydrodynamic mixing, contaminant transport, and water quality of reservoirs and lakes [13, 14, 15, 16, 17]. Dake and Harleman (1969) investigated the analytical and laboratory studies of thermal stratification in lakes [12]. Modiri-Ghareveran et al. (2013) worked on effects of climate change on the thermal regime of a reservoir. They modeled the thermal stratification of Latian dam [18]. Baharim et al. (2011) investigated the effects of thermal stratification on the concentration of iron and manganese in a tropical water supply reservoir [19]. Nazariha et al. (2009, 2010) predicted the thermal stratification in proposed Bakhtiyari reservoir [20]. Nsiri et al. (2016) modeled the thermal stratification and the effect on water quality in four reservoirs in Tunisia [21]. Cossu et al. (2015) investigated the subject under the title of seasonal variability in turbidity currents in Lake Ohau and their influence on sedimentation [22]. Akiyama and Stefan (1984) summarized equations proposed by several investigators for determining the plunge depth [23]. Farrell and Stefan (1986) reported about buoyancy induced plunging flow into reservoirs and coastal regions in a project of Minnesota and studied on mathematical modeling of plunging reservoir flows [24].

Some other researchers studied on effect of water temperature on stratification and sediment transport. the most recent study related this subject is done by Zhong et al. (2020). They worked on impact of cold water mass on suspended sediment transport in the South Yellow Sea [26]. Other recent study was the role of saltwater and waves in continental shelf formation with seaward migrating clinoform, which was done by Iwasaki and Parker in 2020 [27].

Evaluating these literatures and many other studies, it is concluded that there isn't any study about the effect of the water temperature on distribution and transport of the suspended sediment particles. The main use of results of this study is to improve the dam reservoirs or lakes operation. Because it is necessary to predict effects of sediment distribution and loss of storage capacity and its rate for better operation of the reservoirs.

## 2. MATERIAL AND METHOD

Eight scenarios were simulated according to table 2, which will described in section 2.2. Based on these selected scenarios, the temperature range between 4-40 $^o$C . Where, the suspended sediment concentrations were 15 and 20 kg/m$^3$ depending on the selcted simulation. The computational code, which was choosen for this work, the governing equation used by this code and the information about numerical model are explained in sections 2.1 and 2.2.

### 2.1. Governing Equations

A three-dimensional numerical modeling was used in the present study to model the hydrodynamics in reservoirs or lakes. FLOW-3D computational fluid dynamic code was

selected for numerical solutions because of its capabilities and advantages. Continuity, momentum and energy equations are presented as Equation (1), (2) and (3), respectively [25].

$$\frac{\partial \rho}{\partial t} + \frac{\partial}{\partial x}(\rho u) + \frac{\partial}{\partial y}(\rho v) + \frac{\partial}{\partial z}(\rho w) = 0 \tag{1}$$

$$\frac{\partial u}{\partial t} + u. \nabla u = f - \frac{1}{\rho}\nabla P + \upsilon \nabla^2 u \tag{2}$$

$$\frac{\partial \overline{T}}{\partial t} + \overline{u}\frac{\partial \overline{T}}{\partial x} + \overline{v}\frac{\partial \overline{T}}{\partial y} + \overline{w}\frac{\partial \overline{T}}{\partial z} + f\overline{u} = \alpha_{eff}\left(\frac{\partial^2 \overline{T}}{\partial x^2} + \frac{\partial^2 \overline{T}}{\partial y^2} + \frac{\partial^2 \overline{T}}{\partial z^2}\right) \tag{3}$$

Suspended Sediment Transport Equation is an important equation that must be noticed in the case of sediment motion this equation is shown as Equation (4) [25].

$$\frac{\partial c}{\partial t} + u_i\frac{\partial c}{\partial x_i} = \frac{\partial}{\partial x_i}\left(\Gamma\frac{\partial c}{\partial x_i} - \overline{u_i'c'}\right) + S_c \tag{4}$$

In this equation, c is the suspended sediment concentration $\left(\frac{mg}{l}\right)$, $\Gamma$ is the molecular diffusivity coefficient, $S_c$ is the sink or source of c. The term $-\overline{u_i'c'}$ is called the turbulent diffusion of c.

## 2.2. Numerical Model

A reservoir (Figure 2) was designed and defined to FLOW3D, which has an entrance and an outlet. The geometry of reservoir is created using its own modeler (using the Flow 3D GUI and solids modeler). For drawing the geometries, components should be created first. Each model, which created in this study, has a component and 3 subcomponents. FLOW 3D creates subcomponents as solid objects by default, and this is the only option when the subcomponent belongs to a new component. Geometry

of the reservoir has about 390 meters length, 120 meters width and 60 meters depth, when reservoir capacity is completely full.
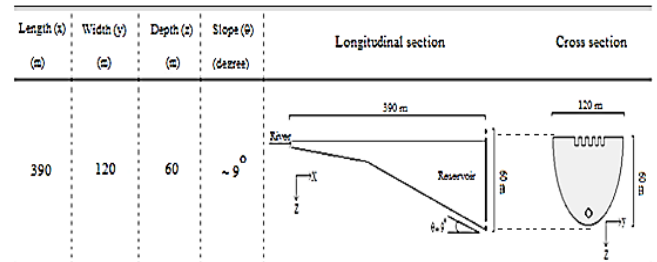


**Figure 2.** The selected dimensions for the models.

Mesh structure of models using for this study consists of four mesh blocks in all simulations. These blocks are Block1, Block2, Block 3 and Block 4, which are represented in Figure 3.
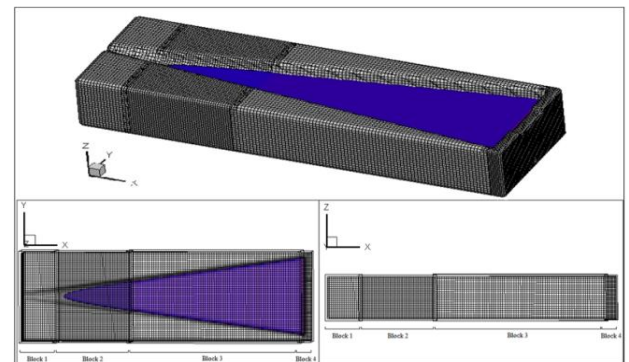


**Figure 3.** Mesh structure of models.

Blocks and grids information of the models are presented in Table 1. The cells in Block 2 and 4 are smaller than the other block. In Block 2, condition is similar to shallow water condition. So, the details are very important in this region. On the other hand, in block 4, a spillway is available. Then, the smaller cells are needed to creation of a good shaped structure of these outlets.

**Table 1.** Mesh and Grid Information of Geometry

| Mesh Block No. | Direction | Total number of real cells | Min. cell size | Max. cell size | Total number of real cells of each block | Total number of real cells in model |
|---|---|---|---|---|---|---|
| I | x | 18 | 2.50 | 2.50 | 17802 | |
| | y | 43 | 2.50 | 2.50 | | |
| | z | 23 | 2.52 | 2.52 | | |
| II | x | 48 | 1.87 | 1.87 | 87552 | |
| | y | 57 | 1.86 | 1.86 | | 201314 |
| | z | 32 | 1.89 | 1.89 | | |
| III | x | 78 | 2.69 | 2.69 | 67080 | |
| | y | 43 | 2.68 | 2.68 | | |
| | z | 20 | 2.65 | 2.65 | | |
| IV | x | 10 | 1.44 | 1.44 | 28880 | |
| | y | 76 | 1.44 | 1.44 | | |
| | z | 38 | 1.43 | 1.43 | | |

$x_{min}$ was selected as the inflow boundary. The defined boundary condition for this point of model was volume

flow rate, which defines the inflow discharges to the e FLOW-3D ($V_{fr}$ or Q). For this boundary condition, inflow

discharge, sediment concentration of inflow water and the thermal information of inflow water were adjusted, depends on the selected models. Here, the values and parameters were set as time-dependent conditions. The boundary condition at $x_{max}$ , in block number 4 in models, was selected as outflow boundary (O), where the body of the dam is located. The outflows were considered as a spillway at the dam crest and the lower outlet near the bottom of the body of dam. In this study, only S models were investigated, which represents models that only spillway operated. The bottom ($z_{min}$), right ($y_{min}$) and left ($y_{max}$) boundary conditions of reservoir were selected as wall type (W). In this type of boundaries, fluid could not be entered to the boundary. Zmax boundary of models was defined as the symmetry condition (S). Figure 4 represents these boundary conditions (BCs).
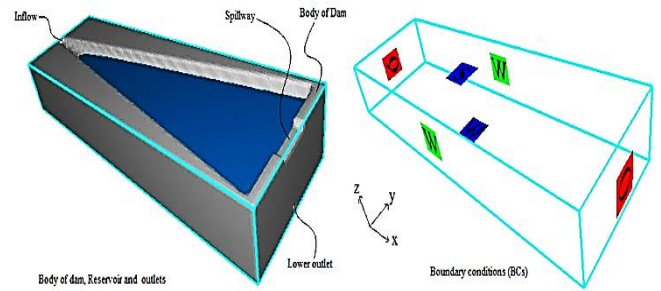


**Figure 4.** Boundary conditions of the models.

Eight separate simulations (scenarios) were performed under the scope of this study. A matrix of simulations performed during this study is represented in Table 2.

**Table 2.** Scenarios modeled using FLOW3D

| Simulation ID (Scenario) | Inflow | | | Reservoir/Lake | | | Outlet Type | Turbulence Model |
|---|---|---|---|---|---|---|---|---|
| | Discharge (m³/sec) | C (kg/m³) | T (ºC) | Discharge (m³/sec) | C (kg/m³) | T (ºC) | | |
| S2 | | | 4 | | | | | |
| S5 | | 20 | 12 | | 15 | | | |
| S8 | | | 24 | | | | | |
| S11 | 50 | | 40 | 50 | | 24 | Spillway | RNG |
| S14 | | | 4 | | | | | |
| S17 | | 15 | 12 | | 20 | | | |
| S20 | | | 24 | | | | | |
| S23 | | | 40 | | | | | |

## 3. RESULTS

The results are compared in different simulation times included: 100 s, 150 s, 200 s, 250 s, 500 s, 750 s, 1000 s, 1500s, 2000 s, 2500 s and 3000 s. These times indicate the time elapsed since the start of modeling. When time is equal to zero, it expresses the time that the inflow water (river) received to the reservoir and it is at the begining point of the reservoir. The results are compared at the middle of the width of the reservoir, where the y is equal to 60 meters. The results are compared each other in two sections of the reservoir, which are shown in Figure 5. One of these sections was selected next to the dam body and the other one was in the middle of the reservoir. These sections are named as section 1 and section 2 withthe distance of

250 m and 375 m from entrance of the reservoir, respectively. Colored temperature and suspended sediment concentration Contours of simulated scenarios are given in the Figure 6.
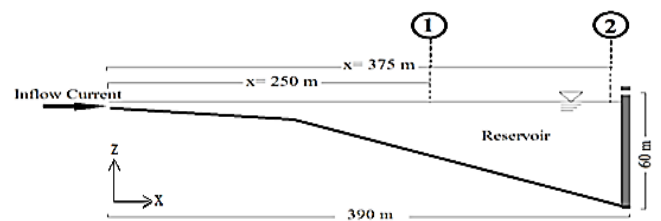


**Figure 5.** Situation of controlling sections.

(a)                                      (b)
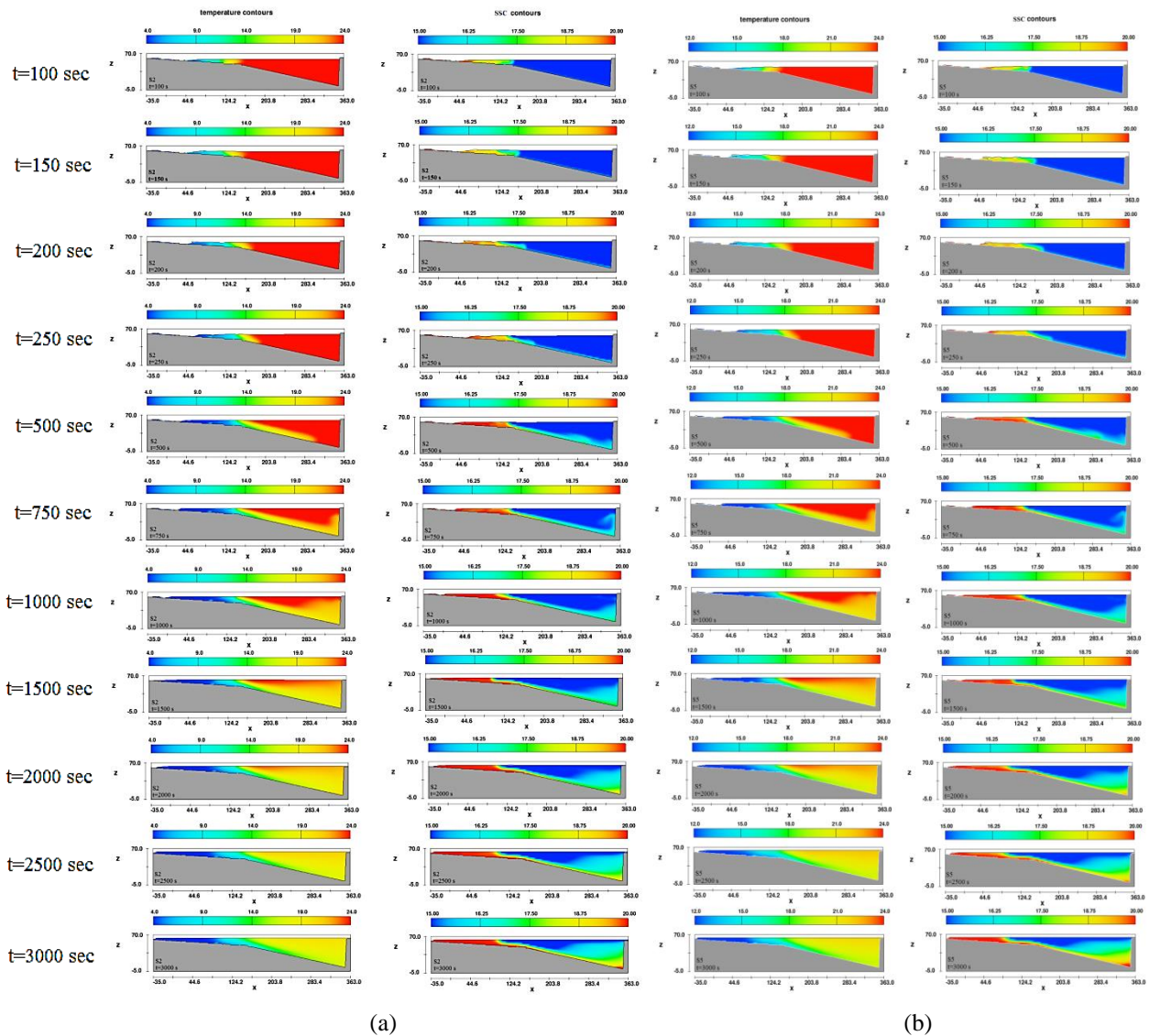
**Figure 6.** Temperature and SSC Contours of Simulation a) S2 and b) S5.

As the suspended sediment concentration of inflow current is higher than the reservoir's one, then the inflow water is denser than the reservoir one. As a result, it is expected that the under flow condition occurred (Figure 6). On the other hand, since the cold water is denser than warm and hot water, the inflow water is denser than the reservoir's one. Then it is expected that the inflow water sinks to the reservoir water and the thermal under flow condition occurs. Evaluating the results for S5 simulation shows that with changing in the temperature of the inflow current's water, the spread of temperature and suspended sediment concentration change. Effect of changings of temperature in inflow currents on distribution of suspended sediments particles are obvious in this simulation. Therefore, it affects the travelling time and distance of suspended particles in dam reservoirs.
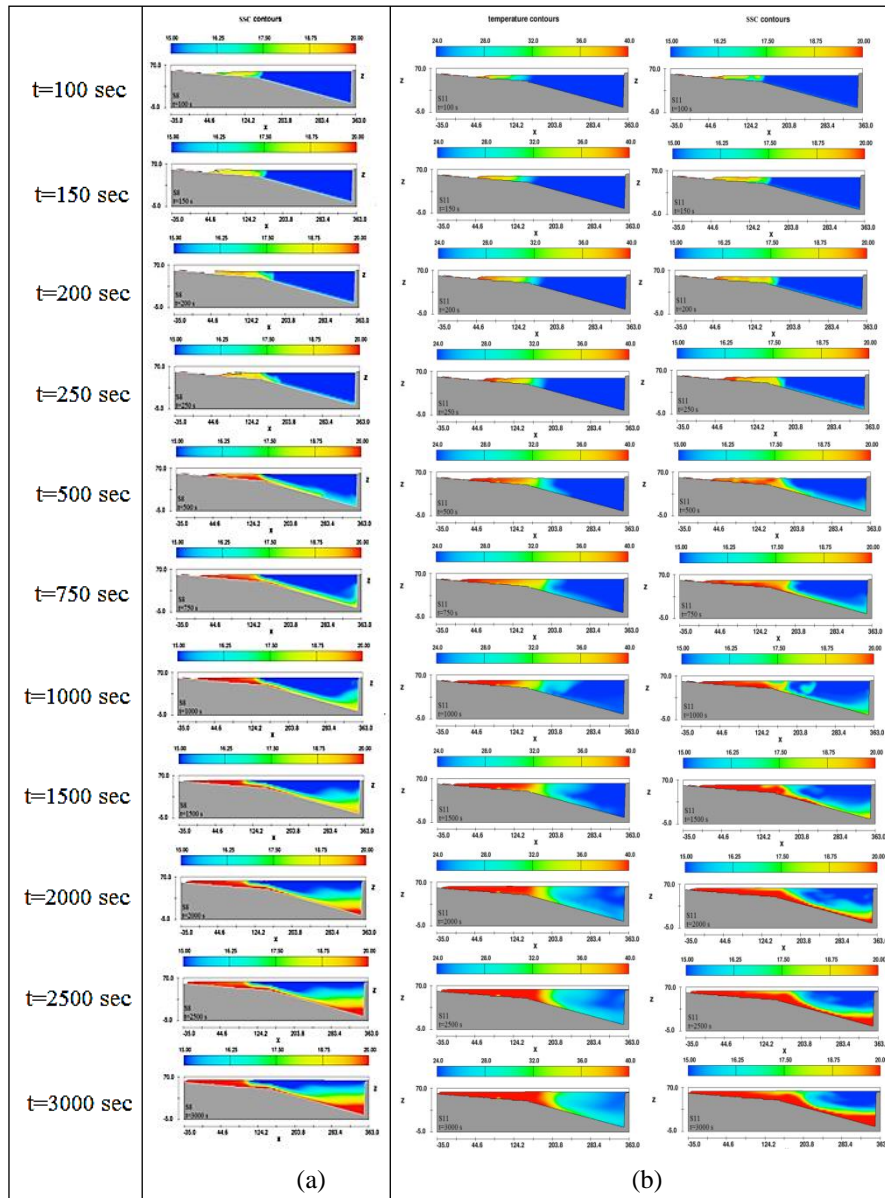
**Figure 7.** Temperature and SSC Contours of Simulations a) S8 and b) S11

In these simulations, velocity is increased at the upper layer of the reservoir. This increasing in velocity at the upper layer of reservoir, rises more near the dam body than the other places farther away from the dam body. It is because of the operation of spillway. As mentioned before, the temperature of inflow's water and reservoir are same and equal to 24 ℃ in simulation S8. It is clear, that this change is also affect the travelling time and distance of suspended sediment particles. As one of the main results it could concluded that temperature affects the plunge point situation of turbidity flows in reservoirs and lakes.

These results are presented as the comparative scatter plots for selected sections of the reservoir in Figure 7, and for different time scales included 1000, 2000 and 3000 seconds after running the simulation.

**Figure 8.** The comparative scatter plots for selected sections 1 and 2.

The spillway starts to operate after the time 700 seconds, approximately. After this time, the velocity at the upper layer of the reservoir and at the surface increases and direction of these velocity vectors are toward the dam body or downstream. So, the distribution of suspended sediment in this layer increase as the given Figure 8. It could conclude that the spillway increases the thickness of layers and helps to decreasing of the stratification.

In the other category of the simulations that were listed in scenario's table (Table 2), in which the concentration of inflow water is less that the concentration of the reservoir water, the inflow and reservoir concentrations were equal to 15 and 20 kg/m$^3$, respectively. So, based on the temperature of water in inflow current and reservoir, the water in reservoir is denser than the inflow water. It is expected that the over flow condition formed in these simulations.
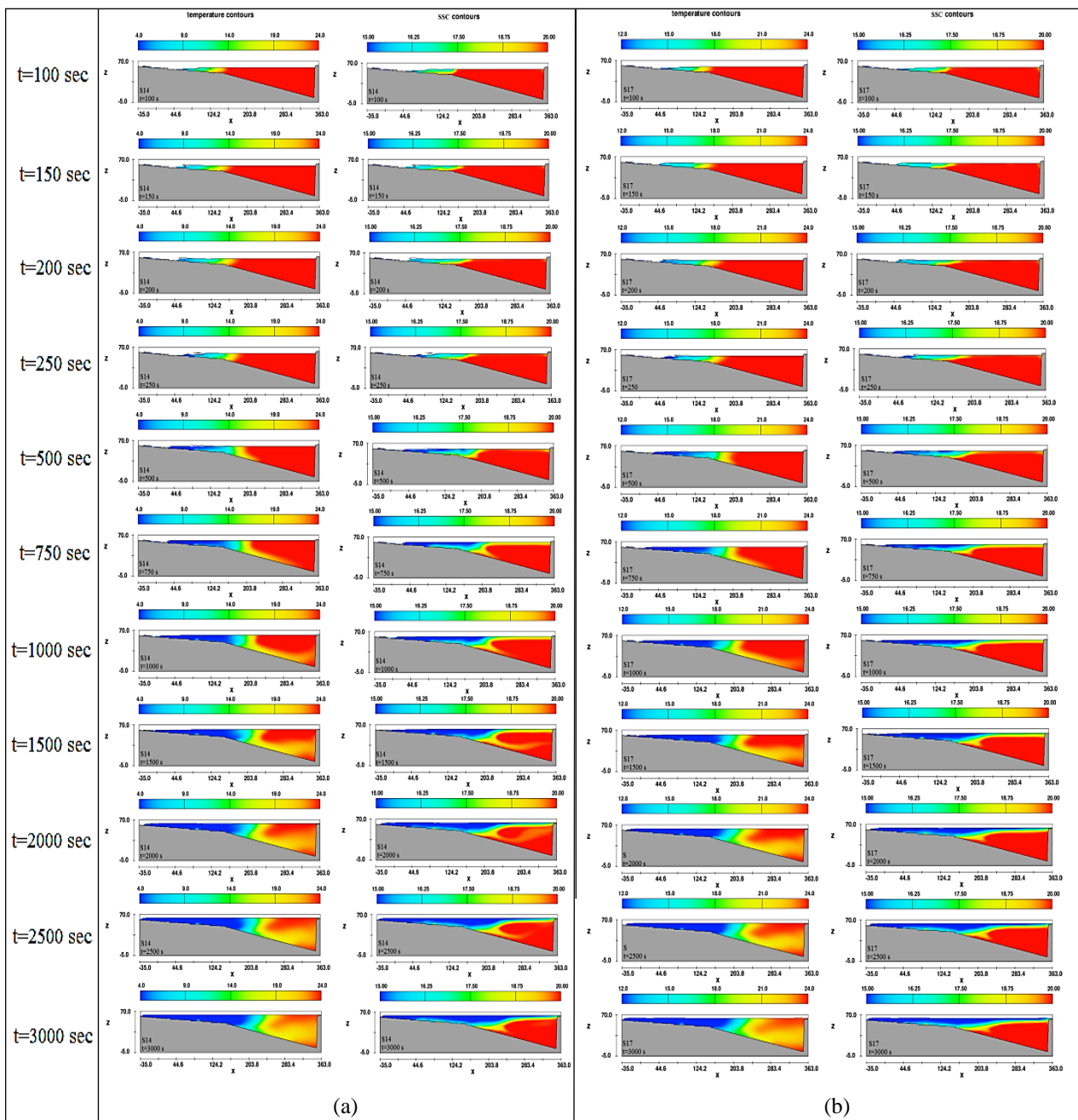
**Figure 9.** Temperature and SSC Contours of Simulation a) S14 and b) S17.

According to Figure 9, in simulation S17 temperature of the inflow current water is still less than the water temperature of the reservoir, as like as the simulation S14. It is a little warmer than the water temperature in simulation S14 and equal to 12 °C. In this simulation, reservoir water temperature is as same as the S14, which is equal to 24 °C. Outlet type is still selected as spillway like other scenarios. About the suspended sediment concentration, the inflow current suspended sediment concentration is less than the reservoir's one.
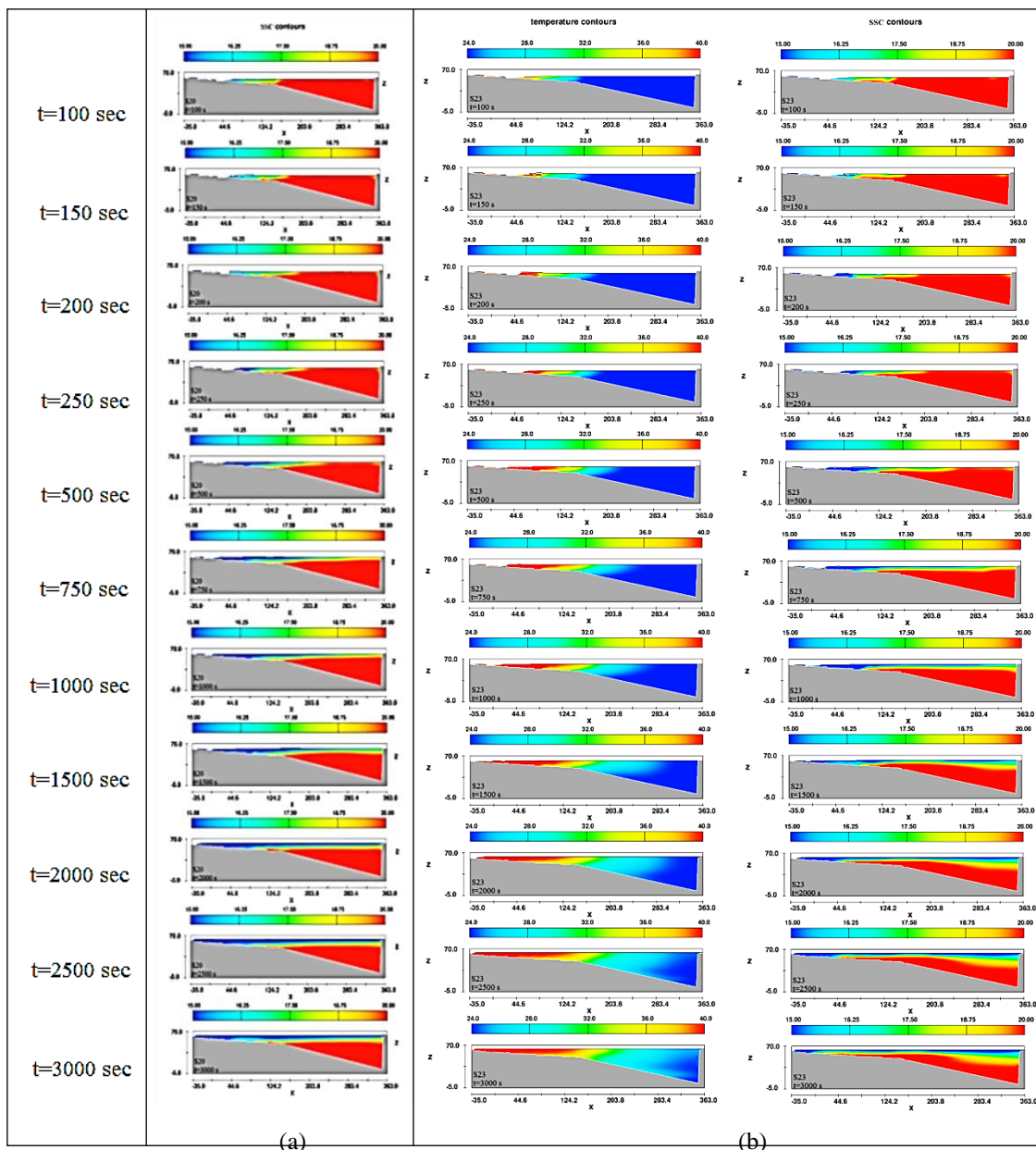
**Figure 10.** Temperature and SSC Contours of Simulation a) S20 and b) S23.

In simulation S20, the water temperature of the inflow current and reservoir are same and equal to 24 ℃. The existence of the spillway outlet affects the distribution pattern for temperature and suspended sediment. This kind of outlets increases the current velocity at the surface of the reservoir. In simulations S14, S17, S20 and S23, the over

flow condition is occurred, obviously. These results are presented as the comparative scatter plots for selected sections of the reservoir and for different timescales included 1000, 2000 and 3000 seconds after running the simulation (Figure 10).

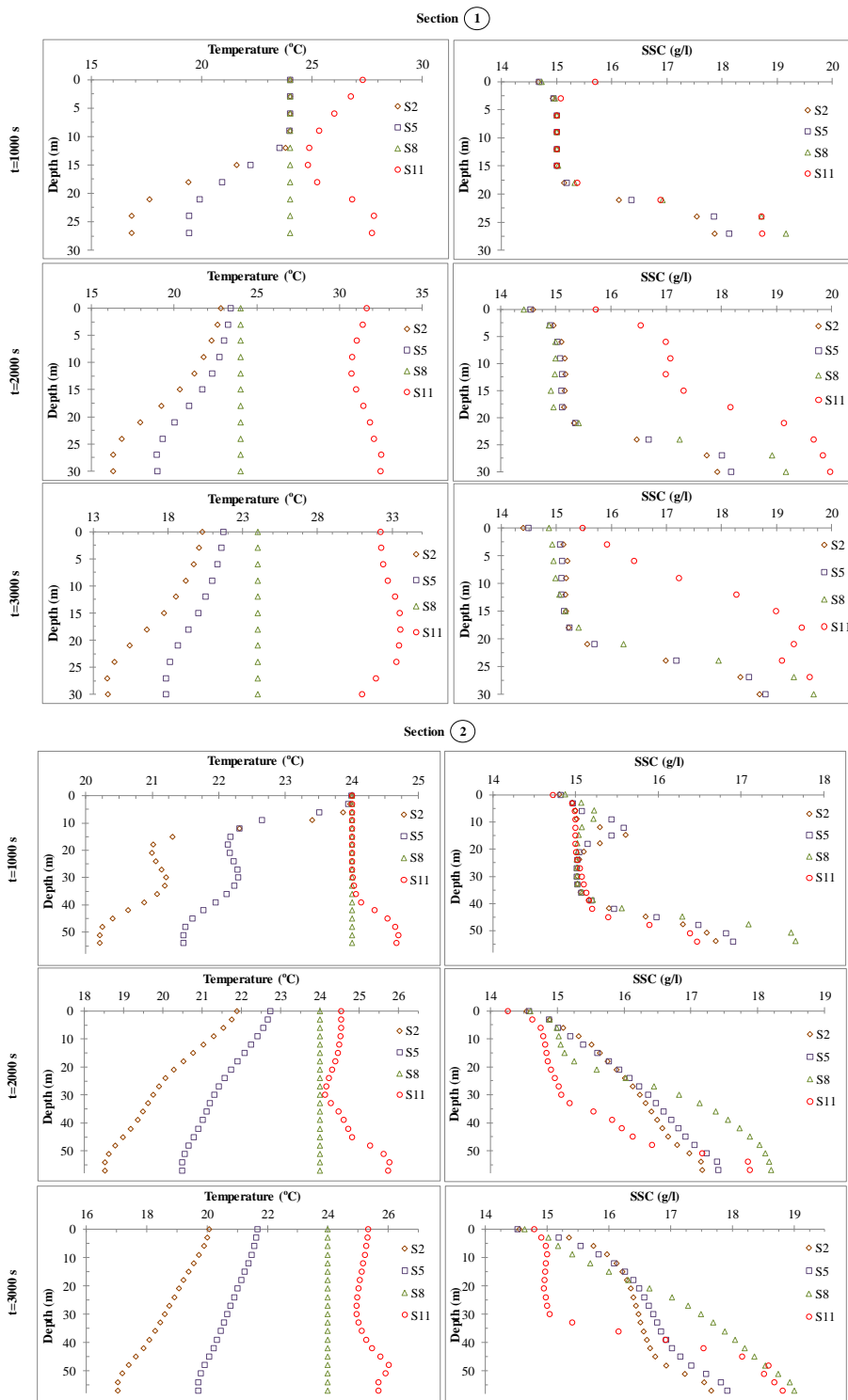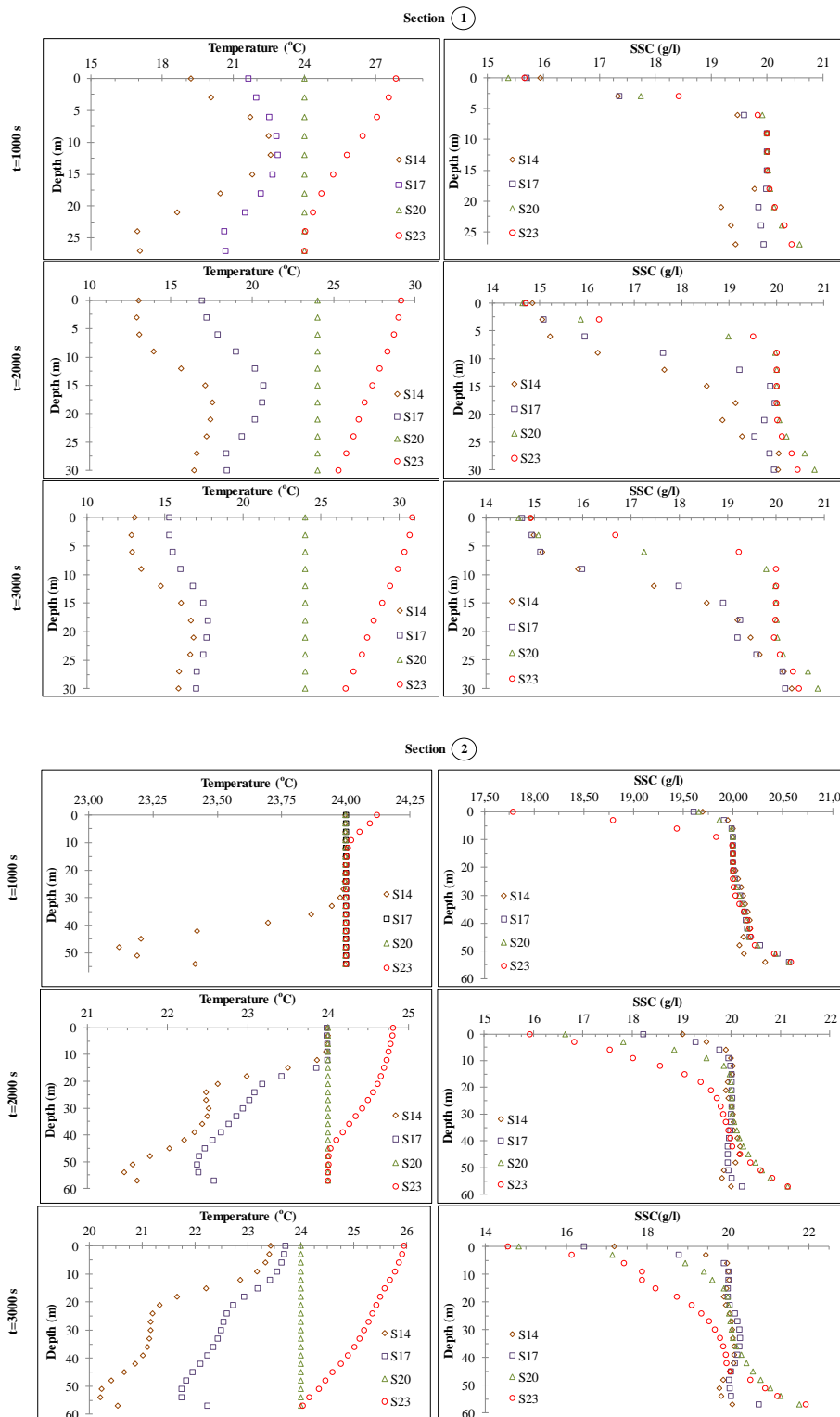**Figure 11.** The comparative scatter plots for selected sections 1 and 2.

From Figure 11, it could be demonstrated that in S2, S5, S8 and S11, the incoming flow into the reservoir is plunge at the beginning of the reservoir into the deeper layers and the turbidity current is formed. The obvious point that could be mentioned here is that the spillway has an important role in distribution of sediment and temperature during the turbidity current phenomenon. Another important point is that the effect of the differences between the inflow's water temperature and suspended sediment concentration and reservoir's water on distribution of the temperature and suspended sediment in the reservoir.

Obtained results, which discussed above, were in a good agreement with the results obtained from studies done by other researchers in terms of water density differences, caused by differences in temperature and suspended sediment concentration. (eg. Zhong et al, 2020; Iwasaki and Parker, 2020; Chen et al., 2019; etc.).

## 4. CONCLUSION

Main aim of this study was to investigate and study on the distribution of the suspended sediment and temperature in lakes and reservoirs. The results of simulations show that the distribution of temperature and suspended sediment is under the effect of changes in some main parameters of inflow current and reservoir/lake. It is concluded that in the same conditions included the inflow water's suspended sediment concentration, reservoir's suspended sediment concentration, reservoir's water temperature and situation of outlet, with changing in inflow water temperature, there are some changes occurred in the situation of plunging point. Magnitude of discharge could affect the plunge point and the formation of the density/turbidity currents. But result of simulations in this study show that without applying any changes in discharge, there will occur some changes in plunging point situation, layers thicknesses, the distribution of suspended sediment and temperature. If density of inflow water is greater than the reservoir's one the density/turbidity currents will be formed obviously.

In simulations S2, S5, S8 and S11, when turbidity/density currents reached to the dam body, the current was moving upward with collision with body of dam and propagated and distributed into the upper layers of the reservoir near dam body. The existence of the spillway type outlet causes to increasing the velocity in layers near dam body and also at the surface of the reservoir. This rising in velocity leads to upward motion of suspended sediment in different layers close to dam body.

The rising in water temperature value leads to settling the suspended sediments faster. Therefore, the temperatures of inflow and reservoir water affect the depositing and settling of suspended sediments. Other words, water temperature could mainly affects the distribution of suspended sediment, the distance traveled by sediment particles and the thickness of formed stratified layers in lakes and reservoirs, directly.

## REFERENCES

[1] M. Nazariha, E. Danayi, S. H. Hashemi, A. H. Izaddustdar, "Camparison of the Thermal Stratification of Under Construction Bakhtiyari Dam at Reservoir and trasitional Area Using CE-QUAL-W2 Model". Enviromental Sciences and Technologies, VOL 13, No.3, 2008 (in Persian).

[2] D. E. Ford, M. C. Johnson, "An Assessment of Reservoir Density Currents and Inflow Processes", Technical Report, E-83-7, Prepared by Ford, Thornton, Nortonand Associates, Ltd, and the Environmental Laboratory, Waterways Experiment Station, for the U. S. Army Engineer Waterway Experiment Station, Vicksburg, Miss, (1983).

[3] M. R. Hipsey, J. D. Brookes, "Pathogen Management in Surface Waters: Practical Considerations for Reducing Public Health Risk", Current Topics in Public Health, Chapter 21, 2013.

[4] J. D. Milliman, "Transfer of River-born Particular Material to the Ocean River Inputs to Ocean Systems", UNEP UNESCO, Switserland, P.5-12, (1981).

[5] L.C. van Rijn, "Sediment transport, part II: suspended load transport." Journal of hydraulic engineering 110.11: 1613-1641, (1984).

[6] G.P. Williams, "Sediment Concentration Versus Water Discharge During Single Hydrological Events in Rivers", Journal of Hydrology, No.111, P.89-106, 1989.

[7] S. Kostic, G. Parker, "Physical and Numerical Modeling of Deltaic Sedimentation in Lakes and Reservoirs", Proceedings, XXX International Association of Hydraulic Research Congress, (2003).

[8] N. L. Salant, M. A. Hassan, C. V. Alonso, "Suspended Sediment Dynamics at High and Low Storm", Hydrological Processes, 22. 1573-1587. 10.1002/hyp.6743, (2008).

[9] O. Algan, C. Gazioglu, Z. Yucel, N. Cagatay, B. Gonencgil, "Sediment and Freshwater Discharges of the Anatolian River into the Black Sea", IOC-BSRC Workshop Report, No.145,Paris,UNESCO,P.38–50, 2000.

[10] H. W. Fang, G. Q. Wang, "Three-dimensional Mathematical Model of Suspended Sediment Transport", Journal of Hydraulic Engineering, Vol. 126, No. 8, ASCE, 2000.

[11] USSD "Modeling Sediment Movement in Reservoirs", Report, Prepared by the United States Society of Dams, Committee on Hydraulics of Dams, Subcommittee on Reservoir Sedimentation, (2015).

[12] J. M. Dake, D. R. F. Harleman, "Thermal Stratification in Lakes: Analytical and Laboratory Studies", Water Resources Research, Vol.5, No.2, 1969.

[13] B.R. Hodges, J. Imberger, A.Saggio, K.B.Winters, "Modeling basin-scale internal waves in a stratified lake". Limnology and oceanography, 45(7), 1603-1620, (2000).

[14] P. Okely, J. Imberger, K. Shimizu, Particle dispersal due to interplay of motions in the surface layer of a small reservoir. Limnology and oceanography, 55(2), 589-603, (2010).

[15] m. Pilotti, G. Valerio, L. Gregorini, L. Milanesi, C.A. Hogg, Study of tributary inflows in Lake Iseo with a rotating physical model. J. Limnol, 73(1), 131-145, (2014).

[16] H.B. Fischer, E.G. List, R.C.Y Koh, J. Imberger, N.H. Brooks, "Mixing in inland and coastal waters". Academic Press, (1979).

[17] R.H. Kennedy, K.W. Thornton, D.E. Ford, "Characterization of the reservoir ecosystem." Microbial Processes in Reservoirs. Developments in Hydrobiology, vol 27. Springer, Dordrecht. https://doi.org/10.1007/978-94-009-5514-1_2, (1985).

[18] M. Modiri-Ghareveran, E. Jabbari, A. Etemad-Shahidi, Proceedings of the Institution of Civil Engineers - Water Management, 167:10, 601-611, 2014.

[19] N. H. Baharim, R. Ismail, M. H. Omar, "Effects of Thermal Stratification on the Concentration of Iron and Manganese in a Tropical Water Supply Reservoir", Sains Malaysiana, 40(8), P.821–825, 2011.

[20] M. Nazariha, E. Danayi, S. H. Hashemi, A. H. Izaddustdar, "Prediction of Thermal Stratification in Proposed Bakhtyari Reservoir with CE-QUAL-W2", World Environmental and Water Resources Congress 2009: Great Rivers, ASCE, 36. 1-8. 10.1061/41036(342)398, (2009).

[21] I. Nsiri, J. Tarhouni, M. Irie, "Modeling of Thermal Stratification and the Effect on Water Quality in Four Reservoirs in Tunisia", J Hydrogeol Hydrol Eng 5:1. doi:10.4172/2325-9647.1000132, (2016).

[22] R. Cossu, A. L. Forrest, H. A. Roop, G. B. Dunbar, M. J. Vandergoes, R. H. Levy, …, S. G. Schladow, "Seasonal Variability in Turbidity Currents in Lake Ohau, New Zealand, and Their İnfluence on Sedimentation, Marine and Freshwater Research", CSIRO Publishing, 2015.

[23] J. Akiyama, H. G. Stefan, "Theory of Plunging Flow into a Reservoir", Internal Memo IM-97, St. Anthony Falls Hydraulic Laboratory, University of Minnesota, Minneapolis, Minn, 1981.

[24] G. J. Farrell, H. Stefan, "Mathematical Modeling of Plunging Reservoir Flows", Journal of Hydraulic Research, 26(5), P.525-537, 1986.

[25] FLOW 3D, "User Manual", Flow Science Inc., (2008).

[26] Yi Zhong, Lulu Qiao, Dehai Song, Yang Ding, Jishang Xu, Wenjing Xue, Cheng Xue, Impact of cold water mass on suspended sediment transport in the South Yellow Sea, Marine Geology, Volume 428, 2020, 106244, ISSN 0025-3227, https://doi.org/10.1016/j.margeo.2020.106244.

[27] Toshiki Iwasaki, Gary Parker, "The role of saltwater and waves in continental shelf formation with seaward migrating clinoform". Proceedings of the National Academy of Sciences Jan 2020, 117 (3) 1266-1273; DOI: 10.1073/pnas.1909572117.

[28] Chen, M., Pattiaratchi, C. B., Ghadouani, A., Hanson, C., "Seasonal and inter-annual variability of water column properties along the Rottnest continental shelf, south-west Australia". Ocean Sci.,Vol:15, 2, 333-348, (2019), DOI:10.5194/os-15-333-2019.

**Academic Platform Journal of Engineering and Science**

# Investigating the Effects of Temperature and Relative Humidity on Performance Ratio of a Grid Connected Photovoltaic System

*[1,2]Ceyda Aksoy Tırmıkçı, [1,2]Cenk Yavuz, [1,2]Talha Enes Gümüş
[1]Sakarya University Innovation Center., Esentepe Campus, 54187, Serdivan, Sakarya, Turkey
[2]Sakarya University Eng. Faculty Electrical and Electronics Eng. Dept., Esentepe Campus, 54187, Serdivan, Sakarya, Turkey
caksoy@sakarya.edu.tr, (iD)
cyavuz@sakarya.edu.tr, (iD)
tgumus@sakarya.edu.tr, (iD)

**Abstract**

The size and the cost of photovoltaic (PV) systems are dependent on the performance ratio of solar cells. Current studies in literature usually determine the size according to the total solar radiation received on the surface of solar modules. However, it is a fact that the energy output of a solar module is also effected by weather conditions of the location where the system is mounted. Thus, for an efficient design, weather conditions must be taken into consideration to determine the size. In this paper, the performance ratio of an existing photovoltaic system was established and the effect of weather conditions on the energy conversion was analyzed. For this purpose, the reference yield of the system was estimated in terms of solar radiation components received on the surface of solar modules for a specific period. Then, the performance ratio was calculated by dividing the measured final yield to the estimated reference yield. In conclusion, the change in performance ratio was discussed for different temperature and relative humidity values. Finally, the effect of meteorological inputs on PV system performance was investigated based on a back propagation artificial neural network approach. In conclusion, theoretical and computational results were evaluated.

*Keywords:* photovoltaic system, final/reference yield, performance ratio, temperature, relative humidity, back propagation artificial neural network

## 1. INTRODUCTION

Turkey is a developing, urbanizing and newly industrialized country with growing energy demands. Primary energy generation sources of the country are 28.1% natural gas, 22.2% coal, 31.2% hydro, 8.5% wind, 6.7% solar and 3.3% other sources. Fossil fuel sources have the largest share to meet the total primary energy demand in the country. Since local reserves of Turkey are not large enough to meet the total fossil fuel demand, the country is heavily dependent on imports [1].

It is a fact that energy access and climate change concerns are the key parameters for a sustainable economic, social and environmental development of societies. Dependence on local fossil fuels sources and imports pose a serious obstacle to sustainable development goals of Turkey. It is urgent for the country to put action plans in place for electricity market and natural gas market liberalization.

Turkey has a favorable geographical position for solar energy applications with annual mean solar radiation of 4.18

kWh/m$^2$ and annual mean sunshine duration of 2741 h [2]. Reports indicate that installed total solar PV capacity of the country increased from 12 MW in 2012 to 832 MW in 2016 due to policy momentum in solar energy market [3]. Distributed solar PV generation appears to be an efficient and effective solution for the country.

Solar PV systems provide energy generation from local and renewable sources with zero greenhouse gas emissions during the operation. In recent years, there is a growing interest in these systems in parallel with energy access and climate change concerns. Solar radiation converted to electrical power by solar PV panels is the key parameter to determine the size and cost of these systems. Solar energy conversion is directly related to environmental conditions, especially temperature and solar radiation.

Solar PV cells are commonly represented by one diode parameter models and two diode parameter models with parameters of photocurrent, diode reverse saturation current, diode quality factor, lumped series resistance and lumped shunt resistance. Equations of given parameters indicate that

*Corresponding Author:Sakarya University Eng. Faculty Electrical and Electronics Eng. Dept., Esentepe Campus, 54187, Serdivan, Sakarya, Turkey

I-V characteristic of a solar PV cell is directly related to temperature and humidity [4 and 5].

In this paper, the effect of temperature and solar radiation on the performance of a 290.400 kWp grid connected solar PV system was investigated in terms of measured energy output data. For this purpose, the most efficient period that solar PV panels of the system receive the largest amount of solar radiation was determined and total daily mean solar radiation for this period was estimated. In the next step, daily performance ratio of the system was calculated to evaluate the relation between solar PV output and daily meteorological parameters; temperature and relative humidity. After that, measured energy output data was processed based on a back propagation artificial network approach to investigate PV system output sensitivity to climate conditions. In conclusion, results obtained from theoretical and computational analyses were presented to correlate PV system performance, temperature and relative humidity.

## 2. METHODOLOGY

IEC 61724 explains the performance ratio (PR) of a solar PV system as total system losses; final system yield ($Y_F$) divided by reference system yield ($Y_R$) [6].

$$PR = \frac{Y_F}{Y_R} \tag{1}$$

Final system is net daily energy output (E) divided by rated output ($P_o$) of a PV array:

$$Y_F = \frac{E}{P_0} \tag{2}$$

Reference system yield is total solar radiation on a tilted surface ($H_T$) divided by reference irradiance of a PV array:

$$Y_R = \frac{H_T \left[\frac{kWh}{m^2}\right]}{1 \left[\frac{kW}{m^2}\right]} \tag{3}$$

Figure 1 presents monthly mean daily global solar radiation data of system location [7]. According to the figure, reference system yield is maximum in June. In this paper, performance ratio of the system is evaluated for different days of June. Therefore, total mean daily solar radiation of the system location is calculated to determine the reference system yield for the selected period.

Total solar radiation ($H_T$) is the sum of beam solar radiation ($H_B$), diffuse solar radiation ($H_D$) and global solar radiation [8]. Beam solar radiation is the difference between the global solar radiation and diffuse solar radiation. Global solar radiation is commonly available for many locations in the world. However, there are few locations measuring the

diffuse component. In this paper, diffuse component for Kocaeli city in June is estimated and used as measured data in further calculations.
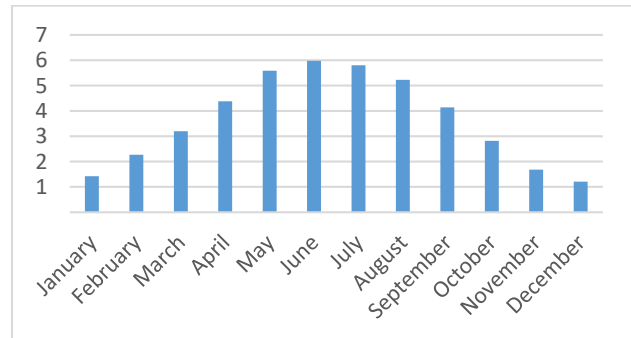


**Figure 1.** Monthly mean daily global solar radiation for Kocaeli city [kWh/m2.day]

In literature, there are many studies to estimate diffuse solar radiation since measured values are not available [9-19]. This paper used current equations correlating the diffuse component with clearness index ($K_T$) and/or sunshine fraction ($K_N$) to obtain new diffuse equations for the system location (Table 1 and Table 2). The most appropriate equation among new nine equations was determined by statistical test indicators (Table 3).

**Table 1.** Current diffuse solar radiation equations

| | | |
|---|---|---|
| (4) | $K_D = 1.00 - 1.13(K_T)$ | [9] |
| (5) | $K_D = 1.0212 - 1.1672(K_T)$ | [10] |
| (6) | $K_D = 0.9885 - 1.4276(K_T) + 0.5679(K_T)^2$ | [11] |
| (7) | $K_D = 1.018 - 1.167(K_T) + 0.024(K_T)^2$ | [12] |
| (8) | $K_D = 1.027 - 1.6582(K_T) + 1.1018(K_T)^2 - 0.4019(K_T)^3$ | [13] |
| (9) | $K_D = 0.6603 - 0.5272(K_N)$ | [14] |
| (10) | $K_D = 0.791 - 0.635(K_N)$ | [15] |
| (11) | $K_D = 0.754 - 0.654(K_N)$ | [16] |
| (12) | $K_D = 0.7434 - 0.8203(K_N) + 0.2454(K_N)^2$ | [14] |
| (13) | $K_D = 0.5562 + 0.1536(K_N) - 1.2027(K_N)^2 + 0.7122(K_N)^3$ | [10] |
| (14) | $K_D = 1.194 - 0.838(K_T) - 0.446(K_N)$ | [17] |
| (15) | $K_D = 1.00 - 0.858(K_T) - 0.235(K_N)$ | [18] |
| (16) | $K_D = 0.945 - 0.675(K_T) - 0.166(K_T)^2 - 0.173(K_N) - 0.079(K_N)^2$ | [12] |
| (17) | $K_D = 0.9593 - 0.8713(K_T) + 0.29191(K_T)^2 - 0.0979(K_T)^3 - 0.28419(K_N) + 0.02653(K_N)^2 - 0.02083(K_N)^3$ | [13] |
| (18) | $K_D = 0.747 - 1.502(K_T) - 4.956(K_T)^2 + 3.321(K_T)^3 - 1.004(K_N) + 1.747(K_N)^2 - 1.226(K_N)^3$ | [12] |

Daily energy output values were obtained from the owner to calculate the final system yield. Table 2 presents measured net daily energy output in June. Rated output of the system was determined by technical specifications of system PV panels under standard test conditions.

**Table 2.** New diffuse solar radiation equations

(19)   $K_D=0.9992-1.1838\ (K_T)$

(20)   $K_D= 0.4504+1.4226\ (K_T) -3.0186\ (K_T)^2$

(21)   $K_D=2.2074 -11.2684\ (K_T)+ 27.1114\ (K_T)^2 -23.5278\ (K_T)^3$

(22)   $K_D=0.7732 -0.5842\ (K_N)$

(23)   $K_D=0.9956 -1.4812\ (K_N)+ 0.8473\ (K_N)^2$

(24)   $K_D=0.9719-1.3355\ (K_N)+0.5582\ (K_N)^2+ 0.1848(K_N)^3$

(25)   $K_D=0.8956-0.6027\ (K_T)-0.3009\ (K_N)$

(26)   $K_D=0.8404-0.3745\ (K_T) -0.3272\ (K_T)^2 -0.2502\ (K_N) -0.0220(K_N)^2$

(27)   $K_D=0.8699 -0.4986\ (K_T)+ 0.0448\ (K_T)^2 -0.354\ (K_T)^3-0.3484\ (K_N) + 0.1629\ (K_N)^2 -0.1099\ (K_N)^3$

**Table 3.** Statistical test results for new nine equations

|  | MABE | MAPE | RMSE | $R^2$ | t |
|---|---|---|---|---|---|
| (19) | 0.1484 | 2.4748 | 0.1836 | 0.9959 | 0.1289 |
| (20) | 0.0828 | 1.2632 | 0.1243 | 0.9981 | 0.0615 |
| (21) | 0.0817 | 1.1869 | 0.1189 | 0.9982 | 0.0729 |
| (22) | 0.1338 | 2.3210 | 0.1664 | 0.9967 | 0.2667 |
| (23) | 0.0464 | 0.8820 | 0.0575 | 0.9996 | 0.1904 |
| (24) | 0.0452 | 0.8706 | 0.0569 | 0.9996 | 0.1871 |
| (25) | 0.0150 | 0.2623 | 0.0256 | 0.9999 | 0.0600 |
| (26) | 0.0145 | 0.2626 | 0.0236 | 0.9999 | 0.1366 |
| (27) | 0.0147 | 0.2625 | 0.0238 | 0.9999 | 0.1412 |
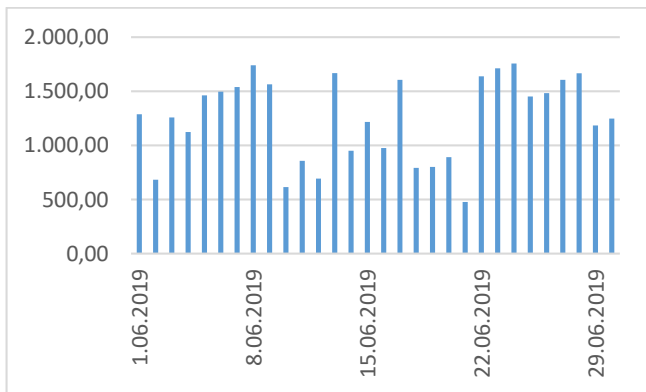


**Figure 2.** Measured net daily energy output of the system [kWh]



**Figure 3.** The structure of BP network

Artificial neural networks (ANNs) are computing systems that imitate the work structure of a biological brain by a collection of connected artificial neurons. Neural networks are widely used in many applications due to their simplicity of implementation [20]. In this paper, final PV system yield was predicted by changing input variables to investigate the effect of temperature and relative humidity effect on PV system performance. In Case 1, temperature and relative humidity data were trained with reference yield data. In Case 2, temperature and reference yield data were selected as input variables. Finally, relative humidity data was trained with reference yield data and called Case 3. Multilayered feedforward topology and back-propagation (BP) algorithm was adopted to train the network.

## 3. RESULTS AND DISCUSSION

Statistical test results of new diffuse solar equation indicate that in equations where the diffuse component is a function of clearness index and sunshine fraction give the vest results for the system location. According to Table 3, results for MABE, MAPE, RMSE and R2 indicators are almost equal. However, the result for t-statistic indicator for Equation 25 is minimum among all t results. Therefore, the best equation to estimate the diffuse component of the system was selected as Equation 25.

$$K_D=0.8956-0.6027\ (K_T)-0.3009 \tag{25}$$

Figure 3 presents temperature and relative humidity values for June 2019. According to the figure, maximum daily mean temperature, minimum daily mean temperature, maximum daily mean relative humidity and minimum daily mean humidity are recorded on 25.06.2019, 05.06.2019, 11.06.2019 and 24.06.2019 respectively.

Performance ratio results presented in Table 5 indicate that 24.06.2019 and 08.06.2019 are the most efficient days for the system. Temperature and relative humidity values for these days were recorded below 35°C and below 50% on 24.06.2019 and below 30°C and nearly 50% on 08.06.2019. Performance ratio values for the days with records to maximum temperature and minimum relative humidity were calculated almost equal, 80.291% on 25.06.2019 and 80.135% on 05.06.2019. These experimental results prove the theoretical results of many studies in the literature indicating that changes in temperature and humidity conditions effect solar energy conversion efficiency significantly in solar PV systems [21 and 22].

**Table 4.** Daily mean values of solar radiation components for the system location [kWh/m$^2$]

|  | H$_D$ | H$_B$ | H$_T$ |
|---|---|---|---|
| 01.06.2019 | 2.2710 | 3.7090 | 5.5566 |
| 02.06.2019 | 2.2755 | 3.7045 | 5.5486 |
| 03.06.2019 | 2.2798 | 3.7002 | 5.5409 |
| 04.06.2019 | 2.2839 | 3.6961 | 5.5337 |
| 05.06.2019 | 2.2877 | 3.6923 | 5.5269 |
| 06.06.2019 | 2.2913 | 3.6887 | 5.5205 |
| 07.06.2019 | 2.2946 | 3.6854 | 5.5145 |
| 08.06.2019 | 2.2977 | 3.6823 | 5.5089 |
| 09.06.2019 | 2.3005 | 3.6795 | 5.5038 |
| 10.06.2019 | 2.3031 | 3.6769 | 5.4990 |
| 11.06.2019 | 2.3055 | 3.6745 | 5.4947 |
| 12.06.2019 | 2.3076 | 3.6724 | 5.4908 |
| 13.06.2019 | 2.3095 | 3.6705 | 5.4873 |
| 14.06.2019 | 2.3111 | 3.6689 | 5.4841 |
| 15.06.2019 | 2.3125 | 3.6675 | 5.4814 |
| 16.06.2019 | 2.3137 | 3.6663 | 5.4791 |
| 17.06.2019 | 2.3146 | 3.6654 | 5.4772 |
| 18.06.2019 | 2.3153 | 3.6647 | 5.4757 |
| 19.06.2019 | 2.3158 | 3.6642 | 5.4746 |
| 20.06.2019 | 2.3160 | 3.6640 | 5.4739 |
| 21.06.2019 | 2.3160 | 3.6640 | 5.4736 |
| 22.06.2019 | 2.3158 | 3.6642 | 5.4736 |
| 23.06.2019 | 2.3153 | 3.6647 | 5.4741 |
| 24.06.2019 | 2.3145 | 3.6655 | 5.4750 |
| 25.06.2019 | 2.3136 | 3.6664 | 5.4763 |
| 26.06.2019 | 2.3124 | 3.6676 | 5.4780 |
| 27.06.2019 | 2.3110 | 3.6690 | 5.4801 |
| 28.06.2019 | 2.3093 | 3.6707 | 5.4826 |
| 29.06.2019 | 2.3074 | 3.6726 | 5.4854 |
| 30.06.2019 | 2.3052 | 3.6748 | 5.4887 |
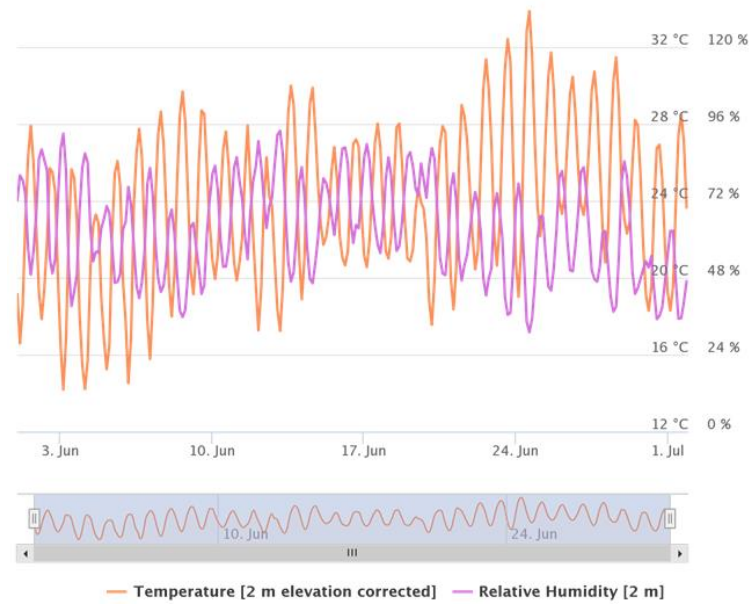


**Figure 4.** Temperature and relative humidity changes in June 2019 [23]

**Table 5.** Y$_F$ [kWh/kWp], Y$_R$ [h] and PR (%) of the system for June

|  | Y$_F$ | Y$_R$ | PR |
|---|---|---|---|
| 01.06.2019 | 3.901667 | 5.5566 | 70.2168 |
| 02.06.2019 | 2.067364 | 5.5486 | 37.25919 |
| 03.06.2019 | 3.813727 | 5.5409 | 68.82866 |
| 04.06.2019 | 3.404727 | 5.5337 | 61.52714 |
| 05.06.2019 | 4.429 | 5.5269 | 80.13534 |
| 06.06.2019 | 4.531394 | 5.5205 | 82.08303 |
| 07.06.2019 | 4.663303 | 5.5145 | 84.56439 |
| 08.06.2019 | 5.271545 | 5.5089 | 95.69143 |
| 09.06.2019 | 4.737818 | 5.5038 | 86.08267 |
| 10.06.2019 | 1.861424 | 5.4990 | 33.85023 |
| 11.06.2019 | 2.596303 | 5.4947 | 47.25104 |
| 12.06.2019 | 2.098788 | 5.4908 | 38.22372 |
| 13.06.2019 | 5.052182 | 5.4873 | 92.07045 |
| 14.06.2019 | 2.880485 | 5.4841 | 52.52429 |
| 15.06.2019 | 3.684576 | 5.4814 | 67.21961 |
| 16.06.2019 | 2.955576 | 5.4791 | 53.94272 |
| 17.06.2019 | 4.866727 | 5.4772 | 88.85429 |
| 18.06.2019 | 2.402788 | 5.4757 | 43.88093 |
| 19.06.2019 | 2.426788 | 5.4746 | 44.32813 |
| 20.06.2019 | 2.702303 | 5.4739 | 49.36705 |
| 21.06.2019 | 1.444909 | 5.4736 | 26.39778 |
| 22.06.2019 | 4.962636 | 5.4736 | 90.66494 |
| 23.06.2019 | 5.187485 | 5.4741 | 94.76416 |
| 24.06.2019 | 5.32303 | 5.4750 | 97.2243 |
| 25.06.2019 | 4.39703 | 5.4763 | 80.29199 |
| 26.06.2019 | 4.494061 | 5.4780 | 82.03835 |
| 27.06.2019 | 4.864455 | 5.4801 | 88.7658 |
| 28.06.2019 | 5.047485 | 5.4826 | 92.06371 |
| 29.06.2019 | 3.588636 | 5.4854 | 65.4216 |
| 30.06.2019 | 3.780303 | 5.4887 | 68.87429 |

Figure 5 indicates the predicted final yield and calculated final yield of the PV system with BP neural network by inputting reference yield, temperature and relative humidity.



**Figure 5**. Predicted and measure $Y_F$ values -Case1

Figure 6 indicates the predicted final yield and calculated final yield of the PV system with BP neural network by inputting reference yield and temperature.



**Figure 6.** Predicted and measure $Y_F$ values –Case2

Figure 7 indicates the predicted final yield and calculated final yield of the PV system with BP neural network by inputting reference yield and relative humidity.



**Figure 7.** Predicted and measure $Y_F$ values –Case3

From the results of Figure 5, Figure 6 and Figure 7, it can be found that predicted values of final system yield match

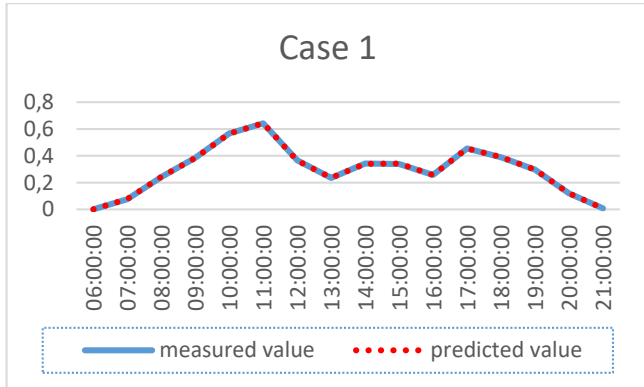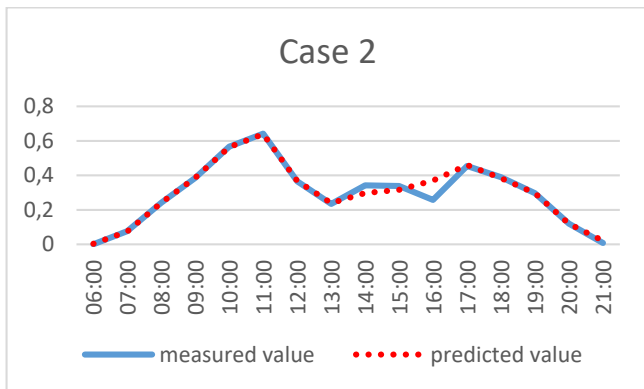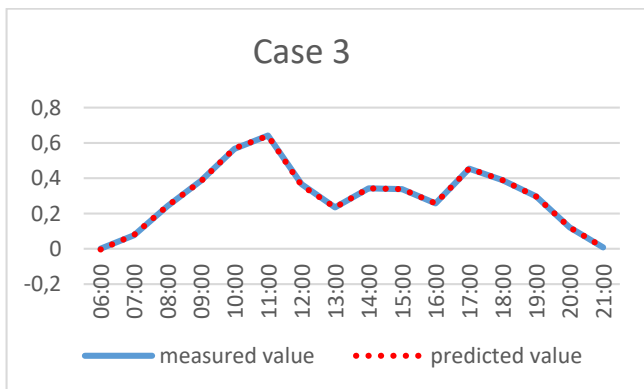calculated final system yield best for Case 1 with input variables-reference system yield, temperature and relative humidity. The results from Case 2 and Case 3 also indicate that PV system performance is more sensitive to relative humidity variable on summer days in Kocaeli city.

## 4. CONCLUSION

Performance ratio of solar PV panels is strongly correlated with solar energy conversion efficiency. The primary condition for a high system performance is maximum solar radiation on the solar surface. Then, comes optimum conditions for meteorological conditions especially for temperature and humidity which change I-V characteristic of the arrays.

In this paper, performance ratio of a 290.400 kWp grid connected solar PV system was estimated for the month of June when the monthly mean global solar radiation was recorded maximum. Performance ratio was calculated according to IEC 61724 standard as final system yield divided by reference system yield. Final system yield data was obtained from the owner and reference yield system data was estimated. For this purpose, new diffuse solar radiation equations were developed in terms of clearness index and/or sunshine fraction and the most appropriate equation for the system location was determined by statistical indicators.

Performance ratio results of the system indicated that the most efficient days of the month 24th and 8th days respectively. On these days, relative humidity values were recorded almost equal. Besides, performance ratio of the system was calculated around 80% on the day with a record to maximum temperature and on the day with a record minimum record. These results indicated that the hottest or the clearest periods were not always recorded with maximum conversion efficiency.

Results obtained from BP network supported theoretical performance ratio results and indicated that success rate of the algorithm increased with more meteorological data inputs. Predicted final system yield values also indicated that in Kocaeli city and locations with similar climate conditions, PV system output was very sensitive to relative humidity in summer months.

It can be concluded that solar energy conversion efficiency changes in parallel with solar radiation, temperature and humidity parameters. Therefore, all these parameters must be evaluated to determine the size of a solar PV system. In the contrary case, it is likely to experience vital problems with especially off grid systems due to low conversion efficiency under unexpected environmental conditions.

## REFERENCES

[1]. IEA, Countries: Turkey, URL: http://iea.org (Reached; January, 1, 2021)

[2]. The Ministry of Energy and Natural Resources, Information Center, URL: http://energy.gov.tr (Reached; August, 14, 2020)

[3]. BP Statistical Review of World Energy (2017), URL: http://bp.com (Reached; May, 1, 2020)

[4]. D.S.H. Chan, J.C.H. Phang, "Analytical methods for the extraction of solar cell single-double model parameters from I-V characteristics", IEEE Transactions on Electron Devices, 34(2), pp.286-293, 1987.

[5]. V.L. Brano, A. Orioli, G. Ciulla, A.D: Gangi, "An improved five-parameter model for photovoltaic modules", Solar Energy Materials and Solar Cells, 94, pp. 1358-1370, 2010.

[6]. F. Ghani, G. Rosengarten, M. Duke, J.K. Carson, "The numerical calculation of single-diode solar-cell modelling parameters", Renewable Energy, 72, pp.105-112, 2014.

[7]. Photovoltaic System Performance Monitoring-Guideliness for Measurement, Data Exchange and Analysis, IEC Standard 61724, 1998.

[8]. The Ministry of Energy and Natural Resources, Solar Energy Potential Atlas (2019), URL: http://yegm.gov.tr (Reached; February, 2, 2020)

[9]. J.K. Page, "The estimation of monthly mean values of daily total short wave radiation on vertical and inclined surface from sunshine records for latitudes 40N-40S", UN Conference on New Sources of Energy, Rome, 1961.

[10]. H. Aras, O. Ballı, A. Hepbaşlı, "Estimating the horizontal diffuse solar radiation over the Central Anatolia Region of Turkey", Energy Convers Manage, 47, pp.2240-2249, 2006.

[11]. S. Tarhan, A. Sari, "Model selection for global and diffuse radiation over the Central Black Sea (CBS) region of Turkey", Energy Convers Manage, 46(4), pp.605–13, 2005.

[12]. Y. Jiang, "Estimation of monthly mean daily diffuse radiation in China", Applied Energy, 86:1458, 2009.

[13]. H. Khorasanizadeh, K. Mohammadi, A. Mostafaeipour, "Establishing a diffuse solar radiation model for determining the optimum tilt angle of solar surfaces in Tabass, Iran", Energy Convers Manage, 78, pp.805–814, 2014.

[14]. S. Barbaro, G. Cannata, S. Coppolino, C. Leone, E. Sinagra, "Diffuse solar radiation statistics for Italy", Solar Energy, 26, pp. 429-435, 1981.

[15]. M. Iqbal, "Correlation of average diffuse and beam R-radiation with hours of bright sunshine", Solar Energy, 23(2), pp.169-173, 1979.

[16]. G. Lewis, "Diffuse Irradiation over Zimbabwe", Sol Energy, 31(1), pp.125–128, 1983.

[17]. K.K. Gopinathan, "Computing the monthly mean daily diffuse radiation from clearness index and percent possible sunshine", Sol Energy, 41(4), pp.379–385, 1988.

[18]. D.G. Erbs, S.A. Klein, J.A. Duffie, "Estimation of the Diffuse Radiation Fraction for Hourly, Daily and Monthly Average Global Radiation", Solar Energy, 28, pp. 293-302, 1982.

[19]. C.A. Tirmikci, C. Yavuz, "Establishing new regression equations for obtaining the diffuse solar radiation in Sakarya (Turkey)", Tehnicki Vjesnik-Technical Gazette, Vol.25, pp.503, 2018.

[20]. J. Kou et al., "Photovoltaic power forecasting based on artificial neural network and meteorological data", TENCON 2013-2013 IEEE Region 10 Conference, Xian, China.

[21]. X. Qing, Y. Niu, "Hourly day-ahead solar irradiance prediction using weather forecasts by LSTM", Energy, 148, pp.462-468, 2018.

[22]. Maitanova M, Telle JS, Hanke B, Grottke M, Schmidt T, von Maydell K, Agert C, "A machine learning approach to low-cost photovoltaic power prediction based on publicly available weather reports", Energies, 13, vol. 735-757, 2020.

[23]. Weather Kocaeli, URL: https://www.meteoblue.com/ (Reached; April, 5, 2020)

# An Approach Integrating Kano Model And Fuzzy Logic Into The Planning Matrix Of Quality Function Deployment: An Application For The Design Of A Baby Diaper

*[1]Derya Haroglu, [2]İzem Leblebici

[1]Erciyes University, Department of Industrial Design Engineering, Kayseri, Turkey, dharoglu@erciyes.edu.tr, 🆔
[2]Erciyes University, Department of Industrial Design Engineering, Kayseri, Turkey, izemleblebici@gmail.com, 🆔

## Abstract

Determining the customer requirements accurately early in the product development process, particularly in highly competitive industries such as baby diapers, would help to prevent design repetitions and consequently wasting time and resources. Quality Function Deployment (QFD) has turned out to be a key methodology to design products by getting the voice of the customer in the first place, as well as converting the customer's voice into product engineering characteristics. In addition, Kano model emphasizes the degree to which a customer is satisfied when a particular customer need is met. In this study, an approach integrating the Kano model into the planning matrix of QFD using Fuzzy logic, was proposed. The importance weights of customer requirements of a baby diaper were calculated using both the proposed Adjusted Kano-Fuzzy-QFD (AKFQFD) and traditional Kano-QFD model. It was demonstrated that the AKFQFD could effectively prioritize the importance weights of customer requirements.

*Keywords:* Quality function deployment, Kano model, Fuzzy logic, baby diaper

## 1. INTRODUCTION

Competitive reactions and changing customer needs are applying an ever-increasing pressure on companies to offer innovative products to the market and to reduce product development cycle-times. Furthermore, according to the research conducted by the Product Development and Management Association (PDMA) in 2012, which included around 453 respondents that were mostly from North America and Asia, and were from several industries (e.g., chemicals and materials, health care), new products have accounted for approximately 31% of sales and profits over the past 5 years of companies [1, 2]. Thus, many quality improvement tools including Quality Function Deployment (QFD), Failure Mode and Effect Analysis (FMEA), and lean six sigma, have been introduced by researchers to help companies to analyze problems effectively and systematically making the development of new products more manageable and successful [3, 4].

QFD, a customer-driven product design approach, was first introduced by Dr. Yoji Akao in Japan in 1966, and became popular with the American Supplier Institute (ASI) in the late 1980s with the "four-phase model" including four matrixes [5, 6]. The first phase is often referred to as the "House of Quality (HOQ)", and translates customer needs (Whats) into engineering characteristics (Hows), which is the most used matrix globally [7, 8]. The second, third, and fourth phase transforms the voice of the customer (VOC) into component

characteristics, key process operations, and production requirements, respectively [9]. Toyota, one of the first companies successfully applied QFD, reduced the new product development costs, and decreased the development time by one third [10, 11]. Furthermore, researchers have integrated ergonomic design criteria (e.g., easy to use) into engineering design with the help of QFD for many years. Zhang et al. [12] used the HOQ to design a ceiling hood and hob. Marsot [13] designed a kitchen knife applying the HOQ. Prasad et al. [14] evaluated the drawing tables for students suffering from musculoskeletal disorders using the HOQ. Demirbilek & Demirkan [15] designed an inner door knocker by using the HOQ. Ergonomics is a scientific discipline that aims to maximize the harmony between human beings, the environment in which they are doing their work and the objects they use by focusing on human health and performance [16, 17]. Therefore, a product or service design with which a person interacts is within the scope of ergonomics.

The Kano model introduced in 1984 by Noriaki Kano, which can be integrated with QFD to deeply understand the voice of the customer, classifies customer requirements into five categories, namely must-be quality, one-dimensional quality, attractive quality, indifferent quality, and reverse quality, based on a customer survey [18]. Kano model emphasizes the degree to which a customer is satisfied when a particular customer need is met. Kano model has been studied in various fields by researchers.

Bayraktaroglu&Ozgen [19] analyzed the user requirements regarding the library services of a state university by applying Kano model. Ma et al. [20] used Kano model to classify the quality characteristics of steering wheels in vehicles. Xu et al. [21] followed an analytical Kano model by using Kano classifiers and a configuration index to measure customer satisfaction quantitatively in design of a car dashboard. He et al. [22] introduced importance-frequency Kano model, and integrated it into QFD using a multi-population adaptive genetic algorithm for designing a home elevator.

Furthermore, since customer interpretations about a product or service quality are typically imprecise and vague, it could make more sense to use Fuzzy set theory to clarify questionnaire results. Fuzzy set theory, first introduced in 1965 by Lotfi Zadeh, provides a quantitative approach to formulate fuzzy data [23]. Lee & Huang [24] presented fuzzy Kano's questionnaire by allowing participants to interpret multiple feeling to reduce the uncertainty of human thought and applied it to the service quality of a theme park. Yadav et al. [25] and Avikal et al. [26] applied fuzzy Kano's questionnaire to categorize aesthetic attributes of a car profile. Wang & Fong [27] analyzed customer preferences for airline services using fuzzy Kano model.

This paper proposes an adjusted Kano model which integrates the Kano model indices, first introduced by Tan & Shen [28], into the formula of satisfaction index (SI) and dissatisfaction index (DI), developed by Berger et al. [29], adding the frequency of reversal quality to the denominator. The present study has shown an approach for fuzzification of Kano model by assigning fuzzy numbers instead of crisp values of Kano model indices, 0.5, 1, and 1.5, for must-be, one-dimensional, and attractive attributes, respectively. Then, the Adjusted Kano-Fuzzy model is integrated into QFD by following the common steps in the planning matrix of HOQ to calculate the absolute and relative importance weights of customer requirements of a baby diaper. According to the literature, limited research [30, 31] has been done on the use of the Kano model to examine the quality characteristics of a textile product.

The baby diapers market size was globally approximately $52.6 billion in 2019, and is forecasted to be $68.3 billion by 2027 with a compound annual growth rate (CAGR) of 5%

from 2021 to 2027 [32]. A baby diaper can be in the form of cloth (reusable) or disposable (single-use), and disposable diapers have dominated the market with more than 90% use [33]. Disposable diapers are included in healthcare and hygiene products in medical textiles, and are made up of nonwoven fabrics. The nonwoven fabrics accounted for 64.29% of global medical textiles market that was approximately $16.7 billion in 2018, and the whole market is expected to grow at a CAGR of 4.9% to $23.3 billion by 2025 [34].

However, disposable diapers may contain chemicals that can cause allergic reactions in infants. In addition, a well-designed baby diaper could be of importance in managing the increasing rate of waste diapers by protecting the environment. In this context, the overall goal of this research is to improve the design of a baby diaper by focusing on the most important customer requirements. In this study, an approach integrating the Kano model into the planning matrix of QFD using Fuzzy logic, was proposed to effectively prioritize the importance weights of customer requirements.

In the next section, some theoretical aspects of QFD, Kano model, Fuzzy logic, and the approaches for integrating Kano model and QFD are discussed. In Section 3, the proposed AKFQFD model is introduced. Applying the proposed model in the design of a baby diaper are presented in Section 4. Discussions and conclusions are presented in Section 5 and 6, respectively.

## 2. LITERATURE REVIEW

### 2.1. Quality function deployment (QFD)

Quality Function Deployment (QFD) is a valid method for designing new products, aiming at customer satisfaction by transforming customer needs into product characteristics, as well as diffusing quality into whole production [35].

A typical HOQ, the first phase of QFD, involves identifying customer needs, determining relative importance of customer needs, detecting major engineering characteristics, building the relationship matrix between customer needs and engineering characteristics, determining tradeoffs in design, obtaining technical performance data of competitors, and setting measurable design targets [7]. Figure 1 shows an example of HOQ including customer needs and engineering characteristics of an airbag.
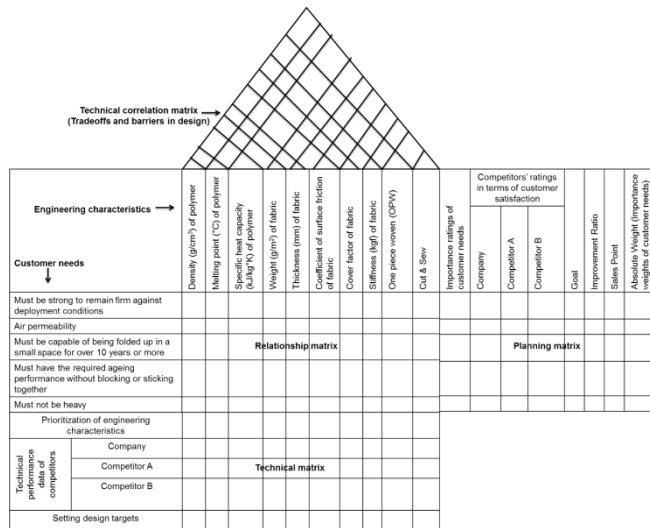
**Figure 1.** House of quality chart

In case of too many customer needs, understanding and prioritizing customer needs accurately may not be guaranteed by traditional HOQ due to complexity in calculations and long implementation times caused by increased matrix sizes. Therefore, integrating quantitative techniques into the HOQ planning matrix can help to diminish computational handicaps.

## 2.2. Kano model

Kano model emphasizes the degree to which a customer is satisfied when a particular customer need is met. The Kano model classifies customer requirements into five categories as follows (Figure 2) [18]:

(1)     Must-be (M): While fulfilling must-be characteristics beyond the expectation does not increase customer satisfaction, the absence of them dissatisfies the customer. For example, a car owner would expect an airbag to deploy properly in case of an accident.

(2)     One-dimensional (O): Customer satisfaction occurs in case of fulfillment of one-dimensional requirements, and dissatisfaction occurs in case of nonfulfillment of them. For example, the more the refrigerator saves energy the more satisfied the customer is.

(3)     Attractive (A): While the presence of attractive characteristics can increase customer satisfaction, the absence of them does not cause any dissatisfaction. These characteristics are mostly not pronounced by customers, and can result in exciting products.

(4)     Indifference (I): It does not matter for customers whether this type of quality is present or not. For instance, package design of a tooth paste may not be an important concern for tooth paste purchasers, which makes this quality as an indifferent characteristic.

(5)     Reverse (R): Customers are satisfied when this type of requirement is nonfulfilled, and they are dissatisfied when it is fulfilled.
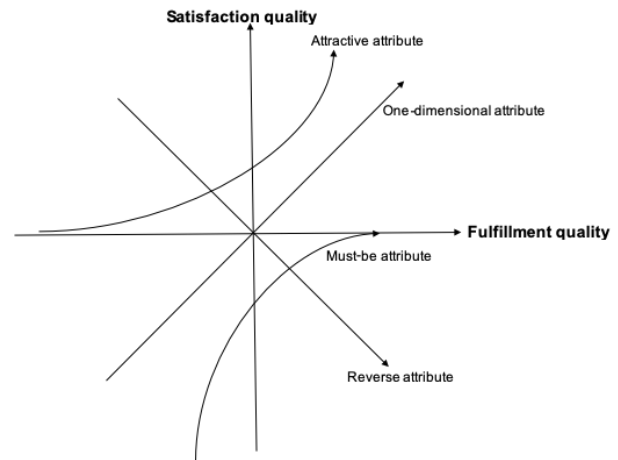


**Figure 2.** Kano model (adapted from [36])

To decide which customer needs are included in which Kano category, a survey should be conducted. To that end, a pair of question, functional and dysfunctional, in case of presence and absence of a particular need how a customer feels, respectively, should be asked. Then, the pair of responses are evaluated according to the Kano table as shown in Table 1. The attribute with the highest response frequency determines the category of the related customer requirement. When customers are either confused or misunderstand the pair of question of a particular need in the survey they do not give logic responses. This type of group is referred to as questionable characteristics (Q).

**Table 1.** Kano evaluation table (adapted from [29])

| Customer Needs | | Dysfunctional Question (e.g., if baby diaper is not soft, how do you feel?) | | | | |
|---|---|---|---|---|---|---|
| | | I like it that way | It must be that way | I am neutral | I can live it that way | I dislike it that way |
| Functional Question (e.g., if baby diaper is soft, how do you feel?) | I like it that way | Q | A | A | A | O |
| | It must be that way | R | I | I | I | M |
| | I am neutral | R | I | I | I | M |
| | I can live it that way | R | I | I | I | M |
| | I dislike it that way | R | R | R | R | Q |

Note: A: attractive, O: one-dimensional, M: must-be, I: indifference, R: reverse, Q: questionable

## 2.3. Fuzzy Set Theory

Lotfi Zadeh who was a professor at the University of California, Berkeley, provided a quantitative approach to formulate vague data by Fuzzy set theory [23]. A fuzzy set is a set of objects in which there is no clear boundary between objects and each object is assigned a degree of membership ranging between zero and one by a membership function [24, 37]. Therefore, fuzzy sets are characterized by membership functions (MFs), where triangular, trapezoidal and Gaussian MFs are commonly used.

A triangular fuzzy number (TFN) $\tilde{A} = (a_1, a_2, a_3)$, in which $a_1 < a_2 < a_3$, and its membership function is defined as follows:

$$\mu_{\tilde{A}}(x) = \begin{cases} 0 & x \leq a_1 \\ \frac{x-a_1}{a_2-a_1} & a_1 \leq a_2 \\ \frac{a_3-x}{a_3-a_2} & a_2 \leq x \leq a_3 \\ 0 & a_3 \leq x \end{cases} \quad (1)$$

To convert the fuzzy set into a numerical (crisp) number the process of defuzzification including center of area, maxima, and bisector methods are carried out. The center of area (gravity) (COA) can be calculated as follows:

$$F_{COA}^{-1} = \frac{\int \mu_{\tilde{A}}(x)x\,dx}{\int \mu_{\tilde{A}}(x)\,dx} \quad (2)$$

According to Gao et al. [38] the calculation of scalar multiplication of a TFN and multiplication of two TFNs can be done as follows:
$\tilde{A} = (a_1, a_2, a_3)$, $a_1 < a_2 < a_3$; and $\tilde{B} = (b_1, b_2, b_3)$, $b_1 < b_2 < b_3$, are two TFNs

$$\lambda * [a_1; a_2; a_3] = [\lambda \times a_1; \lambda \times a_2; \lambda \times a_3] \; \lambda > 0 \quad (3)$$

$$[a_1; a_2; a_3] \times [b_1; b_2; b_3] = [a_1 \times b_1; a_2 \times b_2; a_3 \times b_3] \quad (4)$$

## 2.4. Integration of Kano model into QFD

Since Kano model is helpful for explaining the relationship between the degree of satisfaction and the fulfillment of customer requirements, integrating the Kano model into the planning matrix of HOQ would help deeply to understand the voice of the customer. In this direction, Berger et al. [29] introduced two terms that are satisfaction index (SI) and dissatisfaction index (DI). The SI symbolizes how much a customer satisfaction would be increased in case of fulfillment of a particular customer need, and the DI signifies how much a customer satisfaction would be decreased in case of nonfulfillment of that customer need, which are calculated as follows:

Satisfaction index (SI)= $(f_A + f_O) / (f_A + f_O + f_M + f_I)$ (5)

Dissatisfaction index (DI)= $(-1) (f_O + f_M) / (f_A + f_O + f_M + f_I)$ (6)

Here, $f_A$, $f_O$, $f_M$, $f_I$ are frequency of attractive attribute, frequency of one-dimensional attribute, frequency of must-be attribute, and frequency of indifference attribute, respectively. Furthermore, Wang & Fong [27] and Avikal et al. [26] proposed methods by adding the frequency of reversal attribute ($f_R$) to the denominator to compute the SI and DI. In addition, Tontini [39] introduced the adjustment factor (m) for each customer need, which infuses the Kano result into the importance of a customer requirement, as follows:

$$m = \max\{SI, |DI|\} \quad (7)$$

m: adjustment factor

Tan & Shen [28] proposed a transformation function in which the Kano model indices, k values, are embedded into the original improvement ratio ($IR_o$) that is a component of the planning matrix of HOQ. Here, k values were chosen as 0.5, 1, and 2 for must-be, one-dimensional, and attractive qualities, respectively, to calculate the adjusted improvement ratio ($IR_{adj}$) as follows:

$$IR_{adj} = (IR_o)^{1/k} \quad (8)$$

Chaudha et al. [40] recommended another transformation function to adjust the $IR_o$ using the adjustment factor (m), and Kano model indices, where the k values were 0, 0.5, 1, and 1.5 for indifferent, must-be, one-dimensional, and attractive attributes, respectively, as follows:

$$IR_{adj} = (1+m)^k \times IR_o \quad (9)$$

The original improvement ratio, $IR_o$, a factor determining the importance weights of customer needs, is calculated by dividing the goal by current company rating (Original Improvement Ratio ($IR_o$) = Goal / Current Company Rating). Strategic goals are determined on the basis of the values obtained in the competitive analysis. Furthermore, in most cases, to identify competitors' and company's current ratings whether they meet the customers' requirements, customers are asked how well they are satisfied with the competitors' and company's products utilizing a scale from 1 to 5 with 5 being the most important through mail/e-mail surveys [41, 42]. Similarly, to determine the importance of customer needs customers are usually asked to rank the needs according to a five-point scale through a survey [41, 42]. Then, for both the competitive analysis and the self-stated importance, the value of weighted average performance score for each customer need can be calculated as follows:

$$= \frac{\sum_i (\text{Number of respondents at performance value i}) * i}{\text{Total number of respondents}} \quad (10)$$

$i = 1, 2, 3, 4, 5$

The final importance weights of customer requirements (absolute weights) are generally determined by multiplying the improvement ratio, the self-stated importance, and the value of sales point [28, 29, 42]. The value of sales point for

each customer need is generally determined by the marketing people, which indicates which customer needs, when met, would provide a competitive advantage to the company [6, 7, 42]. In general, three values, 1, 1.2, 1.5, are used for sales points, which are assigned to no competitive advantage or no sales, a slight competitive advantage or medium sales, and a strong competitive advantage or strong sales, respectively [6, 7, 42, 43]. In this study, to illustrate the proposed model efficiently sales point is not taken into account.

## 3. PROPOSED MODEL FOR INTEGRATING KANO MODEL AND FUZZY LOGIC INTO THE PLANNING MATRIX OF HOQ

In this paper, an approach, in which the Kano model indices that are assigned as 0.5, 1, and 1.5 for must-be, one-dimensional, and attractive attributes, respectively, are embedded into the formulae used to calculate the adjustment factor, is proposed by Equations (11-14):

$$w_j = f_j / (f_A + f_O + f_M + f_I + f_R) \qquad j = A, O, M \qquad (11)$$
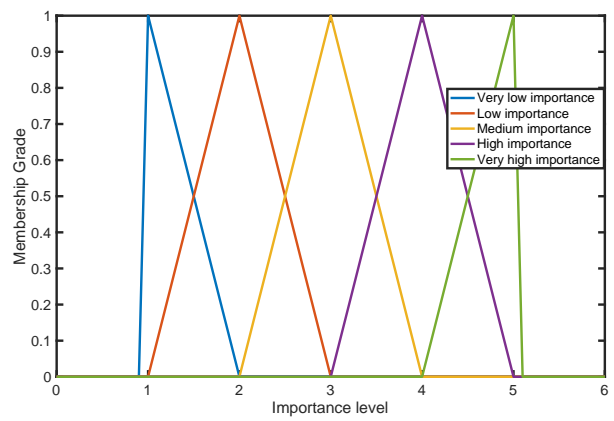
$$SI' = w_A * k_A + w_O * k_O \qquad (12)$$

$$DI' = (-1)(w_O * k_O + w_M * k_M) \qquad (13)$$

$$m' = \max\{SI', |DI'|\} \qquad (14)$$

Here, $k_A$, $k_O$, and $k_M$ represents Kano model indices of attractive, one-dimensional, and must-be qualities, respectively. The integration of Kano model indices to the model would increase the accuracy of understanding the relationship between customer requirements and customer satisfaction by considering the impact factors of each quality attribute. In previous studies it was stated that the quality attributes of Kano model were of different importance, and attractive attributes should be given higher weight since they create more value in terms of customer satisfaction and increase compatibility of products [28, 40, 44, 45]. Tan &Pawitra [44] applied the crisp values of 4, 2, and 1 for attractive, one-dimensional, and must be qualities, respectively as multiplier values for determining relative importance of customer needs. Calisoglu [45] used the Kano model indices 0, 0.5, 1, and 1.5 for indifferent, must-be, one-dimensional, and attractive attributes, respectively, as a multiplier for calculation of sales point. Furthermore, $f_A$, $f_O$, $f_M$, $f_I$, and $f_R$ symbolizes frequencies of attractive, one-dimensional, must-be, indifference, and reversal qualities, respectively. Since reversal quality is included in the Kano model and reflects also customer expectations from a product or service, adding the frequency of reversal quality to the denominator, as shown in Wang & Fong [27] and Avikal et al. [26], would make sense for computing the

adjustment factor, and finally the relative weights of customer needs. The proposed model is illustrated in Table 2.

In the proposed model, the triangular membership function (MF), and the center of area (gravity) (COA) method for the operation of defuzzification are chosen, where MATLAB is used for the calculations. However, other types of MFs (e.g., trapezoidal) could also be used for the proposed model. Figure 3 shows the triangular MF of the importance of customer need, where the fuzzy numbers are used instead of crisp values of 1, 2, 3, 4, and 5 for very low, low, medium, high, and very high significance, respectively. In addition, Figure 4 shows the triangular MF of the Kano model categories, where the Kano model indices that are assigned as 0, 0.5, 1, and 1.5 for indifferent, must-be, one-



dimensional, and attractive attributes, respectively, are indicated by the fuzzy sets. Then, intersection areas are randomly selected as 0.3 for all categories.

**Figure 3.** Triangular membership function of importance of customer need
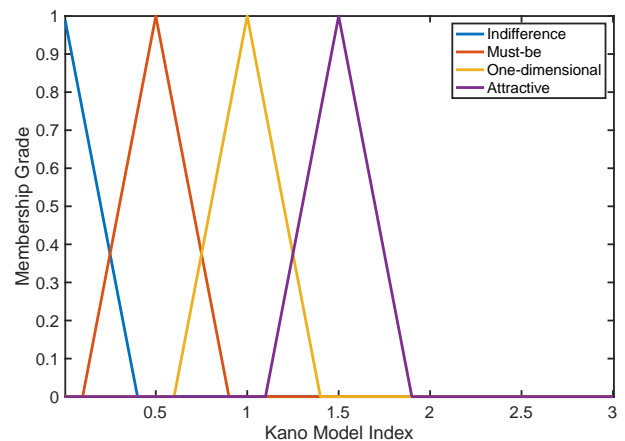


**Figure 4.** Triangular membership function of Kano model categories

**Table2.** Proposed Adjusted Kano-Fuzzy-QFD model

| Steps | Proposed model: Adjusted Kano-Fuzzy-QFD |
|---|---|
| Step 1 | Conducting the preliminary study to identify customer needs. |
| Step 2 | Determining the importance of customer needs by market survey. Here, importance of customer needs are assigned by fuzzy numbers instead of crisp values of 1, 2, 3, 4, and 5 for very low, low, medium, high, and very high significance, respectively. <br><br> <table><tr><td>Very Low</td><td>(1;1;2)</td></tr><tr><td>Low</td><td>(1;2;3)</td></tr><tr><td>Medium</td><td>(2;3;4)</td></tr><tr><td>High</td><td>(3;4;5)</td></tr><tr><td>Very High</td><td>(4;5;5)</td></tr></table> |
| Step 3 | Making Kano questionnaire based on results of market survey. |
| Step 4 | Evaluation of Kano survey according to Kano evaluation table. Attribute gauge chart is plotted to demonstrate how well the respondents agreed with each other for each question (item). |
| Step 5 | Determining the adjustment factor (m′) for each customer need by using the proposed model. Here, Kano model indices are assigned by fuzzy numbers [45]. <br><br> <table><tr><td>Indifference attributes</td><td>(0;0;0.4)</td></tr><tr><td>Must-be attributes</td><td>(0.1;0.5;0.9)</td></tr><tr><td>One-dimensional attributes</td><td>(0.6;1;1.4)</td></tr><tr><td>Attractive attributes</td><td>(1.1;1.5;1.9)</td></tr></table> <br> $w_j = f_j / (f_A + f_O + f_M + f_I + f_R)$        $j = A, O, M$ <br><br> $SI' = w_A * k_A + w_O * k_O$ <br> $DI' = (-1) (w_O * k_O + w_M * k_M)$ <br> $m' = \max\{SI', |DI'|\}$ |
| Step 6 | Doing competitive analysis |
| Step 7 | Setting goal and finding IR |
| Step 8 | Calculation of absolute and relative weights of customer needs |

## 4. APPLYING THE PROPOSED MODEL IN THE DESIGN OF A BABY DIAPER

### 4.1. Body Of A Disposable Baby Diaper

A typical modern disposable baby diaper consists of a topsheet directly contacting with the baby's skin transfering liquid to the underlying layers, a water vapor permeable backsheet forming the outer layer preventing liquid from leaking out of the diaper, and an absorbent core layer positioned between the topsheet and the backsheet [46]. In general, the topsheet consists of a nonwoven structure composed of polypropylene or polypropylene/polyethylene blend, the backsheet is made of polyethylene or polyurethane laminated film, and the core layer comprises superabsorbable polymers (e.g., sodium polyacrylate) and wood pulp covered by cellulose or polypropylene nonwoven fabric [46, 47]. Although the polymers used for diapers are chemically inert materials, the contamination of polymers with monomers, and other impurities (e.g., additives) during the polymerization or manufacturing process can cause allergic reactions in infants [47].

The elastic bands consisting of spandex or synthetic rubber, and the fastening system including adhesives, in the waist and inguinal folds are the other design components for preventing leakage and guaranteeing a good fit to the diaper [47, 48]. However, reports demonstrated that rubber chemicals such as mercaptobenzothiazole, cyclohexylthiophthalimide, and adhesives (e.g., p-tertiary-butylphenol formaldehyde resin) induced contact allergy particulary in case of preceding diaper rash [48–50]. Diaper rash, in other words diaper dermatitis, is a common skin disorder in infants, which occurs mostly in a warm and humid environment with prolonged exposure to urine and feces in the diaper area, making the skin more susceptible to friction and irritation and consequently penetration by substances due to overhydration of skin and maceration [51, 52].

Additionally, diapers could contain dyes (e.g., pigment) for aesthetics purposes, fragrances (e.g. perfume) to mask fecal odor, and lotion, in other words emollients (e.g., zinc oxide, petrolatum) in the topsheet aiming at protecting the skin from overhydration [47, 53]. On the other hand, fragrances (e.g., myroxylonpereirae), disperse dyes, and lotions (e.g., sorbitansesquioleate, lanolin) have been reported as potential allergens in diapers [48, 54].

Since the disclosure of all ingredients of disposable diapers for infants is under no obligation for the manufacturers in the USA and Europe it cannot be possible to trace back all possible chemicals developing allergic reactions [55, 56]. Although it is announced by manufacturers that disposable diapers are approved by dermatologists or pediatricians there is no standardization in this regard [47].

Furthermore, waste absorbent hygiene products including baby diapers account for 1.5%-6.3% of municipal solid waste in Europe [57]. Waste baby diapers that may partially contain also biodegradable materials, have been subject to either incineration or landfilling, causing environmental problems such as greenhouse gas emissions (e.g., methane), and water pollution since the 1970s [58, 59]. Costly, and limited end product quality solutions of current recycling and composting methods of waste diapers pose other handicaps for diapers [58, 60].

### 4.2. Ethical Approval

Ethical approval was obtained from the Social and Human Sciences Ethics Committee of Erciyes University (project number: 222) to conduct surveys for the study. Participation in the study was voluntary.

### 4.3. Applying The Proposed Adjusted Kano-Fuzzy-QFD Model For Determining Of Importance Weights Of Customer Requirements Of A Baby Diaper

#### 4.3.1. Step 1 & Step 2: Conducting The Preliminary Study To Identify Customer Needs And Determining The Importance Of Customer Needs

In the preliminary study, to collect customer needs (CNs), and subsequently enhance the accuracy of data for the Kano customer survey, literature review, market research through commercial websites (e.g., amazon.com), and social networks, one-to-one and face-to-face interviews were conducted. Then, a list of 18 CNs (Table 5) were obtained; however, to find out if there is any missing need a market survey was also carried out.

The market survey had four parts: the first part: informed consent form of the survey; the second part: demographic questions; the third part: a few questions listed in Table 3; the fourth part: respondents were asked to rate the 18 CNs using a five-point scale from 1 to 5, where 1, 2, 3, 4, and 5 signify for very low, low, medium, high and very high importance, respectively.

**Table 3.** Questions of preliminary market survey

| | |
|---|---|
| (i) | What kind of baby diaper do you choose for your baby (i.e., disposable, cloth)? |
| (ii) | What kinds of features did you get from your current baby diaper? |
| (iii) | Which brand do you prefer when you compare the products of different companies? |
| (iv) | What kinds of complaints do you have from your current baby diaper? |
| (v) | What kinds of features do you expect from a baby diaper? |

The survey was deployed to all people in Turkey, where the participation was voluntary. In total, 554 valid responses were received. The results of the third part of the market survey are given in Table 4; all of the respondents were women, and approximately 76% of them had 1 child, 21% of them had two children, and 3% of them had three children.

**Table 4.** Market survey results (N= 554)

| Baby Diaper Type | Response (%) | Diaper Change Frequency Per Day | Response (%) | Brand Preference | Response (%) |
|---|---|---|---|---|---|
| Disposable | 99.46 | 1-3 | 13.18 | Company A | 40.79 |
| Cloth | 0.54 | 4-6 | 65.70 | Company B | 28.88 |
| | | 7-9 | 16.61 | Company C | 15.52 |
| | | >9 | 4.51 | Others | 14.80 |

The majority of the respondents indicated that they have used disposable diapers, and they have changed an average of 4-6 diapers per day, where the results are parallel to those reported in Odio& Friedlander [61] and the UK Environment Agency[62]. In addition, according to the survey the market has been dominated by three companies. Due to confidentiality reasons the company names cannot be declared.

Furthermore, based on the results of the survey it was emphasized that "Baby diaper should not smell of petroleum-based polymers" with the S4 in the list of CNs. The 18 CNs were classified into four categories: aesthetics, performance, safety, and comfort, by considering ergonomic design criteria based on ergonomics literature [12, 17, 63], which is shown in Table 5.

To deal with the last part of the market survey, first, the value of weighted average importance score for each customer need was calculated; second, the corresponding values of the importance that were developed by fuzzy set members were determined and shown in Table 6. The fuzzy numbers used instead of crisp values of 1, 2, 3, 4, and 5, are listed in Table

2 and are shown in Figure 3 for the proposed model.

In order to verify the reliability of the questionnaire, the coefficient of Cronbach's alpha($\alpha$) was calculated as 0.76. Here, a questionnaire with an alpha coefficient of greater than or equal to 0.7 is generally accepted to be reliable in terms of the internal consistency of the items [20, 64].

### 4.3.2. Step 3:Making Kano Survey

The Kano survey had four parts: the first part included the informed consent form of the survey, the second part consisted of 36 questions on 18 baby diaper quality attributes (Table 5), the third part was related to the demographic questions, and the fourth part included the section of competitive analysis for rating the three major brands in the market determined by the market survey, for each quality attribute by using a five point scale from 1 to 5, where the higher the score the higher the perceived satisfaction was.

The second part of the Kano survey was conducted based on the Kano questionnaire including functional and dysfunctional questions as shown in Table 1, which were

The survey was deployed to all people in Turkey, where the participation was voluntary. In total, 344 valid responses were received, where all of the respondents were women, and approximately 77 % of them had 1 child, 21% of them had two children, and 2% of them had three children.

The percent agreement which demonstrates how well the respondents agreed with each other for each question (item) was plotted as shown in Figure 5. The formula of the percent agreement is as follows [65]:

$$\% \text{ Agreement for item i} = \frac{\sum_{l=1}^{k} \binom{number\ of\ responses\ for\ level\ l}{2}}{\binom{N_i}{2}} \quad (15)$$

k = number of levels
$N_i$ = Number of ratings on item i (i = 1,……,n)
n = number of items

The trial version of JMP® 15.1 statistical software was used for the attribute gauge chart shown in Figure 5.

**Table 5.** CNs for a baby diaper

| Primary customer requirements | Item number | Item code | Whats / Customer needs |
|---|---|---|---|
| Aesthetics | 1 | A1 | The package should be well designed |
| | 2 | A2 | The aesthetic appearance (e.g., color, pattern) of the outer surface of baby diaper should be great |
| Performance | 3 | P1 | Baby diaper should not leak pee |
| | 4 | P2 | The waist band of baby diaper should not become deformed when used |
| | 5 | P3 | Baby diaper should have substantially absorptive property |
| | 6 | P4 | Baby diaper should have a good water vapor permeable outer layer |
| | 7 | P5 | Baby diaper leg wraps in the inguinal folds should not be too tight |
| | 8 | P6 | The waist band of baby diaper should exhibit elasticity sufficiently |
| | 9 | P7 | Baby diaper should consist of bio-based (organic) materials |
| Safety | 10 | S1 | Baby diaper should be approved by dermatologists/pediatricians (Baby diaper should be dermatologically tested) |
| | 11 | S2 | Baby diaper should not cause an allergic reaction (Baby diaper should not contain allergenic ingredients) |
| | 12 | S3 | Baby diaper should not cause diaper rash |
| | 13 | S4 | Baby diaper should not smell of chemicals (e.g., petroleum-based polymers) |
| Comfort | 14 | C1 | Baby diaper should contain lotion |
| | 15 | C2 | Baby diaper should be thin |
| | 16 | C3 | Baby diaper should include wetness indicator |
| | 17 | C4 | The smell of pee should not get out of baby diaper |
| | 18 | C5 | Baby diaper should be soft |
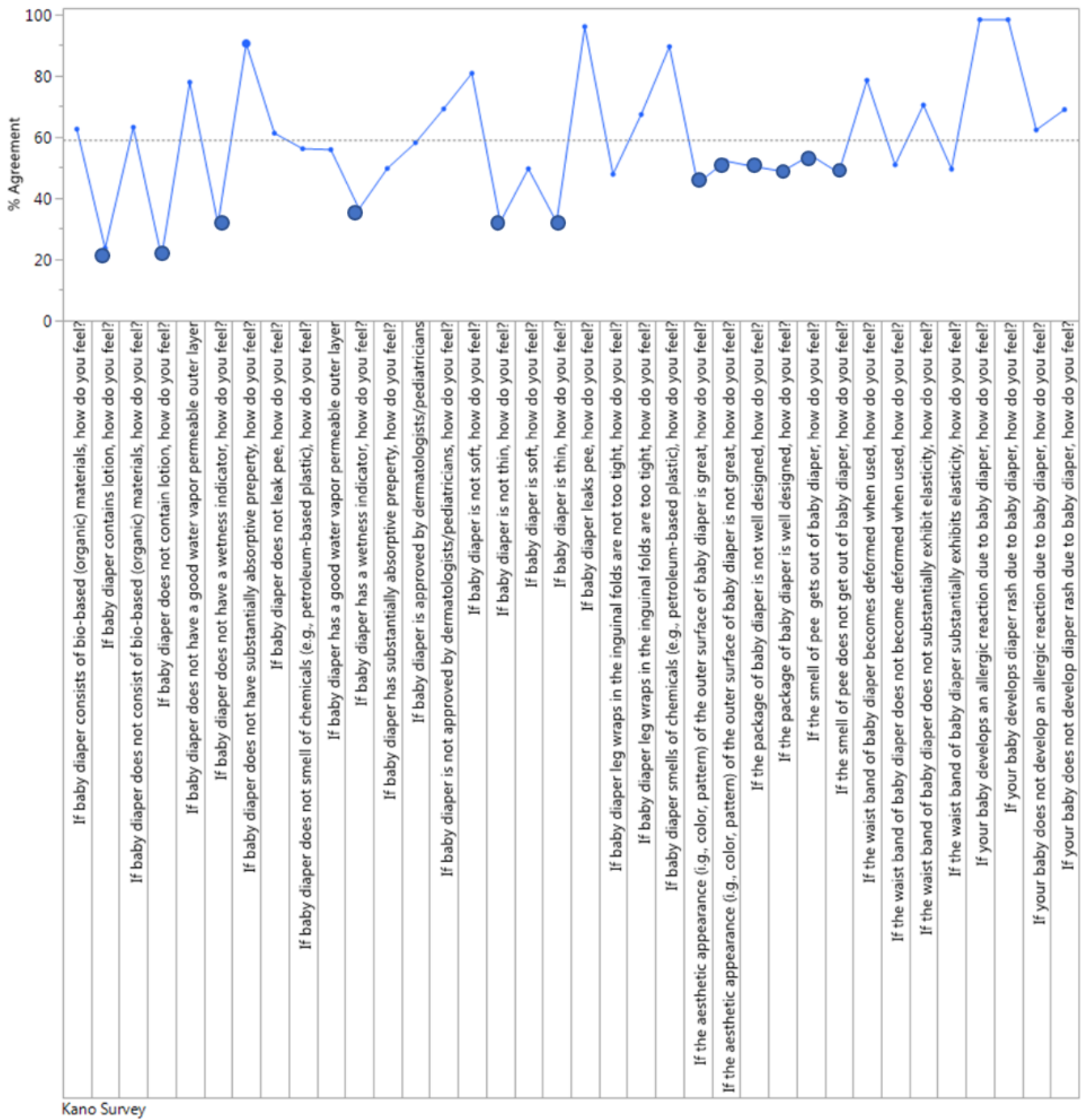
**Figure 5.** Attribute gauge chart of the Kano survey

The points marked with the blue filled circles indicate the six attributes that have lower agreement for their related both functional and dysfunctional questions when compared with those of other attributes. Out of six attributes, two of them belong to the category of aesthetics (A1, A2) and four of them (C1, C2, C3, C4) belong to the category of comfort. Although the lower agreement of the perceptions of aesthetics and comfort could potentially be a consequence of their subjective nature, it increases the variability, and subsequently decreases the internal consistency of the questionnaire.

**4.3.3. Step 4 And Step 5: Evaluation Of Kano Survey According To Kano Evaluation Table And Determining The Adjustment Factors For Each Customer Need**

Table 7 shows the results of the Kano questionnaire, which includes the adjustment factors calculated according to both traditional and proposed method.

The scatter plot of satisfaction index and dissatisfaction index of both methods is shown in Figure 6.

**Table 6.** Importance of customer need and corresponding Fuzzy set members

| Customer needs | Rate of importance | Rate of importance - Fuzzy set members | | |
| --- | --- | --- | --- | --- |
| | | Lower bound | Core | Upper bound |
| A1 | 2 | 1 | 2 | 3 |
| A2 | 3 | 2 | 3 | 4 |
| P1 | 5 | 4 | 5 | 5 |
| P2 | 5 | 4 | 5 | 5 |
| P3 | 5 | 4 | 5 | 5 |
| P4 | 5 | 4 | 5 | 5 |
| P5 | 5 | 4 | 5 | 5 |
| P6 | 5 | 4 | 5 | 5 |
| P7 | 5 | 4 | 5 | 5 |
| S1 | 5 | 4 | 5 | 5 |
| S2 | 5 | 4 | 5 | 5 |
| S3 | 5 | 4 | 5 | 5 |
| S4 | 5 | 4 | 5 | 5 |
| C1 | 3 | 2 | 3 | 4 |
| C2 | 4 | 3 | 4 | 5 |
| C3 | 4 | 3 | 4 | 5 |
| C4 | 4 | 3 | 4 | 5 |
| C5 | 5 | 4 | 5 | 5 |

Equations (5-7) were used for the calculations of the traditional method; whereas Equations (11-14) were used for the calculations of the proposed method. Overall questionable (Q)-rate is not higher than 1%.
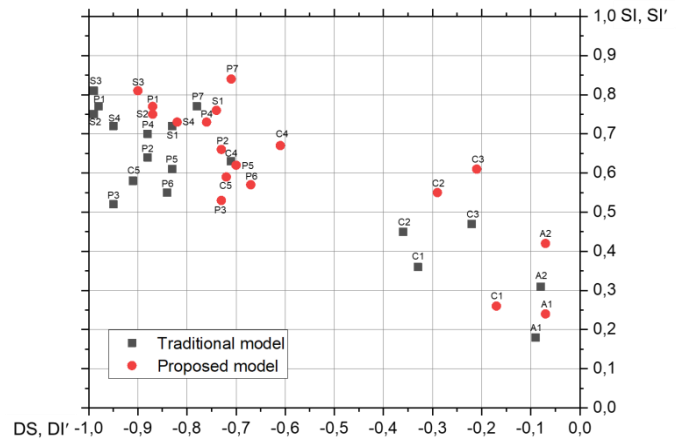


**Figure 6.** Matrix of satisfaction index and dissatisfaction index

### 4.3.4. Step 6 & Step 7: Doing competitive analysis, setting goal and finding IR

The three major brands (competitors) determined by the market survey were rated for each quality attribute, using a five point scale from 1 to 5, with 5 being the highest perceived satisfaction, through the Kano survey. However, since the C1 was found out to be a reverse requirement based on the results of the Kano survey, it was rated as 1. Furthermore, the number of raters for each competitor changed depending on the related brand experienceof the raters.

The value of weighted average performance score for each quality attribute per competitor was calculated; goals were set by the QFD team (here, they are the authors of this paper); and, improvement ratios were found as shown in Table 8.

### 4.3.5. Step 8: Calculation Of Absolute And Relative Weigths Of Customer Requirements

The formula of absolute weight and relative weight are as follows [7, 35]:

Absolute weight$_i$ = $m_i$ x (Importance to customer) x IR$_i$ (16)

$m_i$: the adjustment factor of customer need i

IR$_i$: improvement ratio of customer need i

Relative weight= (absolute weight$_i$)/(maximum absolute weight) (17)

**Table 7.** Results of the Kano questionnaire

| Item code | A | O | M | I | R | Q | Total | Kano category | SI | DI | m | SI′ | DI′ | m′ |
|---|---|---|---|---|---|---|---|---|---|---|---|---|---|---|
| A1 | 43 | 18 | 12 | 270 | | 1 | 344 | I | 0.18 | -0.09 | 0.18 | 0.24 | -0.07 | 0.24 |
| A2 | 80 | 24 | 3 | 232 | 4 | 1 | 344 | I | 0.31 | -0.08 | 0.31 | 0.42 | -0.07 | 0.42 |
| P1 | 2 | 256 | 74 | 5 | | 7 | 344 | O | 0.77 | -0.98 | 0.98 | 0.77 | -0.87 | 0.87 |
| P2 | 18 | 199 | 101 | 21 | 1 | 4 | 344 | O | 0.64 | -0.88 | 0.88 | 0.66 | -0.73 | 0.73 |
| P3 | 4 | 175 | 152 | 12 | 1 | | 344 | O | 0.52 | -0.95 | 0.95 | 0.53 | -0.73 | 0.73 |
| P4 | 22 | 214 | 84 | 19 | | 5 | 344 | O | 0.70 | -0.88 | 0.88 | 0.73 | -0.76 | 0.76 |
| P5 | 8 | 197 | 83 | 48 | 3 | 5 | 344 | O | 0.61 | -0.83 | 0.83 | 0.62 | -0.70 | 0.70 |
| P6 | 15 | 173 | 111 | 40 | 2 | 3 | 344 | O | 0.55 | -0.84 | 0.84 | 0.57 | -0.67 | 0.67 |
| P7 | 44 | 217 | 45 | 32 | | 6 | 344 | O | 0.77 | -0.78 | 0.78 | 0.84 | -0.71 | 0.84 |
| S1 | 26 | 218 | 65 | 30 | | 5 | 344 | O | 0.72 | -0.83 | 0.83 | 0.76 | -0.74 | 0.76 |
| S2 | 1 | 256 | 84 | 1 | | 2 | 344 | O | 0.75 | -0.99 | 0.99 | 0.75 | -0.87 | 0.87 |
| S3 | 1 | 277 | 64 | 2 | | | 344 | O | 0.81 | -0.99 | 0.99 | 0.81 | -0.90 | 0.9 |
| S4 | 8 | 235 | 86 | 10 | 1 | 4 | 344 | O | 0.72 | -0.95 | 0.95 | 0.73 | -0.82 | 0.82 |
| C1 | 27 | 49 | 19 | 114 | 130 | 5 | 344 | R | 0.36 | -0.33 | 0.36 | 0.26 | -0.17 | 0.26 |
| C2 | 71 | 78 | 41 | 141 | 6 | 7 | 344 | I | 0.45 | -0.36 | 0.45 | 0.55 | -0.29 | 0.55 |
| C3 | 95 | 65 | 11 | 168 | 3 | 2 | 344 | I | 0.47 | -0.22 | 0.47 | 0.61 | -0.21 | 0.61 |
| C4 | 32 | 180 | 59 | 64 | 6 | 3 | 344 | O | 0.63 | -0.71 | 0.71 | 0.67 | -0.61 | 0.67 |
| C5 | 11 | 186 | 122 | 21 | 3 | 1 | 344 | O | 0.58 | -0.91 | 0.91 | 0.59 | -0.72 | 0.72 |

Note: A: attractive attribute, O: one-dimensional attribute, M: must-be attribute, I: indifference attribute, R: reversal attribute, Q: questionable attribute, SI: satisfaction index according to the traditional method, DI: dissatisfaction index according to the traditional method, SI′: satisfaction index according to the proposed method, DI′: dissatisfaction index according to the proposed method, m: adjustment factor according to the traditional method, m′: adjustment factor according to the proposed method

The absolute and relative weight results of customer needs according to both proposed and traditional models are shown in Table 9. The lower bound, core, and upper bond of the absolute weight for each CN for the proposed model was calculated taking into account SI′ or $|DI'|$ whichever had the higher score. The fuzzy numbers shown in Table 2, and the center of area (gravity) (COA) method for the operation of defuzzification were applied through MATLAB.

**Table 8.** Competitive analysis, setting goal and finding IR

| Customer needs | Company A (N = 255) | Company B (N=231) | Company C (N= 207) | Our Product | Goal | Improvement Ratio (IR) |
|---|---|---|---|---|---|---|
| A1 | 4.2 | 4.1 | 3.9 | 1 | 4 | 4 |
| A2 | 4.2 | 4.1 | 3.9 | 1 | 4 | 4 |
| P1 | 4.1 | 3.6 | 3.4 | 1 | 5 | 4 |
| P2 | 4.3 | 4.1 | 3.9 | 1 | 4 | 4 |
| P3 | 4.3 | 3.7 | 3.5 | 1 | 4 | 4 |
| P4 | 4.1 | 3.9 | 3.6 | 1 | 4 | 4 |
| P5 | 4.2 | 3.9 | 3.8 | 1 | 4 | 4 |
| P6 | 4.3 | 4.0 | 3.9 | 1 | 4 | 4 |
| P7 | 3.2 | 4.3 | 3.4 | 1 | 5 | 5 |
| S1 | 4.1 | 4.3 | 4.1 | 1 | 4 | 4 |
| S2 | 4.2 | 4.1 | 3.9 | 1 | 5 | 5 |
| S3 | 4.3 | 3.9 | 3.7 | 1 | 5 | 5 |
| S4 | 3.2 | 4.3 | 3.6 | 1 | 5 | 5 |
| C1 | 1 | 1 | 1 | 1 | 1 | 1 |
| C2 | 4.3 | 3.7 | 3.3 | 1 | 4 | 4 |
| C3 | 4.3 | 4.2 | 4.0 | 1 | 4 | 4 |
| C4 | 3.8 | 3.4 | 3.4 | 1 | 4 | 4 |
| C5 | 4.3 | 3.9 | 3.6 | 1 | 4 | 4 |

## 5. RESULTS AND DISCUSSION

Based on the results of the Kano questionnaire evaluation (Table 7), among the 18 customer needs, 13 were classified as one-dimensional, 4 were classified as indifferent, and 1 was classified as reverse. Here, the most frequent responses were categorized as one-dimensional or indifferent. It can be argued that this could be slightly different. For example, P3, having a baby diaper that should have substantially absorptive property, was classified as a one-dimensional attribute. On the other hand, P3 is considered as a primary function of a baby diaper and, it is expected to be a must-be attribute. However, commenting on the subject to the participants may cause subjective bias.

Figure 7 and 8 show the graphs of relative importance of customer requirements according to the proposed and traditional model, respectively.
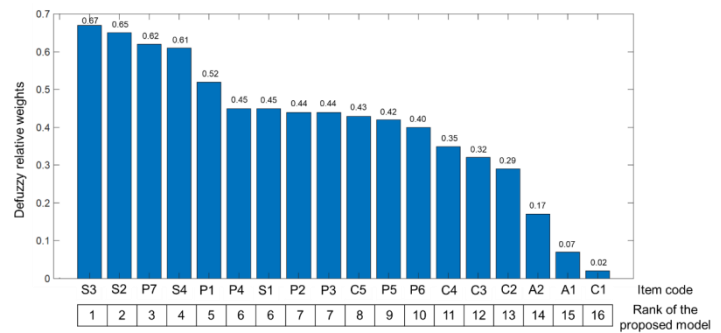


**Figure 7.** Defuzzy relative weights of the proposed model
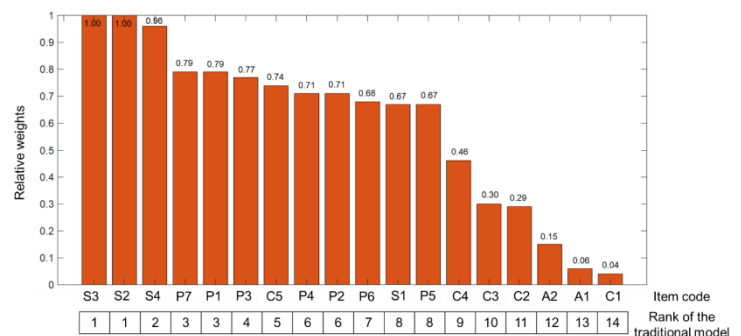


**Figure 8.** Relative weights of the traditional model

According to the relative weights of both models, the safety and performance design criteria have the highest priority which are followed by the comfort criteria, and the aesthetic design criteria are of the least importance. However, the comfort and aesthetic design criteria could be the future attractive attributes [40, 66]. Since C1 was found out to be a reverse attribute it is ranked at the end of the list. Although the frequency of reverse attribute for the requirements other than C1 are negligible, it cannot be ignored for CN1 due to the allergic ingredients potentially included in lotions. In addition, leading diaper manufacturers differ in whether to add lotion to the top sheet.

When the two models are compared, there are some changes in the ranking lists. While in the traditional model, 8 customer needs share 4 ranks: S3 and S2 = rank#1, P7 and P1= rank#3, P2 and P4= rank#6, P5 and S1= rank#8; in the proposed model just 4 customer needs share 2 ranks: P4 and S1= rank#6, P2 and P3= rank#7. Unlike the traditional model, in the proposed model, P7, having a baby diaper that should consist of bio-based materials, is the third significant customer need ranked before S4, having a baby diaper that should not smell of chemicals. Here, the result of the proposed model seems to be logical. On the contrary to the traditional model, in the proposed model, P4, having a baby diaper with a good water vapor permeable outer layer is ranked before P3, having a baby diaper with substantially

**Table 9.** Absolute and relative weight results of both proposed model and traditional model

| Customer needs | Absolute weights | | | Relative weights | | | Defuzzy relative weights of the proposed model | Absolute weights of the traditional model | Relative weights of the traditional model |
|---|---|---|---|---|---|---|---|---|---|
| | Lower bound | Core | Upper bound | Lower bound | Core | Upper bound | | | |
| A1 | 0.68 | 1.92 | 3.74 | 0.02 | 0.06 | 0.12 | 0.07 | 1.44 | 0.06 |
| A2 | 2.39 | 5.04 | 8.66 | 0.07 | 0.16 | 0.27 | 0.17 | 3.72 | 0.15 |
| P1 | 7.64 | 17.39 | 25.22 | 0.24 | 0.54 | 0.78 | 0.52 | 19.6 | 0.79 |
| P2 | 6.09 | 14.68 | 21.74 | 0.19 | 0.45 | 0.67 | 0.44 | 17.6 | 0.71 |
| P3 | 5.59 | 14.59 | 22.20 | 0.17 | 0.45 | 0.69 | 0.44 | 19 | 0.77 |
| P4 | 6.46 | 15.10 | 22.14 | 0.20 | 0.47 | 0.68 | 0.45 | 17.6 | 0.71 |
| P5 | 5.97 | 14.07 | 20.68 | 0.18 | 0.43 | 0.64 | 0.42 | 16.6 | 0.67 |
| P6 | 5.39 | 13.40 | 20.06 | 0.17 | 0.41 | 0.62 | 0.40 | 16.8 | 0.68 |
| P7 | 10.57 | 20.93 | 28.65 | 0.33 | 0.65 | 0.89 | 0.62 | 19.5 | 0.79 |
| S1 | 7.52 | 15.16 | 20.92 | 0.23 | 0.47 | 0.65 | 0.45 | 16.6 | 0.67 |
| S2 | 9.47 | 21.78 | 31.73 | 0.29 | 0.67 | 0.98 | 0.65 | 24.75 | 1.00 |
| S3 | 10.03 | 22.46 | 32.37 | 0.31 | 0.69 | 1.00 | 0.67 | 24.75 | 1.00 |
| S4 | 8.80 | 20.44 | 29.88 | 0.27 | 0.63 | 0.92 | 0.61 | 23.75 | 0.96 |
| C1 | 0.35 | 0.79 | 1.41 | 0.01 | 0.02 | 0.04 | 0.02 | 1.08 | 0.04 |
| C2 | 4.45 | 8.76 | 14.49 | 0.14 | 0.27 | 0.45 | 0.29 | 7.2 | 0.29 |
| C3 | 5.04 | 9.71 | 15.88 | 0.16 | 0.30 | 0.49 | 0.32 | 7.52 | 0.30 |
| C4 | 5.04 | 10.70 | 18.35 | 0.16 | 0.33 | 0.57 | 0.35 | 11.36 | 0.46 |
| C5 | 5.77 | 14.40 | 21.59 | 0.18 | 0.44 | 0.67 | 0.43 | 18.2 | 0.74 |

absorptive property. Here, to obtain a baby diaper with substantially absorptive property leading diaper manufacturers use superabsorbable polymers that reduce the leakage values below 2% [67]. Furthermore, a baby diaper with a good water vapor permeable outer layer is critical in terms of not developing diaper rash. Such being the case, P4 involves more design challenges than P3, which makes the results of the proposed model valid. In addition, S1, having a baby diaper with the approval of dermatologists/pediatricians, is ranked before C5, having a soft baby diaper, in the proposed model unlike the traditional model. Here, S1 is included in the safety design criteria, and is related to baby health; thus, S1 is not expected to be less important than C5.

As the quality attributes used to calculate customer SI and customer DI are not equal as stated in the current literature [28, 40] the integration of the Kano model indice of k to the computation of the adjustment factor (m) would finally adjust the original improvement ratio, and consequently final importance of customer requirements. Furthermore, reversal attribute sometimes can alert unrecognized things related to a requirement as shown in C1. Therefore, adding the frequency of reversal quality to the denominator of the customer SI and customer DI formula would be meaningful while obtaining final importance values. Since customer interpretations about a product or service are typically vague, it could make more sense to use fuzzy membership functions instead of crisp numbers to clarify questionnaire results.

In recent years, fuzzy Kano's questionnaire (FKQ) has been introduced, which deals with multiple answers rather than a single answer, unlike the traditional Kano's questionnaire (TKQ) [24]. However, like the TKQ, the FKQ is still conducted with functional and dysfunctional question pair for each CN, in which the Kano evaluation table is used for every participant's answer pair for each CN. Therefore, FKQ can be said to take more time than TKQ, and still to maintain uncertainties regarding human judgements.

However, since this study focused on just one product, further research is required to investigate the proposed model by taking into account the plausible values of the attribute-driven Kano model indices for designing of different products. In addition, the integration of the proposed model with other methodologies including Artificial Neural Networks (ANNs), Analytical Hierarchy Process (AHP) should be studied to evaluate its performance in prioritizing customer requirements.

## 6. CONCLUSION

In this study, the Adjusted Kano-Fuzzy-Quality Function Deployment (QFD) (AKFQFD) approach is presented in order to better understand the relationship between customer requirements and customer satisfaction, and consequently to increase the accuracy of determining the importance weights of customer requirements in product design. It is aimed to improve the existing Kano-QFD approaches by considering

the impact factor of each quality attribute, that is Kano model indices, while calculating the adjustment factor (m) which is embedded into the QFD. Furthermore, fuzzy logic has been proposed by assigning fuzzy numbers instead of crisp values of Kano model indices, 0.5, 1, and 1.5, for must-be, one-dimensional, and attractive attributes, respectively, to manage the vagueness of customer interpretations about a product. In addition, since the reverse quality also reflects customer expectations in product or service design it makes sense to add its frequency to the denominator of the satisfaction index and dissatisfaction index.

The proposed AKFQFD model was applied for determining the importance weights of CNs of a baby diaper, in which the CNs were divided into four categories: aesthetics, performance, safety, and comfort. It has been shown that the proposed model helps to distinguish the CNs within the same category, and to prioritize the CNs of a baby diaper effectively. Hence, considering the impact factor of each Kano quality category while determining customer satisfaction or customer dissatisfaction, would facilitate decisions of companies in product design by effectively prioritizing customer needs.

However, it is generally accepted that dealing with the subjectivity is complex, and this paper develops an approximate method for the adjustment factor. Further study is needed to examine the potential values of the attribute-driven Kano model indices. Furthermore, future work should focus on studying the integration of the proposed approach with other methodologies such as Analytical Hierarchy Process (AHP) to improve the model.

## Conflicts of interest

The authors declare that there are no conflicts of interest

## REFERENCES

[1]     Markham, SK., Lee, H., "Product development and management association's 2012 comparative performance assessment study", *Journal of Product Innovation Management,* 30(3):408–429. DOI 10.1111/jpim.12025, 2013.

[2]     Lee, H., Markham, SK., "PDMA Comparative Performance Assessment Study (CPAS): Methods and Future Research Directions", *Journal of Product Innovation Management,* 33:3–19. DOI 10.1111/jpim.12358, 2016.

[3]     Page, AL., "Assessing New Product Development Practices and Performance: Establishing Crucial Norms", *Journal of Product Innovation Management,* 10(4):273–290, 1993.

[4]     Thia, CW., Chai, KH., Bauly, J., Xin, Y., "An exploratory study of the use of quality tools and techniques in product development", *The Total Quality Management Magazine,* 17(5):406–424. DOI 10.1108/09544780510615924, 2005.

[5]     Daetz, D., "Planning for customer satisfaction with quality function deployment", *in Proceedings of the Eighth International Conference of the ISQA,* (November, Jerusalem, Israel, 1990)

[6]     Bicknell, BA., Bicknell, KD., *The road map to repeatable success: using QFD to implement change.* USA: CRC Press, 1995

[7]     Cohen, L., *Quality function deployment: how to make QFD work for you.* USA: Addison Wesley Longman, Inc., 1995.

[8]     Cristiano, JJ., Liker, JK., White, CC., "Customer-Driven Product Development Through Quality Function Deployment in the U.S. and Japan", *Journal of Product Innovation Management,* 17(4):286–308. DOI 10.1111/1540-5885.1740286, 2000.

[9]     Urban, GL., Hauser, JR., *Design and Marketing of New Products.* UK: Pearson Education Limited, 1993.

[10]     Sullivan, PL., "Quality Function Deployment", *Quality Progress,* 39–50, 1986.

[11]     Herrmann, A., Huber, F., Algesheime, R., Tomczak, T., "An empirical study of quality function deployment on company performance", *International Journal of Quality & Reliability Management,* 23(4):345–366. DOI 10.1108/02656710610657576, 2006.

[12]     Zhang, F., Yang, M., Liu, W., "Using integrated quality function deployment and theory of innovation problem solving approach for ergonomic product design", *Computers and Industrial Engineering,* 76(1):60–74. DOI 10.1016/j.cie.2014.07.019, 2014.

[13]     Marsot, J., "QFD: A methodological tool for integration of ergonomics at the design stage", *Applied Ergonomics,* 36(2):185-192. DOI 10.1016/j.apergo.2004.10.005, 2005.

[14]     Durga, Prasad, KG., Prasad, MV., Hima, Gireesh, C., Chaitanya, VVVNK., *QFD-Based Ergonomic Design of Drafting Table for Engineering Students: A Case Study.* In: Ray, PK., Maiti, J. editors. Ergonomic Design of Products and Worksystems - 21st Century Perspectives of Asia. USA: Springer, 139–153, 2018.

[15]     Demirbilek, O., Demirkan, H., "Universal product design involving elderly users: A participatory design model", *Applied Ergonomics,* 35(4):361–370. DOI 10.1016/j.apergo.2004.03.003, 2004.

[16]     Tayyari, F., Smith, JL., *Occupational ergonomics: principles and applications.* USA: Springer, 1997.

[17]     Dul, J., Bruder, R., Buckle, P., Carayon, P., Falzon, P., Marras, WS. et al., "A strategy for human factors/ergonomics: developing the discipline and profession", *Ergonomics,* 55(4):377–395. DOI 10.1080/00140139.2012.661087, 2012.

[18]     Kano, N., "Attractive quality and must-be quality", *The Journal of Japanese Society for Quality Control,* 14:39–48, 1984.

[19]     Bayraktaroğlu, G., Özgen, Ö., "Integrating the Kano model, AHP and planning matrix QFD application in library services", *Library Management,* 29(4–5):327–351. DOI 10.1108/01435120810869110, 2008.

[20]     Ma, M., Chen, C., "Using Kano model to differentiate between future vehicle-driving services", *International Journal of Industrial Ergonomics,* 69:142–152. DOI 10.1016/j.ergon.2018.11.003, 2019.

[21]     Xu, Q., Jiao, RJ., Yang, X., Helander, M., Khalid, HM., Opperud, A., "An analytical Kano model for customer need analysis", *Design Studies,* 30(1):87–110. DOI 10.1016/j.destud.2008.07.001, 2009.

[22]     He, L., Song, W., Wu, Z., Xu, Z., Zheng, M., Ming, X., "Quantification and integration of an improved Kano model into QFD based on multi-population adaptive genetic algorithm", *Computers and Industrial Engineering,* 114, 183–194. DOI 10.1016/j.cie.2017.10.009, 2017.

[23]     Zadeh, LA., "Fuzzy sets", *Information and Control,* 8(3):338–353. DOI 10.1016/S0019-9958(65)90241-X, 1965.

[24]     Lee, YC., Huang, SY., "A new fuzzy concept approach for Kano's model", *Expert Systems with Applications,* 36(3):4479–4484. DOI 10.1016/j.eswa.2008.05.034, 2009.

[25]     Yadav, HC., Jain, R., Shukla, S., Avikal, S., Mishra, PK., "Prioritization of aesthetic attributes of car profile", *International Journal of Industrial Ergonomics,* 43(4):296–303. DOI 10.1016/j.ergon.2013.04.008, 2013.

[26]     Avikal, S., Singh, R., Rashmi, R., "QFD and Fuzzy Kano model based approach for classification of aesthetic attributes of SUV car profile", *Journal of Intelligent Manufacturing,* 31(2):271–284. DOI 10.1007/s10845-018-1444-5, 2020.

[27]     Wang, CH., Fong, HY., "Integrating fuzzy Kano model with importance-performance analysis to identify the key determinants of customer retention for airline services", *Journal of Industrial and Production Engineering,* 33(7):450–458. DOI 10.1080/21681015.2016.1155668, 2016.

[28]     Tan, KC., Shen, XX., "Integrating Kano's model in the planning matrix of quality function deployment", *Total Quality Management,* 11(8):1141–1151. DOI 10.1080/095441200440395, 2000.

[29]     Berger, C., Blauth, R., Boger, D., "Kanos methods for understanding customer defined quality", *Center for Quality of Management Journal,* 2(4):2–28, 1993.

[30]     Salahuddin, M., Lee, YA., "Identifying key quality features for wearable technology embedded products using the Kano model", *International Journal of Clothing Science*

*and Technology,* 33(1), 93–105:DOI 10.1108/IJCST-08-2019-0130, 2020.

[31] Jeyaraj, KL., Muralidharan, C., Senthilvelan, T., Deshmukh, SG. (2014) Customer Needs and Customer Satisfaction Analysis in a Textile Dyeing Process. *Clothing and Textiles Research Journal,* 32(4):282–295. DOI 10.1177/0887302X14546362, 2014.

[32] Allied Market Research, www.alliedmarketresearch.com/baby-diapers-market, Baby Diapers Market by Product Type: Global Opportunity Analysis and Industry Forecast, 2021-2027 (Visited on May 24, 2021).

[33] EDANA, https://www.edana.org, Sustainability Report 2011 (Visited on Sept. 10, 2020).

[34] GVR, https://www.grandviewresearch.com/industry-analysis/medical-textiles-market, Medical Textiles Market Size & Share | Global Industry Report, 2025 (Visited on Sept. 10, 2020).

[35] Akao, Y., QFD: *Intergating Customer Requirements into Product Design.* UK: Taylor and Francis Ltd., 1990.

[36] Kametani, T., Nishina, K., Suzuki, K., *Attractive quality and must-be quality from the viewpoint of environmental lifestyle in Japan.* In Lenz, HJ., Wilrich, PT., Schmid, W. editors, Frontiers in Statistical Quality Control 9. USA: Springer, 315–327, 2010.

[37] Kahraman, C., Cebeci, U., Ulukan, Z., "Multi-criteria supplier selection using fuzzy AHP", *Logistics Information Management,* 16(6), 382–394. DOI 10.1108/09576050310503367, 2003.

[38] Gao, S., Zhang, Z., Cao, C., "Multiplication Operation on Fuzzy Numbers. Journal of Software", 4(4), 331–338, 2009.

[39] Tontini, G., "Integrating the Kano Model and QFD for Designing New Products", *Total Quality Management,* 18(6), 599–612. DOI 10.1080/14783360701349351, 2007.

[40] Chaudha, A., Jain, R., Singh, AR., Mishra, PK., "Integration of Kano's Model into quality function deployment (QFD)", *International Journal of Advanced Manufacturing Technology,* 53, 689–698. DOI 10.1007/s00170-010-2867-0, 2011.

[41] Francheschini, F., *Advanced Quality Function Deployment.* USA: CRC Press, 2001.

[42] Chan, LK., Wu, ML., "Quality Function Deployment: A Comprehensive Review of Its Concepts and Methods", *Quality Engineering,* 15(1):23–35. DOI 10.1081/QEN-120006708, 2002.

[43] Akao, Y., *Quality function deployment: integrating customer requirements into product design.* UK: Productivity Press, 1990.

[44] Tan, KC., Pawitra, TA., "Integrating SERVQUAL and Kano's model into QFD for service excellence development", *Managing Service Quality,* 11(6):418–430. DOI 10.1108/EUM0000000006520, 2001.

[45] Calisoglu, C., "An integrated approach to innovative product development using fuzzy logic, kano model and quality function deployment", MSc. thesis, Bogazici University Institute of Engineering and Science, İstanbul, 2013.

[46] Kosemund, K., Schlatter, H., Ochsenhirt, JL., Krause, EL., Marsman, DS., Erasala, GN., "Safety evaluation of superabsorbent baby diapers", *Regulatory Toxicology and Pharmacology,* 53(2):81–89. DOI 10.1016/j.yrtph.2008.10.005, 2009.

[47] Yu, J., Treat, J., Chaney, K., "Potential allergens in disposable diaper wipes, topical diaper preparations, and disposable diapers: under-recognized etiology of pediatric perineal dermatitis", *Dermatitis,* 27(3):110–118. DOI 10.1097/DER.0000000000000177, 2016.

[48] Di Altobrando, A., Gurioli, C., Vincenzi, C., Bruni, F., Neri, I., "Allergic contact dermatitis caused by the elastic borders of diapers", *Contact Dermatitis,* 82(1):71–72. DOI 10.1111/cod.13401, 2020.

[49] Belhadjali, H., Giordano, Labadie, F., Rance, F., Bazex, J., ""Lucky Luke" contact dermatitis from diapers: A new allergen?", *Contact Dermatitis,* 44(4):246–263. DOI 10.1034/j.1600-0536.2001.440409-3.x, 2001.

[50] Jacob, SE., Herro, EM., Guide, S., Cunningham, B., Connelly, EA., "Allergic Contact Dermatitis to PampersTMDrymax", *Pediatric Dermatology,* 29(5):672–674. DOI 10.1111/j.1525-1470.2011.01588.x, 2012.

[51] Muniz, AE., Dermatitis. In Baren J, editor. *Pediatric emergency medicine.* USA: Elsevier, 859–870, 2008.

[52] Ojeda, AB., Mendez, MD., *Diaper Dermatitis.* USA: StatPearls Publishing, 2020.

[53] Runeman, B., "Skin interaction with absorbent hygiene products", *Clinics in Dermatology,* 26(1):45–51. DOI 10.1016/j.clindermatol.2007.10.002, 2008.

[54] Cohen, B., "Differential Diagnosis of Diaper Dermatitis", *Clinical Pediatrics,* 56(5):16S-22S. DOI 10.1177/0009922817706982, 2017.

[55] Code of Federal Register (CFR), https://www.accessdata.fda.gov/scripts/cdrh/cfdocs/cfcfr/CFRSearch.cfm?fr=701.3, US FDA designation of ingredients (Visited on Dec. 5, 2020).

[56] Lee, BM., Choi, M., Shin, I., Kim, J., Choi, Z., Kim, K. et al., "Risk communication for labeling all ingredients in consumer products", *Journal of Toxicology and Environmental Health,* Part A, 83(13–14):509–524. DOI 10.1080/15287394.2020.1780174, 2020.

[57] EDANA, https://www.edana.org, Sustainability Report 5th Edition (Visited on Nov. 8, 2020).

[58] Cordella, M., Bauer, I., Lehmann, A., Schulz, M., Wolf, O., "Evolution of disposable baby diapers in Europe: Life cycle assessment of environmental impacts and identification of key areas of improvement", *Journal of Cleaner Production,* 95:322–331. DOI 10.1016/j.jclepro.2015.02.040, 2015.

[59] Karimi, H., Yu, QL., Brouwers, HJH., "Valorization of waste baby diapers in concrete", *Resources, Conservation and Recycling,* 153:1045-1048. DOI /10.1016/j.resconrec.2019.104548, 2020.

[60] Manuel, J., Mendoza, F., Popa, SA., D'aponte, F., Gualtieri, D., Azapagic, A., "Improving resource efficiency and environmental impacts through novel design and manufacturing of disposable baby diapers", *Journal of Cleaner Production,* 210:916–928, 2019.

[61] Odio, M., Friedlander, SF., "Diaper dermatitis and advances in diaper technology", *CurrentOpinion in Pediatrics,* 12(4):342–346, 2000.

[62] UK Environment Agency, www.environment-agency.gov.uk, Life Cycle Assessment of Disposable and Reusable Nappies in the UK (Visited on Oct. 11, 2020).

[63] Wellings, T., Williams, M., Tennant, C., "Understanding customers' holistic perception of switches in automotive human-machine interfaces", *Applied Ergonomics,* 41(1):8–17. DOI 10.1016/j.apergo.2009.03.004, 2010.

[64] Hair, JF., Black, WC., Babin, BJ., Anderson, RE., *Multivariate Data Analysis.* UK: Pearson Education Limited, 2013.

[65] JMP, www.jmp.com, The Attribute Gauge Chart and Reports (Visited on May 24, 2021).

[66] Kano, N., "Life Cycle and Creation of Attractive Quality", *in Proceedings of the 4th International QMOD Conference Quality Management and Organizational Development,* (LinkopingsUniversitet, Sweden, 2001).

[67] Sannino, A., Demitri, C., Madaghiele, M., "Biodegradable cellulose-based hydrogels: Design and applications", *Materials,* 2(2):353–373. DOI 10.3390/ma2020353, 2009.

**Academic Platform Journal of Engineering and Science**

*journal homepage:* *https://dergipark.org.tr/tr/pub/apjes*

# Feature Selection Based Data Mining Approach for Coronary Artery Disease Diagnosis

*[1]Kemal Akyol

[1]Kastamonu University, Department of Computer Engineering, Kastamonu, 37100, Turkey, kakyol@kastamonu.edu.tr,

**Abstract**

Cardiovascular diseases responsible for many deaths are very common and important health problems. According to World Health Organization, each year 17.7 million people die because of them. Coronary artery disease is the most important type of cardiovascular diseases that cause serious heart problems in patients, affecting the heart's function negatively. Being aware of the important attributes for this disease will help field-specialist in the analysis of routine laboratory test results of a patient coming internal medicine or another medicine unit except for the cardiology unit. In this study, it is aimed to determine the significance of attributes for coronary artery disease by utilizing Stability Selection method. In experiments, the attributes; 'Age', 'Atypical', 'Blood pressure', 'Current smoker', 'Diastolic murmur', 'Dyslipidemia', 'Diabetes mellitus', 'Ejection fraction', 'Erythrocyte sedimentation rate', 'Family history', 'Hypertension', 'Potassium', 'Nonanginal', 'Pulse rate', 'Q wave', 'Regional wall motion abnormality', 'Sex', 'St Depression', 'Triglyceride', 'Tinversion', 'Typical chest pain' and 'Valvular heart disease' were found important for each sub-dataset. Besides, the performances of four traditional machine learning algorithms were evaluated to detection of this disease. Logistic Regression algorithm outperformed others with %90.88 value of accuracy, 95.18% value of sensitivity, and 81.34% value of specificity.

*Keywords:* Medical data, coronary artery disease, attribute selection, stability selection, machine learning.

## 1. INTRODUCTION

Cardiovascular diseases responsible for many deaths are very common and important health problems. World Health Organization[1] reports that every year 17.7 million people die and 31% of all deaths occur as a result of cardiovascular diseases. 80% of cardiovascular deaths are heart attacks and strokes. Tobacco use, unhealthy diet and physical inactivity are among the causes that increase the risk of heart attack and stroke. They cause blood pressure, glucose, and lipids in addition to causing overweight and obesity for individuals. Coronary artery disease (CAD) is the most important type of cardiovascular diseases that cause serious heart problems in patients, affecting the heart's function negatively [1].

People who have high cardiovascular risk should be routinely controlled because there are many known and unknown risk factors considered to cause this disease [2]. Therefore, various learning algorithms have been used by researchers in order to find out these risk factors so far. For example, Alizadehsani et al. examined the effectiveness of features information by using Gain and Confidence methods. They achieved 94.08% classification accuracy [1]. Chagas et al. examined the dealing between alcohol consumption and

CAD severity. They divided alcohol consumption into three categories: no, moderate and heavy. According to their study, the relationship between moderate alcohol consumption and severity of CAD is less than the relationship between heavy alcohol consumption and severity of CAD [3]. Yadav et al. presented an application based on association rule data mining in order to identify the hidden knowledge from medical dataset for the detection of CAD [4]. Ghadiri and Saniee used the Particle Swarm Optimization algorithm with a boosting approach to extract rules for detecting CAD patients [5]. Alizadehsani et al. (2) examined a preprocessing algorithm, rule-based and feature-based classifiers on the Z-Alizadeh Sani dataset. They evaluated the performances of different classifiers with 10-fold cross validation [6]. Nithya et al. improved the classification accuracy of the Support Vector Machine by utilizing the fuzzy logic. They evaluated their proposed model on the PIMA and Z-AlizadehSani [7]. Arabasadi et al. introduced a hybrid method that is the combine of Genetic Algorithm and Neural Network. The proposed hybrid method achieved highly accurate results on the Z-Alizadeh Sani dataset [8]. Alizadehsani (3) et al examined the effectiveness of a preprocessing algorithm on the Z-Alizadeh Sani dataset. They extracted three new features from the

---

[1] http://www.who.int/topics/cardiovascular_diseases/en/

* Corresponding Author: Kastamonu University, Department of Computer Engineering, Kastamonu, 37100, Turkey. e-mail: kakyol@kastamonu.edu.tr, Tel: +90 366 280 2978

dataset and used them to enrich the primary dataset. Then, Naive Bayes, Sequential Minimal Optimization, K-Nearest Neighbors and C4.5 algorithms were employed with 10-fold cross validation in their study [9]. Qin et al. introduced an algorithm that investigates the validity and materiality of feature selection on the Z-Alizadeh Sani dataset [10]. Babič et al. focused on predictive analysis, which consists of some classifiers, and descriptive analysis which consists of association and decision rules. According to their studies, the Support Vector Machine provided the best accuracy with 86.67% on the Z-Alizadeh Sani dataset. [11]. In another study, Pathak et al. investigated the CAD in women. According to their studies, it was lower than men but it rose steadily after fifth decade and there is an immediate need to better understand cardiac symptoms in order to facilitate the diagnosis and treatment of the disease in women [12]. Recently, Shahid and Singh proposed hybridized emotional neural networks with particle swarm optimization. They used four different feature selection methods to improve the performance of their study, and so offered 88.34% accuracy with 10-fold cross validation. [13]. Velusamy and Ramasamy applied the ensemble voting technique, which included K-Nearest Neighbor, Random Forest, and Support Vector Machine. Moreover, they conducted experiments on original and balanced datasets containing 5 selected attributes using the random forest-based Boruta wrapper and the attribute significance of the SVM. According to their studies, the authors achieved 98.97% and 100% classification accuracies on the original and balanced datasets, respectively [14]. Nasarian et al. studied the heterogeneous hybrid feature selection method and the performance of different classifiers on balanced datasets. The authors achieved 92.58% classification accuracy with the Synthetic Minority Oversampling Technique (SMOTE) and eXtreme Gradient Boosting (XGBoost) classifier they used in their proposed approach [15].

Understanding risk factors associated with CAD, adopting healthy lifestyle and preventive strategies, and early detection can be crucial to the management and elimination of such cardiovascular diseases. This disease has been proven to be the leading cause of death in both developed and developing countries [16]. Therefore, there is a need for a machine learning approach-based expert system that can diagnose heart disease more accurately in these countries with a shortage of medical resources and field experts. Moreover, the detection of properties important for this disease is used to increase the success of such a system. Being aware of the important attributes for this disease will help field-specialist in the analysis of routine laboratory test results of a patient coming internal medicine or another medicine unit except for the cardiology unit. By taking this data into consideration, the relevant physician will be able to guide the patient to the cardiology field-specialist and thus an important step will be taken for the patient's health. Based on these information, it is aimed to determine the significance of attributes for CAD by utilizing Stability

Selection (SS) method in this study. Machine learning was carried out on the training and test sets which includes 22 features that intersect among the features that are found important in each fold with the SS method. So, it is thought that the results obtained from this study will be useful or give an idea to the field-specialists investigating the causes of this disease at least. And also, the best algorithm is investigated for detecting this disease.

In this context, the rest of this paper is organized as follows: Section 2 describes the material and methods. Section 3 offers the experimental results and discussion. Finally, Section 4 concluded the study with final remarks.

## 2. MATERIAL AND METHODS

### 2.1. Medical Dataset

The Z-Alizadeh Sani dataset[2] which consists of 303 people data in Tehran's Shaheed Rajaei Cardiovascular, Medical and Research Center are used in this study. This dataset consists of 55 attributes including 51 test values and personal information such as age and weight, and 1 outcome attribute which has two possible categories, "CAD" or "Normal". If patient's CAD diameter value is greater than or equal to 50%, the patient is categorized as "CAD", otherwise, the patient is categorized as "normal".

### 2.2. Attribute Selection

Attributes set describes an information about any disease. But, all attributes may not be related to disease. Attribute selection is substantial step in order to avoid over-fitting and detect the best features. Feature selection is widely used in traditional machine learning based models [17–22], as well as in deep learning based models [23–28].

SS method provides information about the attributes for the result variable. In this method, the dataset is randomly shuffled many times. The combination of the "Least Absolute Contraction and Selection Operator" (LASSO) and its sequential regressions are performed to determine the significance of the feature [29]. Random Lasso, also known as SS, introduced in [30] offers consistent variable selection. Support Vector Regression generally has good generalization, and LASSO regression includes the L1 constraint in choosing a small subset of features in the dataset to explain the target variable [29].

### 2.3. Data mining

The purpose of data mining, which is a discipline that includes statistics and computer science algorithms, is to discover meaningful information from data [31]. Compared to statistical techniques, data mining techniques are often more powerful, flexible and effective for the knowledge discovery [32]. The performances of machine learning

---

[2] https://archive.ics.uci.edu/ml/datasets/Z-Alizadeh+Sani#

algorithms are handled for data mining. These algorithms perform the knowledge inference from data by using mathematical and statistical methods. So, unknown data are classified or predicted by utilizing the model. In this study, the classification performances of Random Forest (RF), Logistic Regression (LR), Multi-layer Perceptron (MLP), and Diagonal Linear Discriminant Analysis (DLDA) algorithms which are introduced in [33], respectively are examined.

## 2.4. K-fold cross validation

The *k*-fold cross validation technique splits the dataset into sub-datasets in order to provide consistent data distribution. k-1 piece of the sub-datasets is used as training set, the remaining one sub-dataset is used as test set. This process is repeated until all sub-datasets are tested. So, the performances of the learning algorithms are evaluated k times. The average of these performances is considered as the overall success rate [34].

## 2.5. Performance metrics

Accuracy (Acc), Sensitivity (Sen) and Specificity (Spe) metrics are used to evaluate the performances of the algorithms. The Acc metric indicates the ratio of the number of correctly classified CAD and non-CAD samples to the number of all instances. The Sen metric is ratio of the number of correctly classified CAD patients to the number of all CAD patients. The Spe metric is ratio of the number of correctly classified control samples called non-CAD to the number of all control samples. These metrics are presented in between Equations 1 and 3 [35]:

$$Accuracy = \frac{TP+TN}{TP+FN+TN+FP} \qquad (1)$$

$$Sensitivity = \frac{TP}{TP+FN} \qquad (2)$$

$$Specificity = \frac{TN}{TN+FP} \qquad (3)$$

Here, TP: true positive, TN: true negative, FP: false positive, FN: false negative.

## 3. EXPERIMENTS

In this study, experiments are carried out by using Python 2.7 imported "mlpy and sklearn" machine learning libraries. Firstly, the dataset is cleaned and prepared within the frame of three steps:
  a) The records which include null value(s) are excluded from the raw dataset.
  b) Categorical information like yes/no in the raw data file are converted to 1/0 categorical values.
  c) All data in dataset are normalized into range from 0 to 1.

In this context, 158 records, which include 43 patients having CAD and 115 patients having non-CAD, are prepared for experimental studies. In later stage, the dataset is divided into 80-20% training and test sets within the frame of 5-fold cross-validation technique. That is, the sub-datasets are generated 5 times. Hence, 234 training and 59 test sets are obtained in each iteration. After this step, the SS attribute selection method is applied to these sub-datasets to detect the most effective attributes for target variable and avoid over-fitting. Randomized Lasso is used for computing the importance of attributes on each resampling. Its parameters settings are presented in Table 1.

**Table 1.** The Randomized Lasso model parameters setting.

| Parameter | Meaning | Value type | Value |
|---|---|---|---|
| alpha | The regularization parameter | float | 0.001 |
| scaling | Scale | float | 0.5 |
| sample_fraction | The fraction of samples | float | 0.75 |
| n_resampling | Number of randomized models | integer | 200 |
| selection_threshold | A treshold value for a question of "which features should be selected?" | float | 0.25 |
| normalize | Normalization | boolean | True |
| max_iter | Maximum number of iterations | integer | 500 |

## 4. RESULTS AND DISCUSSION

The significance values of attributes are presented in Figure 1. It is noted that the order of the attributes in this figure is

the same as the public dataset used in this study. Also, the number of important attributes for each sub-dataset is presented in Table 2.
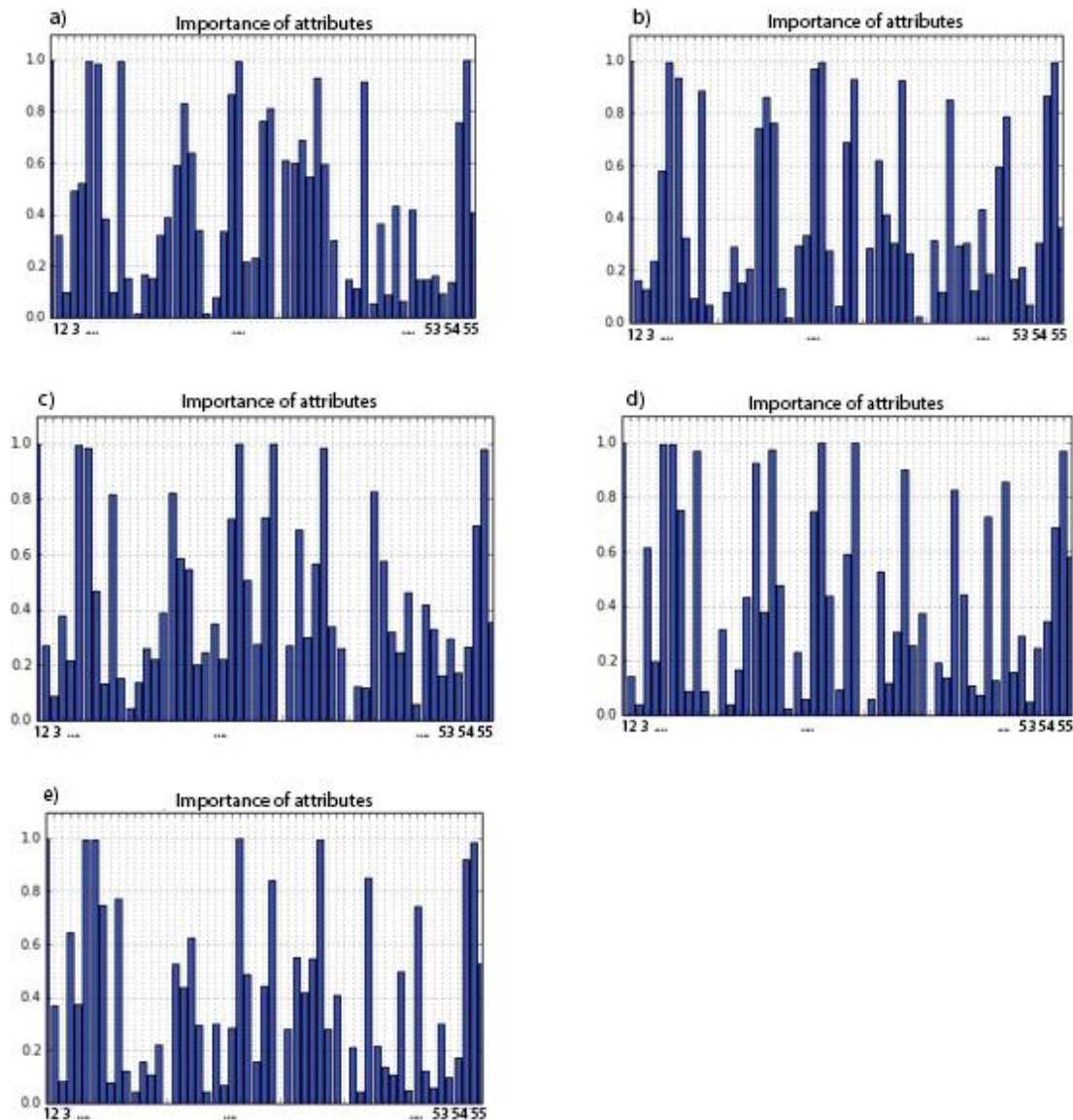
**Figure 1.** The significance values of attributes: a) Training data no. #1, b) Training data no. #2, c) Training data no. #3, d) Training data no. #4, e) Training data no. #5.

**Table 2.** Information about the significances of attributes.

| Datasets | The number of important features |
|---|---|
| Training data no. #1 | 33 |
| Training data no. #2 | 34 |
| Training data no. #3 | 37 |
| Training data no. #4 | 31 |
| Training data no. #5 | 32 |

The study showed that 'Age', 'Atypical', 'Blood pressure', 'Current smoker', 'Diastolic murmur', 'Dyslipidemia', 'Diabetes mellitus', 'Ejection fraction', 'Erythrocyte sedimentation rate', 'Family history', 'Hypertension', 'Potassium', 'Nonanginal', 'Pulse rate', 'Q wave', 'Regional wall motion abnormality', 'Sex', 'St Depression', 'Triglyceride', 'Tinversion', 'Typical chest pain' and 'Valvular heart disease' attributes are found important for each sub-dataset. What is meant by this sentence is that

empirical studies performed on all sub-datasets show that these 22 attributes given in Table 3 are found important in each fold. For example, the 'Current smoker' attribute is found important for CAD in the sub-datasets. On the other hand, 'Exertional CP' and 'BBB' attributes are insignificant for the sub-datasets. In addition, the important attributes which are found out as significant for all sub-datasets are presented in Figure 2.

**Table 3.** The weight information of the important attributes.

| | Training data no. #1 | Training data no. #2 | Training data no. #3 | Training data no. #4 | Training data no. #5 |
|---|---|---|---|---|---|
| Age | 1 | 1 | 1 | 1 | 1 |
| Atypical | 0.745 | 0.705 | 0.735 | 0.54 | 0.535 |
| Blood pressure | 0.74 | 0.63 | 0.8 | 0.395 | 0.36 |
| Current Smoker | 0.345 | 0.48 | 0.335 | 0.76 | 0.77 |
| Diastolic Murmur | 0.85 | 0.695 | 0.96 | 0.725 | 0.27 |
| Dyslipidemia | 0.645 | 0.81 | 0.745 | 0.92 | 0.485 |
| Diabetes mellitus | 0.98 | 0.995 | 0.995 | 1 | 1 |
| Ejection fraction | 0.845 | 0.7 | 0.85 | 0.685 | 0.855 |
| Erythrocyte sedimentation rate | 0.49 | 0.435 | 0.4 | 0.655 | 0.48 |
| Family history | 0.985 | 0.865 | 0.9 | 0.975 | 0.775 |
| Hypertension | 0.995 | 0.985 | 0.91 | 0.985 | 1 |
| Potassium | 0.505 | 0.415 | 0.605 | 0.875 | 0.73 |
| Nonanginal | 0.835 | 0.99 | 0.94 | 0.98 | 0.925 |
| Pulse rate | 0.625 | 0.515 | 0.765 | 0.995 | 0.63 |
| Q Wave | 0.62 | 0.595 | 0.62 | 0.5 | 0.645 |
| Regional wall motion abnormality | 0.99 | 0.975 | 0.99 | 0.94 | 1 |
| Sex | 0.46 | 0.32 | 0.275 | 0.7 | 0.575 |
| St Depression | 0.575 | 0.625 | 0.255 | 0.335 | 0.485 |
| Triglyceride | 0.945 | 0.845 | 0.805 | 0.775 | 0.885 |
| T inversion | 0.9 | 0.995 | 0.91 | 0.895 | 1 |
| Typical Chest Pain | 1 | 0.99 | 0.99 | 1 | 1 |
| Valvular heart disease | 0.45 | 0.35 | 0.405 | 0.605 | 0.545 |
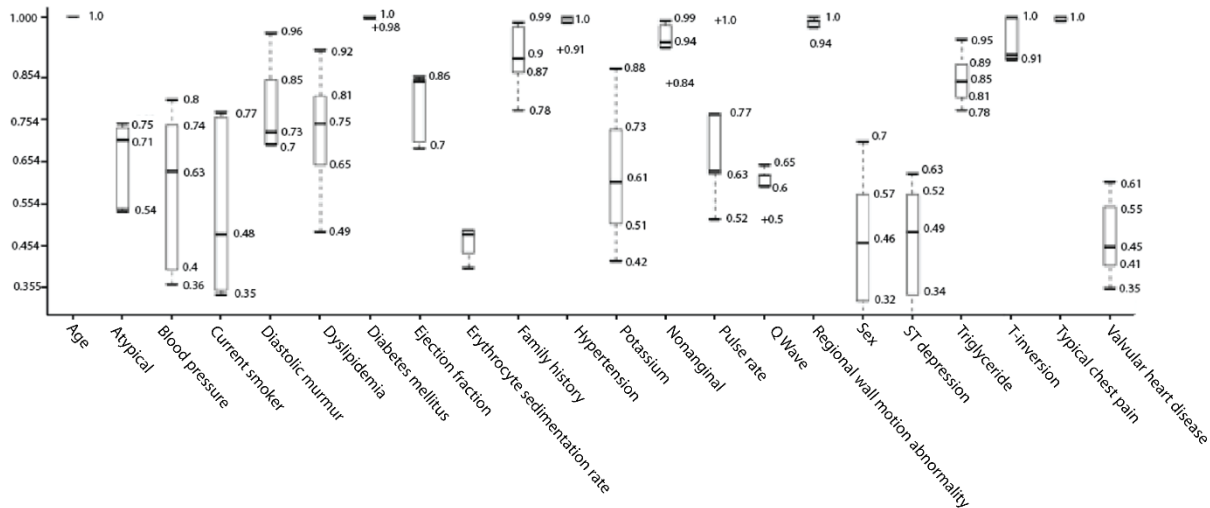


**Figure 2.** The weights of important attributes.

In further stage, the training and test sets which include best attributes are obtained respectively. By sending the sub-datasets as input data to the RF, LR, MLP and DLDA classifier algorithms, the machine learnings are carried out one by one. Table 4 presents detail settings about these algorithms' parameters. The prediction results are presented in Table 5 for sub-datasets including the best attributes. For example, 89.47% Acc, 92.86% Sen and 80.0% Spe measures are achieved on the test dataset no. 1 (Fold no. 1) by LR algorithm. According to Figure 3, the LR algorithm superior to others in terms of the Acc and Spe metrics. Also, the Sen metric of this algorithm quite near to the RF algorithm.

**Table 4.** The parameters setting of the learning algorithms.

| Algorithm | Parameter | Value |
|---|---|---|
| RF | *n_estimators* | *10* |
| | *criterion* | *gini* |
| | max_features | *auto* |
| | *bootstrap* | *True* |
| | *min_samples_split* | 2 |
| | *min_samples_leaf* | 1 |
| LR | penalty | l2 |
| | C | 1.0 |
| | solver | liblinear |
| | max_iter | 100 |
| MLP | solver | lbfgs |
| | *hidden_layer_sizes* | len(attributes), 2* len(attributes)+1 |
| | *activation* | *relu* |
| | alpha | 1e-5 |
| | *learning_rate* | *'constant'* |
| | *learning_rate_init* | *0.001* |
| DLDA | delta | *0.1* |

**Table 5.** Experimental results.

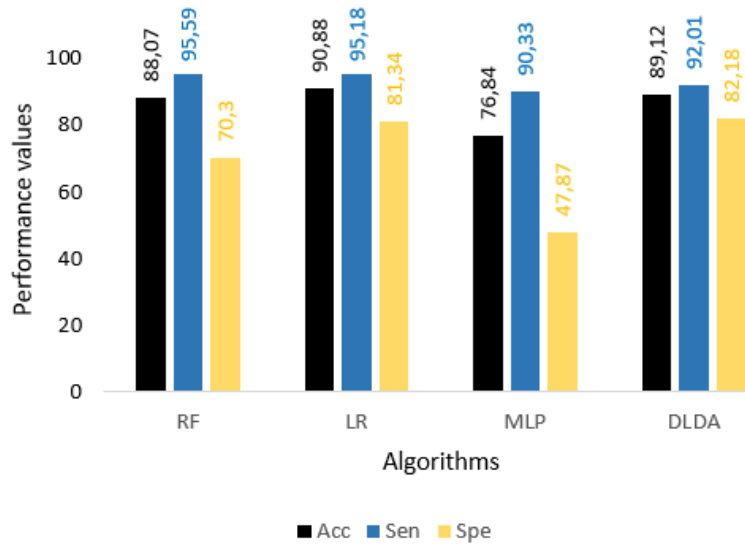| | Learning Algorithms | Acc % | Sen % | Spe % |
|---|---|---|---|---|
| Fold no. 1 | RF | 85.96 | 97.62 | 53.33 |
| | LR | 89.47 | 92.86 | 80.00 |
| | MLP | 82.46 | 88.10 | 66.67 |
| | DLDA | 87.72 | 92.86 | 73.33 |
| Fold no. 2 | RF | 87.72 | 97.30 | 70.00 |
| | LR | 91.23 | 100.00 | 75.00 |
| | MLP | 64.91 | 100.00 | 0.00 |
| | DLDA | 85.96 | 89.19 | 80.00 |
| Fold no. 3 | RF | 87.72 | 95.00 | 70.59 |
| | LR | 92.98 | 95.00 | 88.24 |
| | MLP | 77.19 | 87.50 | 52.94 |
| | DLDA | 92.98 | 95.00 | 88.24 |
| Fold no. 4 | RF | 85.96 | 95.00 | 64.71 |
| | LR | 87.72 | 95.00 | 70.59 |
| | MLP | 75.44 | 90.00 | 41.18 |
| | DLDA | 85.96 | 90.00 | 76.47 |
| Fold no. 5 | RF | 92.98 | 93.02 | 92.86 |
| | LR | 92.98 | 93.02 | 92.86 |
| | MLP | 84.21 | 86.05 | 78.57 |
| | DLDA | 92.98 | 93.02 | 92.86 |



**Figure 3.** Average results of the algorithms.

In addition, the performance of the proposed study was compared with the existing methods given in Table 6. According to this table, the performance of the proposed study is slightly lower compared to other studies, except for [11,13].

However, the studies of [1,4,7–9] were not focused on feature selection. They only simply classified the data. On the other hand, the studies of [14,15] focused on feature selection.

**Table 6.** The comparison of the relevant studies.

| Study | Method | Acc (%) | Sen (%) | Spe (%) |
|---|---|---|---|---|
| Alizadehsani et al. [1] | Gain and Confidence | 93.40 ±5.53 | 95.83 | 87.36 |
| Yadav et al. [4] | Association rule | 93.75 | 95.65 | 91.53 |
| Nithya et al. [7] | SVM and fuzzy logic | 97.03 | 97.16 | 96.85 |
| Arabasadi et al. [8] | Combination of Genetic Algorithm and Neural Network | 93.85 | 97.00 | 92.00 |
| Alizadehsani et al. [9] | Preprocessing and Sequential Minimal Optimization classifier | 92.09 | 97.22 | --- |
| Babič [11] | SVM | 86.67 | --- | --- |
| Shahid and Singh [13] | PSO based emotional neural networks | 88.34 | 91.85 | 78.98 |
| Velusamy and Ramasamy [14] | Feature selection and ensemble voting technique Original dataset Balanced dataset | 98.97 100 | 100 100 | 96.3 100 |
| Nasarian et al. [15] | Feature selection, SMOTE and XGBoost classifier | 92.58 | 92.99 | --- |
| **Proposed Method** | **Feature selection and LR** | **90.88** | **95.18** | **81.34** |

## 5. CONCLUSION

CAD is the most important type of cardiovascular diseases that cause serious heart problems in patients, affecting the heart's function negatively. Having knowledge about the important attributes for this disease will help the field-specialist in evaluating a patient's routine laboratory test results. Based on these information, it is aimed to determine the significance of attributes for CAD by utilizing SS method in this study. And also, the best algorithm is investigated for detection of this disease. Experimental results clearly show that LR, RF, MLP and DLDA machine learning algorithms are successful for best attributes datasets. The LR algorithm is just a little greater than the others within the frame of overall accuracy. It gives 90.88% accuracy. In this context, it can be said that the detection of best attributes is successful. And these attributes can be useful for field-specialists and health care systems in order to evaluate the condition of the patients. In future works, it is aimed to work with big datasets which include more attributes in order to obtain better achievement and more significant results. Also, it is aimed at experiments with the deep learning approaches that are between [33-35].

### Acknowledgements

## REFERENCES

[1]     R. Alizadehsani, J. Habibi, M.J. Hosseini, H. Mashayekhi, R. Boghrati, A. Ghandeharioun, B. Bahadorian and Z.A. Sani, "A data mining approach for diagnosis of coronary artery disease", Comput. Methods Programs Biomed. vol. 111, no. 1, pp. 52–61, 2013.
[2]     R. Roberts, "A genetic basis for coronary artery disease", Trends Cardiovasc. Med. vol. 25, no. 3, pp. 171–178, 2015.
[3]     P. Chagas, L. Mazocco, J. da C.E. Piccoli, T.M. Ardenghi, L. Badimon, P.R.A. Caramori, L. Pellanda, I. Gomes and C.H.A. Schwanke, "Association of alcohol consumption with coronary artery disease severity", Clin. Nutr. vol. 36, no. 4, pp. 1036–1039, 2017.
[4]     C. Yadav, S. Lade and M.K. Suman, "Predictive Analysis for the Diagnosis of Coronary Artery Disease using

Association Rule Mining", International Journal of Computer Applications, vol. 87, pp. 9-13, 2014.

[5]    N. Ghadiri Hedeshi and M. Saniee Abadeh, "Coronary artery disease detection using a fuzzy-boosting PSO approach", Comput. Intell. Neurosci. vol. 2014, pp. 1-13, 2014.

[6]    R. Alizadehsani, M.J. Hosseini, R. Boghrati, A. Ghandeharioun, F. Khozeimeh and Z.A. Sani, "Exerting Cost-Sensitive and Feature Creation Algorithms for Coronary Artery Disease Diagnosis", Int. J. Knowl. Discov. Bioinforma. vol. 3, no. 1, pp. 59–79, 2013.

[7]    S. Nithya, C. Suresh and G. Dhas, "Fuzzy Logic Based Improved Support Vector Machine (F-Isvm) Classifier for Heart Disease Classification", ARPN Journal of Engineering and Applied Sciences, vol. 10, no. 16, pp. 6957-964, 2015.

[8]    Z. Arabasadi, R. Alizadehsani, M. Roshanzamir, H. Moosaei and A.A. Yarifard, "Computer aided decision making for heart disease detection using hybrid neural network-Genetic algorithm", Comput. Methods Programs Biomed. vol. 141, 19–26, 2017.

[9]    R. Alizadehsani, M.J. Hosseini, Z.A. Sani, A. Ghandeharioun and R. Boghrati, "Diagnosis of coronary artery disease using cost-sensitive algorithms", in: Proc. - 12th IEEE Int. Conf. Data Min. Work. ICDMW, Brussels, Belgium, pp. 9–16, 2012.

[10]    C.J. Qin, Q. Guan and X.P. Wang, "Application of ensemble algorithm integrating multiple criteria feature selection in coronary heart disease detection", Biomed. Eng. - Appl. Basis Commun. vol. 29, no. 6, pp. 1-11, 2017.

[11]    F. Babic, J. Olejar, Z. Vantova and J. Paralic, "Predictive and descriptive analysis for heart disease diagnosis", in: Proc. 2017 Fed. Conf. Comput. Sci. Inf. Syst. FedCSIS 2017, Institute of Electrical and Electronics Engineers Inc., pp. 155–163, 2017.

[12]    L.A. Pathak, S. Shirodkar, R. Ruparelia and J. Rajebahadur, "Coronary artery disease in women", Indian Heart J. vol. 69, no. 4, pp. 532–538, 2017.

[13]    A.H. Shahid and M.P. Singh, "A Novel Approach for Coronary Artery Disease Diagnosis using Hybrid Particle Swarm Optimization based Emotional Neural Network", Biocybern. Biomed. Eng. vol. 40, no. 4, pp. 1568–1585, 2020.

[14]    D. Velusamy and K. Ramasamy, "Ensemble of heterogeneous classifiers for diagnosis and prediction of coronary artery disease with reduced feature subset", Comput. Methods Programs Biomed. vol. 198, pp. 1-13, 2021.

[15]    E. Nasarian, M. Abdar, M.A. Fahami, R. Alizadehsani, S. Hussain, M.E. Basiri, M. Zomorodi-Moghadam, X. Zhou, P. Pławiak, U.R. Acharya, R.S. Tan and N. Sarrafzadegan, "Association between work-related features and coronary artery disease: A heterogeneous hybrid feature selection integrated with balancing approach", Pattern Recognit. Lett. vol. 133, pp. 33–40, 2020.

[16]    A.K. Malakar, D. Choudhury, B. Halder, P. Paul, A. Uddin and S. Chakraborty, "A review on coronary artery disease, its risk factors, and therapeutics", J. Cell. Physiol. vol. 234, no. 10, pp. 16812–16823, 2019.

[17]    D. Effrosynidis and A. Arampatzis, "An evaluation of feature selection methods for environmental data", Ecol. Inform. vol. 61, pp. 1-10, 2021.

[18]    K.P. Muhammed Niyas and P. Thiyagarajan, "Feature selection using efficient fusion of Fisher Score and greedy searching for Alzheimer's classification", J. King Saud Univ. - Comput. Inf. Sci., in press, 2021. https://doi.org/10.1016/j.jksuci.2020.12.009.

[19]    K.K. Kavitha and A. Kangaiammal, "Correlation-based high distinction feature selection in digital mammogram", Mater. Today Proc., vol. 147, no. 5, e218-e227, 2020.

[20]    P.D. Sheth, S.T. Patil and M.L. Dhore, "Evolutionary computing for clinical dataset classification using a novel feature selection algorithm", J. King Saud Univ. - Comput. Inf. Sci., in press, 2020. https://doi.org/10.1016/j.jksuci.2020.12.012.

[21]    F. Amini and G. Hu, "A two-layer feature selection method using Genetic Algorithm and Elastic Net", Expert Syst. Appl. vol. 166, pp. 1-10, 2021.

[22]    S.B. Chen, Y.M. Zhang, C.H.Q. Ding, J. Zhang and B. Luo, "Extended adaptive Lasso for multi-class and multi-label feature selection", Knowledge-Based Syst. vol. 173, pp. 28–36, 2019.

[23]    A.U. Haq, A. Zeb, Z. Lei and D. Zhang, "Forecasting daily stock trend using multi-filter feature selection and deep learning", Expert Syst. Appl., vol. 168, pp. 1-8, 2021.

[24]    M. Toğaçar, B. Ergen and Z. Cömert, "Classification of white blood cells using deep features obtained from Convolutional Neural Network models based on the combination of feature selection methods", Appl. Soft Comput. J. vol. 97, pp. 1-10, 2020.

[25]    T. Niu, J. Wang, H. Lu, W. Yang and P. Du, "Developing a deep learning framework with two-stage feature selection for multivariate financial time series forecasting", Expert Syst. Appl. vol. 148, pp. 1-17. 2020.

[26]    W. Tian, Z. Liu, L. Li, S. Zhang and C. Li, "Identification of abnormal conditions in high-dimensional chemical process based on feature selection and deep learning", Chinese J. Chem. Eng. vol. 28, no. 7, pp. 1875-1883, 2020.

[27]    W. Kim, Y. Han, K.J. Kim and K.W. Song, "Electricity load forecasting using advanced feature selection and optimal deep learning model for the variable refrigerant flow systems", Energy Reports. vol. 6, 2604–2618, 2020.

[28]    H. Shi, H. Li, D. Zhang, C. Cheng and X. Cao, "An efficient feature generation approach based on deep learning and feature selection techniques for traffic classification", Comput. Networks. vol. 132, pp. 81–98, 2018.

[29]    F. Mordelet, J. Horton, A.J. Hartemink, B.E. Engelhardt and R. Gordân, "Stability selection for regression-based models of transcription factor-DNA binding specificity", Bioinformatics, vol. 20, no. 13, i117-125, 2013.

[30]    N. Meinshausen and P. Bühlmann, "Stability selection", J. R. Stat. Soc. Ser. B. vol. 72, no. 4, pp. 417–473, 2010.

[31]    C. Zucco, "Data Mining in Bioinformatics", Encycl. Bioinforma. Comput. Biol., Elsevier, vol. 1, pp. 328–335, 2019.

[32]    M. Kantardzic, Data mining : concepts, models, methods, and algorithms, 3rd Edition, 2019.

[33]    T. Hastie, R. Tibshirani and J. Friedman, Elements of Statistical Learning, 2nd edition, 2009.

[34]    R. Kohavi, "A Study of Cross-Validation and Bootstrap for Accuracy Estimation and Model Selection", IJCAI'95: Proceedings of the 14th international joint conference on Artificial intelligence, vol. 2, pp. 1137–1143, 1995.

[35]    S.A. Shaikh, "Measures Derived from a 2 x 2 Table for an Accuracy of a Diagnostic Test", J. Biom. Biostat. vol. 2, no. 5, pp. 1–4, 2011.

# Sentiment analysis of Twitter texts using Machine learning algorithms

*1Hawar Sameen Ali Barzenji

1 Department of Computer Engineering, Faculty of Computer and Information Sciences, Sakarya University, Sakarya, Turkey,
hawar.al-barzenji@ogr.sakarya.edu.tr, iD

**Abstract**

Since the two last decades social media networks have become a part of our daily life. Today, getting information from social media, tracking trends in social media, learning the feelings and emotions of people on social media is very essential. In this study, sentiment analysis was performed on Twitter text to learn about the subjective polarities of the writings. The polarities are positive, negative, and neutral. At the first stage of the sentiment analysis a public data set has been obtained. Secondly, natural language processing techniques have been applied to make the data ready for machine learning training procedures. Lastly sentiment analysis is performed by using three different machine learning algorithms. We reached 89% accuracy with Support Vector Machines, 88% accuracy with Random Forest, and 72% accuracy with Gaussian Naive Bayes classifier.

*Keywords:* Natural Language Processing, Machine Learning, Random Forest, Support Vector Machines, Gaussian Naive Bayes, Sentiment Analysis

## 1. INTRODUCTION

With the rise of the modern era, our life faced a new way of communicating, a new way of social interaction [1]; which is the social media platforms. Willy-nilly if we accept it or not, SM became a phenomenon in our daily life; it became an essential part of our recent lifestyle.

Nowadays, people use social media not only for sharing their emotional, desire, and ideas about a particular subject [2]; but also, they use it for marketing [3], political messages, and etc. A huge attention for the latter mentioned category is Twitter's platform. It is clear that most of the politicians around the world are using Twitter as their no. one's favorite platforms, but we should not forget that this platform has its own positive and negative effects on the decision of the people, and what is familiar among the people about all of the social media platforms is that most of the time, its negative side is more than its positive side.

For the all above important reasons of social media, it's the right time to put our focus on this new phenomenon, from philosophy to machine learning (ML), NLP and other evaluating techniques in data analysis, can be used to analyze the activities on this platform.

The Twitter's account of President Donald Trump has about 88 million followers [4] of Twitter users, and many of them are using his account as a way of news and information resource [5]. His frequent use of the social media account and his influence as President of the US, has made his tweets an essential source in a variety of scientific and research studies, like evaluating his tweets [6] [7], applying sentiment analysis, etc.

In this study, sentiment analysis is performed on Twitter text. The tweets which are used in this research are Trump's tweets published freely online [8]. Obtained tweets were firstly prepared for ML algorithms by using natural language processing techniques (NLP). Then three ML classifiers were trained using the data. The ML techniques are Random Forest, Support Vector Machines (SVM), and Gaussian Naive Bayes (GNB).

### 1.1. NLP

NLP is a subfield of Computer science and AI (particularly the field of machine learning). It deals with the language of the human being and how it understood by the computer. This technique can be obtained with the help of the computational linguistics. To understand the natural language needs a lot of information about lexicon, semantics, syntax, and information about our real world [29, 30, 31].

We can talk about NLP as a synthesis of philosophy of linguistics, computer science, and artificial intelligence. This branch of science deals with the interactions between human language and computers (Robot agent). This field cares about how to code and program computers, in order to process and analyze the data of natural language.

---

*1 Corresponding author: Sakarya University, Sakarya, Turkey, hawar.barznji@gmail.com, +90 552 353 2395
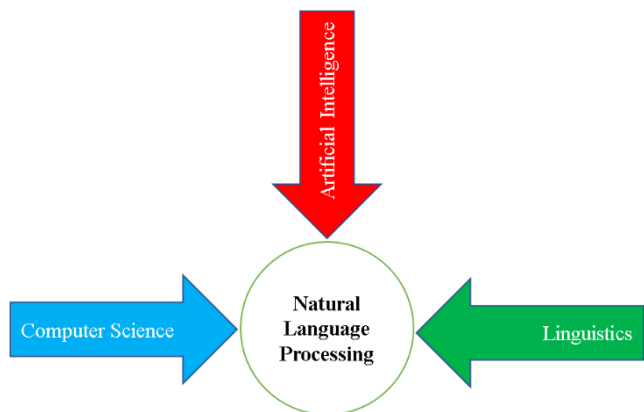
**Figure 1.** The synthesis of NLP

## 1.2 ML classifeirs

Machine learning is about taking out knowledge from raw data, and learning from past experience in order to predict the next upcoming data. This research field is an intersection of AI, statistics, and computer science. The usage of machine learning methods in recent years is very useful in nowadays life. Starting from automatic suggestions of which videos to be watched, or what type of fast-food to order or which items to buy, and for customizing the podcasts; most of the modern portals and devices have machine learning algorithms at their kernel; and ML can do all of these based on learning from experiences, the more training the classier, the more accurate the prediction is.
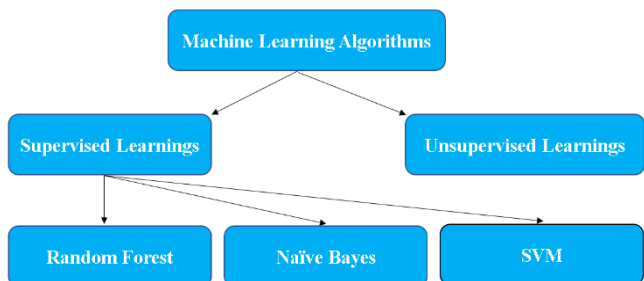


**Figure 2.** The diagram of ML approach

## 1.2.1 Random Forest

Originally Random Forest derives from Decision Tree, this means, it shares all the benefits of decision trees, but historically it refers back to an American computer scientist at IBM Watson Health (Tin Kam Ho) in 1995 with the term of (random decision forests) [9]. After a while (Leo Breiman) coined the Random Forest term in 2001 [10].
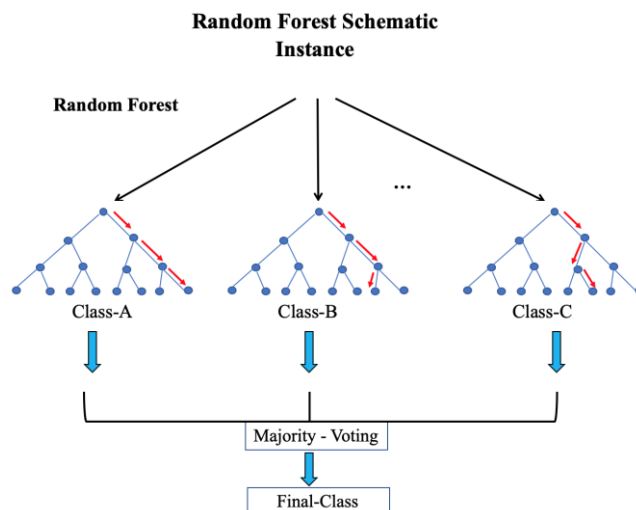


**Figure 3.** Random Forest schematic

## 1.2.2. Gaussian Naïve Bayes

Naive Bayes is a kind of probabilistic or statistical supervised ML algorithm. It builds a probability model on the category description for all feature vectors in the training set. It works based on Bayes theorem [11], which calculates conditional probability. Gaussian distribution, is one of the most usual and main technique in calculating statistics and probability field, stating the "naive" supposition of conditional independence between every pair of attributes given the value of the class variable [12].
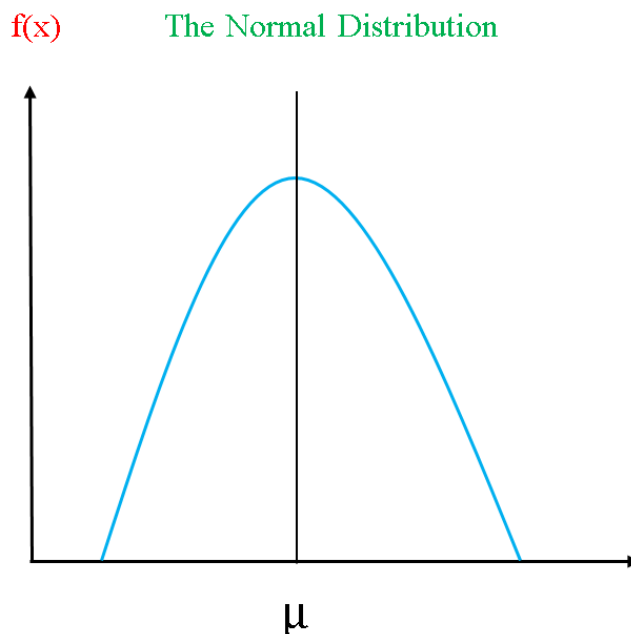


**Figure 4.** The Gaussian distribution

### 1.2.3. Support Vector Machine

Support Vector Machine (SVM) or originally Support Vector Networks (SVN), is a type of supervised ML algorithm that was coined by both C. Cortes and V. Vapnik in 1995 [13]. It can be used in both classification and regression tasks. This prediction tool uses ML theory to maximize required accuracy and automatically avoids overfitting of the data. This supervised learning ML uses in two group classification problems. It can solve linear and non-linear. This algorithm is efficient when dealing with high dimensional data such textual data. The idea of SVM is simple, its objective is to find a hyperplane that has the largest edge (side), i.e. the decision boundary that separates the support vectors to the farthest.

**Table 1.** The number of input features with the required number of hyperplanes

| Input features | Output hyperplane |
|----------------|-------------------|
| 2-features | 1-line hyperplane |
| 3-features | 2-dimentional plane |

In SVM, we are trying to find those points which are the closest to the line from both the classes, the points are called *support vectors*. Then, the distance between the line and the support vectors will be calculated, this distance is called the margin [32]. The goal of SVM is to maximize the margin, as it shown in below figure.
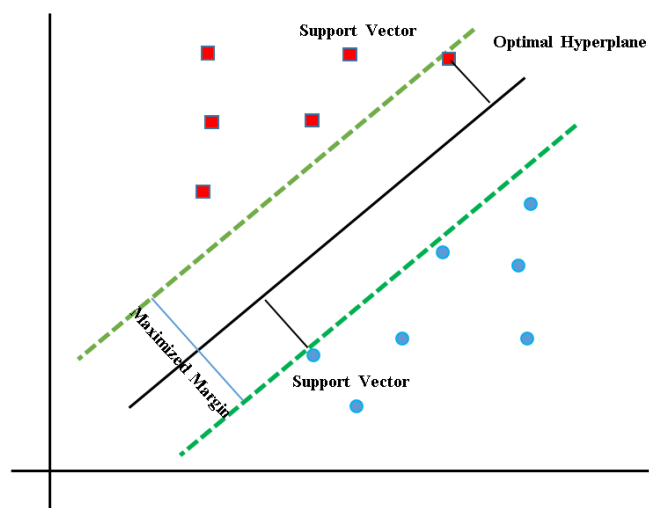


**Figure 5.** Optimal Margin

Finally, since every approach is measured by its outcomes, Random Forest classifier has been applied to get the following targets; *Accuracy*, *Precision, F1 Score*, and *Recall* metrics [14] [15]. Also, the data size of cleaned text with its original source have been compared and tested in macOS

operating system for information purpose; the results have been showed in tables and related figures.

The suggested research paper can have a good impact in many scientific areas and can have a good contribution to science. The proposed system can be used in pre- and post-scraping processes. It can be used during web page scraping before the crawled data is going to be saved in the form of csv file; or after saving the crawled page.

Also, it can be used in various fields; It can be used in Digital Image Processing (DIP) and Pattern Recognition (PR); since there are images that contain textual data, it can be extracted by one of the mentioned proceedings, and the proposed system can be applied on it, of course, the more gathered data, the more accurate it will.

Also, it can be used in AI and robotics; the agents can use the suggested method in converting speech-to-texts, which is famous as Speech Recognition (SR) for cleaning the noisy speech in order to understand and perform the required given orders, with the help of time, the agent can get more experience and gradually becomes smarter.

Since philosophy is one of the closest fields to AI and NLP, it can be used in social sciences, like the philosophy of linguistics, we shall not forget that philosophy as the mother of all sciences, raised the first and most early questions about language and a thinker machine.

Also, the mathematical results in confusion matrix, classification report table can be used in the field of data analysis and statistical purposes.

The framework of this research paper will be as follows: In section 1; a general introduction about the whole study (i.e. the problem definitions) is given, like NLP, all three types of ML classifiers; also, other related topics like scopes, and the suggested solutions have been given too. In section 2; the closest studies in the same area (i.e. related work) have been given. In section 3; which is the material and methods; a full detailed explanation about and text cleaning procedure (i.e. pre-processing) with all of its included steps have been given. In section 4; is the results in confusion matrices, classification report, and the conclusion with our recommendations for the future upcoming studies.

### 2. RELATED WORK

Nowadays Twitter sentiment analysis gained most of the researcher's attention [16]. These concise texts are used as a raw material for data analysis. By using text polarities (positive, neutral, and negative), emotions (angry, sad, loved, etc.) are judging on each text's subjectivities.

Before going deeper into our own study. We will give a brief overview about the previous articles (i.e. Literature Review) that have been done in the same area which is the combination of NLP and ML.

In [17] they proposed a study for detecting fake news spread through images from SM like Facebook, Twitter, etc. They proposed K-means clustering (based on issuing day) to get a general outline of how the images were used throughout the time.

In [18] they introduce a hybrid method which is a combination of NLP and ML techniques to guess and recognize hate speech from social network websites. After gathering the hate speech, steaming, tokenizing, unwanted character removal was applied on it. Finally, they classified the texts into neutral, offensive, and hate (in our study, we classified the tweets into positive, neutral, negative) language. The performance of the system is then evaluated using overall accuracy, f1 score, and precision and recall metrics. The system achieved an accuracy of 98.71%.

In [19] they applied NLP techniques to analyze tweets with regard to mental health. They used Deep Learning (DL) models to classify each tweet regarding of the following emotions: angry, anticipation, disgust, frighten, delight, sadness, surprise, and confidence.

In [20] a group of researchers made a comparison study of the Naïve Bayes algorithm and NLP on the dataset of Twitter. Their comparison is in two categories: *accuracy* and *speed.* Their experimental results showed that the Naïve Bayes algorithm got 63.5% accuracy, which is lower than that achieved by the NLP method. But in the processing speed analysis, the ML method performance is 5.4 times higher than that of the NLP method.

In [21] they used sentiment analysis to extract human feeling and evaluate whether it's negative, positive or neutral. Through unconstructed text by using NLP. They also Machine learning in order to train and test the dataset. They compared the results using different ML classifier, like Naïve Bayes, Random Forest, Support Vector Machine, and etc.

In [22] USSAMA YAQUB applied sentiment analysis on trump's tweets during the early appearance of the coronavirus pandemic (i.e. COVID-19) in the United States. Statistically, he discovered a negative correlation between the sentiments of his tweets and the no. of cases in the United States. One thing which is very important in his study research is that he noticed a gradual shifting in his tweets from positive to negative sentiments polarities while he is mentioning China and COVID-19 together. What USSAMA did is amazing, but his study is not a hybrid method, which means he didn't apply ML classifier after his sentiment analysis, this makes his research stay in the domain of data analysis and NLP techniques.

In [23] In this paper, they analyzed the relationship between the tweets written by POTUS (stands for the President of the United States) and his approval rating using sentiment analytics and data visualization tools. They applied all the NLP requirements on the tweets of POTUS; they mined, cleaned, and gave a quantitative measure based on the content, which they named the "sentiment score". By comparing tweets before the election, during the election and inauguration, and after the inauguration, they found that the "sentiment score" of Trump's tweets feed has been increased with an average in time by a factor of 60%. By using cross-correlation analysis, they find a preliminary causative relationship between POTUS Twitter activity and approval rating. Still, their study is one-sided research, it seems something is missing. What we do with sentiment analysis and NLP techniques, somehow leaves the problem unsolved. By using ML methods, we can train our data in a way that can recognize the next upcoming data which gives to the system, so the robot can predict it.

In [24] this paper, they used social media content to forecast real-world result. In particular, they used the chatter from Twitter platform to predict box office incomes for movies. They revealed that the tweets which are generated about specific movies can perform better in market-based predictors. They applied sentiment analysis on the extracted Twitter data, but they didn't mention which method they did the forecasting.

From all above research studies and articles, we can notice that most of them have a combination method, which means a duality of NLP and ML algorithms. It seems that without combining those two fields, the suggested work would be incomplete. In our research, after applying NLP techniques on the Twitter texts, Random Forest classifier, GNB, and SVM have been to train and test the cleaned texts.

## 3.   MATERIALS AND METHODS

In this section, which covers the most important part of our study, talks about the most required methods and algorithms that need to be applied to our dataset in order to get the target results.

As it already mentioned above, the aim of this study is to apply sentiment analysis on Twitter's textual data and performing text polarities on it. At the final step, the Random Forest classifier, GNB, and SVM have been used to train and test the data. The accuracy and time of the used classifier have been compared. The results showed the proposed method is working well. The details of the results will be given in a confusion matrix in the result section.
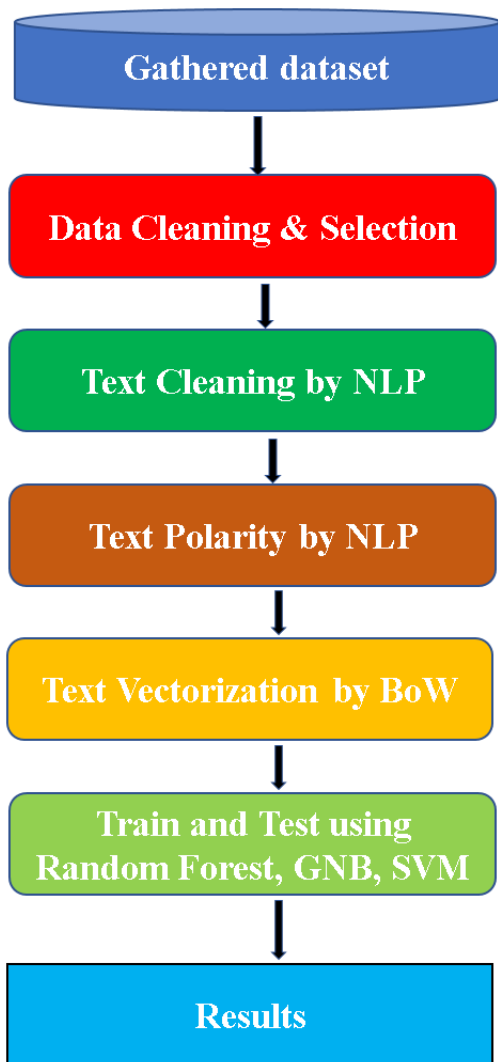
**Figure 6.** A quick overview of the proposed study

The above diagram displays the most essential steps in the proposed research. It starts with the collected tweets and applies the most required processes which are the data cleaning and selection level. In text cleaning which represents all the NLP techniques that have been used in order to prepare the text for conversion. At text polarity level, each cleaned tweet has been judged regarding their subjectivity. At text to number level, BoW has been applied for converting the categorical data (i.e. textual data) into numerical data. Finally, in the ML level, Random Forest classifier, GNB, and SVM have been used to train and test the data for getting the required results.

### 3.1. Gathered dataset

In this study, an already prepared dataset has been used from kaggle online community for data scientists and ML practitioners, the dataset is Trump's tweets. It can be found and downloaded from the cited link [25].



**Figure 7.** The first five records of our host dataset

### 3.2. Data cleaning and selection

Whenever there is a dataset, there should be data analysis too, for the reason that any dataset needs some special commands to manipulate them. Data analysis performs most of the actions that need to be done on any dataset, including importing the dataset, performing most of the actions on its columns and rows, appending and deleting the records, and etc. without data analysis, applying NLP and ML algorithms would be impossible. Deciding which features should be used and which one should be eliminated, will be occurred in this step in any studying research in the same area.

As it clear, data visualization (like charts, infographics, etc.) is giving a good way to represent the important information based on the dataset, but what if your raw data is textual-based document? The solution is using Wordcloud which is available in Python programing language. Wordcloud refers to a cloud filled with lots of words in different shapes and sizes. The size of each of the word represents the frequency or the importance of each word; bigger size, means more repeated word. From the below figure, you will see the Wordcloud of our dataset for the feature of "content".
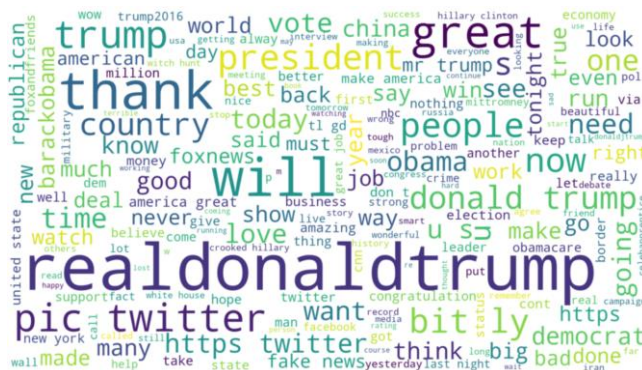


**Figure 8.** Wordcloud for Trump's tweet

From the Wordcloud above, the words with bigger size represent the most repeated words in the tweet dataset.

### 3.3. Text Cleaning

The data (in our case Twitter texts) needs to be fully cleaned and prepared before applying any classifier algorithms. In every text, there are many (mentions, hashtags, emoticons, unconventional punctuation, spaces, symbols), that do not have any value on classifying, have to remove (filter out). One of the biggest advantages of this step is that it makes our data smaller which saves our storage capacity. Decreasing the size of the hosted dataset can have a good effect on the performance of the work and the data size can be used for information purpose. (Details have been given in the result section).

In the experimental part, the following text cleaning which includes the following steps have been applied in the dataset: first, stopwords have been removed, then word lemmatizing has been applied in order to change the words into their roots, finally, regular expressions have been applied for removing the links and emails, etc.

### 3.4. Detecting text polarity

This part is one of the main goals of the study. What we do from the beginning until the final step, is to prepare the text for subjective sentiment polarities (or in some resources, sentiment score). Text polarity is a method to detect each tweet's subjectivity. Since the tweets have been written by human as a subject, and he is tweeting his own ideas about a specific event or anything else, so the tweets are not objective. It needs to be detected in order to be classified into three levels, which are positives, negatives, and neutrals.

In our experimental work, in each sentence has been judged after being cleaned by NLP techniques. Each textual data (In our case is Twitter tweet) is labeled with three possible values: negative, positive or neutral. In this work, we first determined the sentiment polarity of each tweet by adapting the following measurement [26] [27],

$$Sentiment\ Score\ (C) = \frac{Positive - Negative}{Positive + Negative + 2} \qquad (1)$$

Where,
Positive represents total number of the positive words; and negative counts the negative words in the tweet. We represent it by a separate two valued with variable C, which represents the sentiment class:
$C \in \{-1, 1\}$.

Where,
C can hold three values, since of having different thresholds,

$$C = \begin{cases} 1\ (Positive) & if\ Sentiment\ score \geq 0.1 \\ -1\ (Negative) & if\ Sentiment\ score < 0.1 \\ 0\ (Neutral) & if Sentiment\ score = 0 \end{cases} \qquad (2)$$

In the Python programming language, there is a library for text polarity, with the name of TextBlob (Also VADER can be used).

From the experiment result, the total of (41122) records, the distribution of sentiment polarities will be as follows:

Positive tweets: $\frac{22274}{41122} = 54.16\%$

Negative tweets: $\frac{7148}{41122} = 17.38\%$

Neutral tweets: $\frac{11700}{41122} = 28.45\%$

If we put all the results in one table, we will get,

**Table 2.** Sentiment polarities of our dataset

| Sentiment polarities | No. of occurrences | Percentages |
|---|---|---|
| Positive | 22274 | 54.16% |
| Negative | 7148 | 17.38% |
| Neutral | 11700 | 28.45% |
| Total | 41122 | 100% |

As it can be seen from the result table above, the majority of the tweets are positive, and we got the least number of negative tweets, also about 12000 neutral tweets. The graphical distribution of the tweets will be as follows,
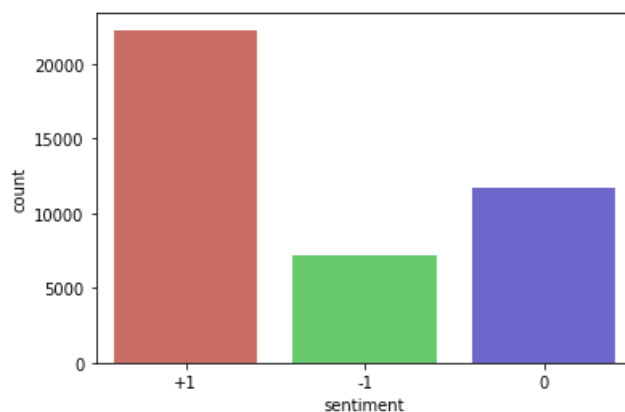


**Figure 9.** Sentiment polarity distribution of the tweets

### 3.5. Text Vectorization

Since all of the ML classifiers are dealing with numbers only, the cleaned text has to be changes into a matrix of numbers, and the field will be ready for the training and test process. Text vectorization is a technique of changing texts into quantitative data.

There are some popular types of text vectorization, which they all do the same task but in different ways. Some of them are:

1. Bag of Words (BoW)

2. TF-IDF

3. Word2Vec

### 3.5.1. Bag of Words

Simply, BoW is a method for representing text in the form of numbers. This model is used for simplifying representation which is used in NLP and information retrieval (IR). In this method, a list of all the text will be considered as a bag of its words, with ignoring the grammar and even the order of the words, but protecting variety.

Simply, BoW is a link between NLP and the ML classifier. It connects NLP techniques to ML.



**Figure 10.** BoW as a link between NLP and ML

In order to clarify BoW concept, in the example below, let's

take three sentences:

Sentence 1: "*The wolf sat*"

Sentence 2: "*The wolf sat on the hill*"

Sentence 3: "*The wolf with the hill*"

We will construct a vector form, from all the unique words in the above three sentences. This vector contains six words which are: 'The', wolf', sat, 'on', 'hill', 'with'. Finally, we will make a table for the results,

**Table 3.** The BoW table

|  | the | wolf | sat | on | hill | with |
|---|---|---|---|---|---|---|
| Sentence 1 | 1 | 1 | 1 | 0 | 0 | 0 |
| Sentence 2 | 2 | 1 | 1 | 1 | 1 | 0 |
| Sentence 3 | 2 | 1 | 0 | 0 | 1 | 1 |

So, the numerical ouotputs for each sentence will be a vector

as follows:

Vector 1: [1, 1, 1, 0, 0, 0]

Vector 2: [2, 1, 1, 1, 1, 0]

Vector 3: [2, 1, 0, 0, 1, 1]

### 3.6. Splitting into train and test

Every used machine learning algorithm needs to a technique which is a kind of division. In this process, the whole dataset will be divided into two parts: Training and Testing. It's up to the researcher divides each part into how many percentages. It can 80%, 20% for both training and testing respectively. Also 70%, and 30%. This method is used to evaluating the performance of the used machine learning algorithm. As we said earlier, this process requires taking the dataset and dividing it into two subsets:

***Training set***: Used to fit and train the machine learning model.
***Testing set***: Used to evaluate the fit machine learning model.

This technique is an important step in any supervised learnings. While the agent does not have any default information about the environment, this procedure gives that ability to the agent to learn from the experiences by training more than half of the data. In most of the cases, 70% of the dataset is given to the agent in order to learn from the training; and the remaining part which is 30% is put for the test to see the accuracy of the used classifier, in order to check whether it works good or not. In case if the suggested ML algorithm is not doing well, another classifier has to be applied on the hosted data. The figure below will explain the procedure of splitting in ML.

For example, in our case, the total records of the dataset equal 41122 records. The mathematical calculating of the splitting method (30% and 70%) for the three proposed classifiers will be as follows:

**Training set:** $70\% \times 41122 = \frac{70}{100} \times 41122 = 0.7 \times 41122 = 28785$ records

**Testing set:** $30\% \times 41122 = \frac{30}{100} \times 41122 = 0.3 \times 41122 = 12337$ records
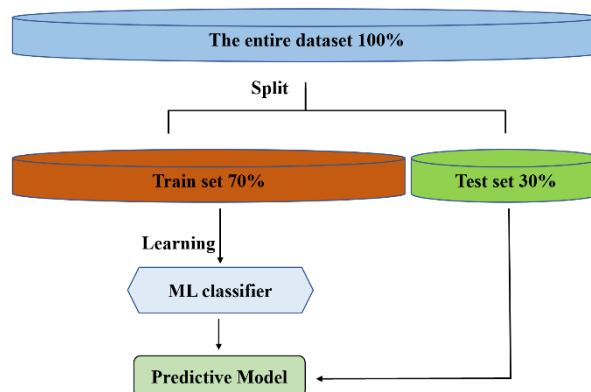


**Figure 11.** The procedure of splitting dataset in ML

## 4. RESULT AND DISCUSSION

This section has been divided into two part. In the first part, a formula of each rule has been given, and examples in order to clarify each used formula. In the second part, the experimental results have been discussed and the output of the confusion matrix have been evaluated; in additional, with checking the size of the dataset before and after cleaning.

We used macOS operating system; with the following technical specifications (which is shown in the below table) for training and testing each classifier:

**Table 4.** The technical specifications of the used host computer

| Computer manufacture | Type of OS | Processor | Amount of RAM |
|---|---|---|---|
| MacBook Pro | macOS Big Sur 2020 | Intel Core i5, ~2.6 GHz | 8GB |

### 4.1. The evaluation metrics

This metrics measurements concludes the following results:

1. Accuracy,
2. Precision,
3. Recall metrics,
4. F1 score.
5. Required time for training and testing
6. Data size

Accuracy is calculated as the total number of correct predictions, over the total number of the dataset (i.e. all correct / all). The rule of accuracy is,

$$Accuracy = \frac{TP + TN}{TP + TN + FN + FP} \quad (3)$$

The rule of precision is,

$$Precision = \frac{True\ Positive\ (TP)}{True\ Positive\ (TP) + False\ Positive\ (FP)} \quad (4)$$

The rule of recall is,

$$Recall = \frac{True\ Positive\ (TP)}{True\ Positive\ (TP) + False\ Negative\ (FN)} \quad (5)$$

Recall works on the horizontal lines (i.e. the rows) of our table.

The solution for the misleading performance of accuracy on imbalanced data, is F1 score. We use F1 score when our data is imbalanced. F1 score is the average of precision and recall.

The rule of F1 score is,

$$F1\ score = 2 \times \frac{Precision \times Recall}{Precision + Recall} \quad (6)$$

In order to understand the above rules, we will take an example.

Consider a classification system that has been trained to classify (or recognize) the pictures of three types of animals: phoenix, owl, and wolf. The system gave the results in a confusion matrix. Assume that the number of animals are given to the system which are 30 animals; there where 10 phoenixes, 8 owls, 12 wolves.

**Table 5.** Confusion matrix for three samples of animals

| | | Predicted class | | | Total no. of each |
|---|---|---|---|---|---|
| | | phoenix | owl | wolf | |
| Actual class | phoenix | 6 | 3 | 1 | 10 |
| | owl | 1 | 5 | 2 | 8 |
| | wolf | 0 | 1 | 11 | 12 |

In this confusion matrix 3 by 3 table, out of 10 actual phoenixes, the system predicted that 3 were owls, and 1 was a wolf; and of the 8 owls, it predicted 1 was a phoenix, and 2 were wolves; and out of 12 wolves, predicted 1 was owls. The green colors are the true actual values for each class.

Considering the confusion matrix above, the corresponding table of confusion which is (Table 5), for the phoenix, owl, and wolf classes, would be as follows:

**Table 6.** Confusion matrix for phoenix class

| 6 true positive (actual phoenixes that were correctly classified as phoenixes) | 1 false positive (owls that were incorrectly labeled as phoenixes) |
|---|---|
| 3, 1 false negative (phoenixes that were incorrectly marked as owls, and wolf respectively) | 19 true negative (all the remaining animals, correctly classified as non-phoenixes) |

**Table 7.** Confusion matrix for owl class

| 5 true positive (actual owls that were correctly classified as an owl) | 3, 1 false positive (phoenixes and wolf that were incorrectly labeled as owl respectively) |
|---|---|

| 1, 2 false negative (owls that were incorrectly marked as phoenix and wolf respectively) | 18 true negative (all the remaining animals, correctly classified as non-owls) |
|---|---|

**Table 8.** Confusion matrix for wolf class

| 11 true positive (actual wolves that were correctly classified as wolves) | 1, 2 false positive (phoenix and owls that were incorrectly labeled as wolves) |
|---|---|
| 1 false negative (wolf that was incorrectly marked as owls) | 15 true negative (all the remaining animals, correctly classified as non-phoenixes) |

The results of (Table 5) will be as follows,

$$Overall\ accuracy = \frac{(5 + 6 + 11)}{30} = \frac{22}{30}$$
$$= 0.73 \times 100\% = 73\%$$

$$Precision\ for\ phoenix\ class = \frac{6}{(6 + 1 + 0)} = \frac{6}{7}$$
$$= 0.85 \times 100\% = 85\%$$

$$Precision\ for\ owl\ class = \frac{5}{(5 + 3 + 1)} = \frac{5}{9}$$
$$= 0.55 \times 100\% = 55\%$$

$$Precision\ for\ wolf\ class = \frac{11}{(11 + 2 + 1)} = \frac{11}{14}$$
$$= 0.78 \times 100\% = 78\%$$

$$Overall\ average\ precision = \frac{(0.85 + 0.55 + 0.78)}{3}$$
$$= \frac{2.18}{3} = 0.72 \times 100\% = 72\%$$

$$Recall\ for\ phoenix\ class = \frac{6}{(6 + 3 + 1)} = \frac{6}{10}$$
$$= 0.6 \times 100\% = 60\%$$

$$Recall\ for\ owl\ class = \frac{5}{(5 + 2 + 1)} = \frac{5}{8}$$
$$= 0.62 \times 100\% = 62\%$$

$$Recall\ for\ wolf\ class = \frac{11}{(11 + 1 + 0)} = \frac{11}{12}$$
$$= 0.91 \times 100\% = 91\%$$

$$Overall\ average\ recall = \frac{(0.60 + 0.62 + 0.91)}{3} = \frac{2.13}{3}$$
$$= 0.71 \times 100\% = 71\%$$

$$F1\ score = 2 \times \frac{(0.72 \times 0.71)}{(0.72 + 0.71)} = 2 \times \frac{0.5112}{1.43}$$
$$= 2 \times 0.357 = 0.71 \times 100\% = 71\%$$

### 4.2. Evaluating the experimental results

From the three tables below, all the results from the classification report for the three algorithms will be as below,

**Table 9.** Classification report for Gaussian Naïve Bayes classifier

| Types of polarity | Precision | Recall | F1-score |
|---|---|---|---|
| Positive | 0.95 | 0.60 | 0.74 |
| Negative | 0.54 | 0.73 | 0.62 |
| Neutral | 0.65 | 0.96 | 0.78 |
| **Accuracy** | 72% | | |

**Table 10.** Classification report for SVM classifier

| Types of polarity | Precision | Recall | F1-score |
|---|---|---|---|
| Positive | 0.96 | 0.91 | 0.93 |
| Negative | 0.90 | 0.73 | 0.80 |
| Neutral | 0.81 | 0.98 | 0.88 |
| **Accuracy** | 89% | | |

**Table 11.** Classification report for Random Forest classifier

| Types of polarity | Precision | Recall | F1-score |
|---|---|---|---|
| Positive | 0.93 | 0.91 | 0.92 |
| Negative | 0.88 | 0.67 | 0.76 |
| Neutral | 0.81 | 0.95 | 0.87 |
| **Accuracy** | 88% | | |

From the results above, it can be noticed that the applied algorithms work on both positive and neutral polarities better than negative tweets, this due to the total no. of negative tweets which lesser that other polarities. As it's given in (Table 1) the total no. of the whole records are 41122 tweets; from this number, 33974 tweets (which is about 83% of the dataset) are both positive and neutral, only 7148 tweets are negative; which is equal to,

$$\frac{7148}{41122} \times 100\% = 0.1738 \times 100\% = 17.38\%$$

17% of the whole dataset; that's why we notice from the CM table, the proposed algorithms are not working well on negative polarities. Since the agent does not have any previous knowledge about the dataset, it has to be trained a lot, the more data for training, the more accuracy results will get.

In some cases, we may face imbalanced data, which means the data in the host dataset are not coherent. Due to this reason, measuring the accuracy alone is not enough. It has to be compared with the result of F1-score. If their results are near to each other, it means it performs well. In the case of Random Forest, for positive and neutral tweets, the results of F1 score are 92% and 87% respectively; with regarding to overall accuracy result which is 88% it means they are near in each other.
Also, in order to test the performance of the suggested classifier, the overall accuracy of Random Forest classifier with GNB and SVM have been compared as it shows in the table below,

**Table 12.** The accuracy comparison between the classifiers with their required time

| ML Classifier | Accuracy | Required time | |
|---|---|---|---|
| | | Training | Prediction |
| **Random Forest** | 88% | 7min 5s | 2.12 s |
| **GNB** | 72% | 1.64 s | 367 ms |
| **SVM** | 89% | 15min 37s | 1min 42s |

The accuracy result shows 88%, 73%, and 89% respectively. From the comparison, it seems that the Ransom forest classier works better than GNB. So, the author is suggesting Random Forest over GNB, but in the case of Random Forest with SVM, we can notice one-degree difference in their accuracies, but SVM has the problem of time requiring. The table above which contains the required time for each classifier, in the used macOS system (the hardware specification is given in Table 2). The results show that GNB needs the least amount of time, while SVM needs the most amount of time, with is a huge difference from the two other classifiers.

Another way for testing the proposed system is to check the data size of the dataset before and after cleaning processes for information purpose. Reducing the size of the data, means the used cleaning method has worked well on the dataset; also, it causes and essential impact on the performance of the work, the less and more cleaned data, means the faster system is.

Thus, cleaning-out the noisy, or wrong samples in the original training dataset; is a very important step for the training dataset methods in enhancing the classification accuracy [28].

The figure below, shows the text before and after cleaning, in the macOS system, the differences can be noticed between both CSV files,
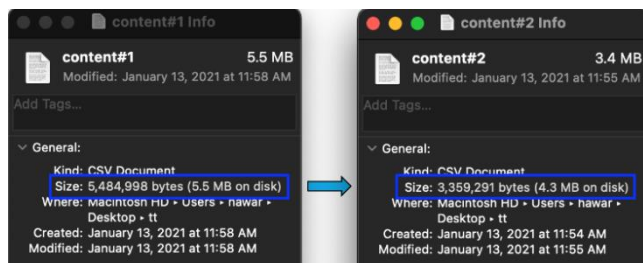


**Figure 12.** Both saved "content" with "cleaned content" features in macOS hard drive

One of the benefits of cleaning textual data is reducing capacity. We succeeded to decrease the size of our dataset about 1.2 MB (from 5.5 MB to 4.3 MB).

This decreasing of size leads to apply the ML algorithms faster. For example, in the case of Random Forest, the training and testing technique on the macOS took 7min 5s, and 2.12 s respectively.
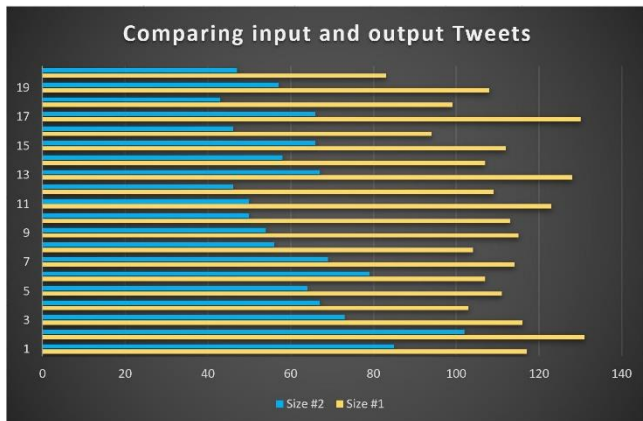
**Figure 13.** Comparing the sizes of In/Out texts

This decreasing of size leads to apply the ML algorithms faster. For example, in the case of Random Forest, the training and testing technique on the macOS took about 7min. This is useful in those situations that have a dataset with a huge amount of information and a small with a determined amount of capacity.

## CONCLUSION

In the proposed research paper, sentiment analysis as the use of use NLP and ML classifiers have been applied on Trump's tweet dataset. After data preparation, the most important sentiment analysis procedures have been applied on the host dataset, like cleaning the dataset in order to be ready for text vectorization. Cleaning the dataset, which includes removing stopwords, word lemmatization, regular expression and tokenization. We succeeded in reducing the size of content feature with the target of taking fewer capacity. With the rapid growth of social media networks, it became a challenged task to know the subjective polarities of tweets. Therefore, we judged each sentence regarding their polarities whether they are *positive*, *negative* or *neutral*. At the end, the accuracies of Random Forest classifier with both GNB and SVM have been compared. Other related results to the confusion matrix and classification report tables have been given in the result and dissection section.

The author is suggesting Random Forest over other two classifiers, which are GNB, and SVM, since Random Forest has a good percent of accuracy and need less time compared to SVM.

For the future studies, detecting text polarities can be classified into 7 levels (strong, moderate, weak) each with 0.25 degrees of threshold. Also, we recommend the same system for not only on texts, but for speech recognition and cleaning noisy data in practical AI and Robotics.
The proposed method can be used in AI industries, and applied linguistics.

## REFERENCES

[1]    Duncombe, Constance. "The politics of Twitter: emotions and the power of social media." International Political Sociology 13.4 (2019): 409-429.

[2]    Akram, Waseem, and Rekesh Kumar. "A study on positive and negative effects of social media on society." International Journal of Computer Sciences and Engineering 5.10 (2017): 347-354.

[3]    Ajjoub, Carl, Thomas Walker, and Yunfei Zhao. "Social media posts and stock returns: The Trump factor." International Journal of Managerial Finance (2020).

[4]    Social Blade Organization, "Twitter Stats Summary," *User Statistics for RealDonalTrump*. https://socialblade.com/twitter/user/realdonaldtrump (accessed Dec. 7, 2020).

[5]    Wells, Chris, et al. "Trump, Twitter, and news media responsiveness: A media systems approach." New Media & Society 22.4 (2020): 659-682.

[6]    Clarke, Isobelle, and Jack Grieve. "Stylistic variation on the Donald Trump Twitter account: A linguistic analysis of tweets posted between 2009 and 2018." PloS one 14.9 (2019): e0222062.

[7]    Yaqub, Ussama, et al. "Analysis of political discourse on twitter in the context of the 2016 US presidential elections." Government Information Quarterly 34.4 (2017): 613-626.

[8]    Kaggle Data science Company, "Datasets," *Datasets*. https://www.kaggle.com/austinreese/trump-tweets (accessed Nov.7, 2020).

[9]    Kam, Ho Tin. "Random decision forest." Proceedings of the 3rd International Conference on Document Analysis and Recognition. Vol. 1416. Montreal, Canada, August, 1995.

[10]   Breiman, Leo. "Random forests." Machine learning 45.1 (2001): 5-32. Cutler, Adele, D. Richard Cutler, and John R. Stevens. "Random forests." Ensemble machine learning. Springer, Boston, MA, 2012. 157-175.

[11]   Scikit-learn Software. https://scikit-learn.org/stable/modules/naive_bayes.html (accessed May 2, 2021)

[12]   Syafie, Lukman, et al. "Comparison of Artificial Neural Network and Gaussian Naïve Bayes in Recognition of Hand-Writing Number." 2018 2nd East Indonesia Conference on Computer and Information Technology (EIConCIT). IEEE, 2018.

[13]   Cortes, Corinna, and Vladimir Vapnik. "Support-vector networks." Machine learning 20.3 (1995): 273-297.

[14]   Tharwat, Alaa. "Classification assessment methods." *Applied Computing and Informatics* (2020).

[15]   Kulkarni, Ajay, Deri Chong, and Feras A. Batarseh. "Foundations of data imbalance and solutions for a data

democracy." Data Democracy. Academic Press, 2020. 83-106.

[16] Elbagir, Shihab, and Jing Yang. "Twitter sentiment analysis using natural language toolkit and VADER sentiment." Proceedings of the International MultiConference of Engineers and Computer Scientists. Vol. 122. 2019.

[17] Li, Irene, et al. "What Are We Depressed About When We Talk About COVID-19: Mental Health Analysis on Tweets Using Natural Language Processing." International Conference on Innovative Techniques and Applications of Artificial Intelligence. Springer, Cham, 2020.

[18] Al-Makhadmeh, Zafer, and Amr Tolba. "Automatic hate speech detection using killer natural language processing optimizing ensemble deep learning approach." Computing 102.2 (2020): 501-522.

[19] Vishwakarma, Dinesh Kumar, Deepika Varshney, and Ashima Yadav. "Detection and veracity analysis of fake news via scrapping and authenticating the web search." *Cognitive Systems Research* 58 (2019): 217-229.

[20] Back, Bong-Hyun, and Il-Kyu Ha. "Comparison of sentiment analysis from large Twitter datasets by Naïve Bayes and natural language processing methods." *Journal of information and communication convergence engineering* 17.4 (2019): 239-245.

[21] Jindal, Kanika, and Rajni Aron. "A systematic study of sentiment analysis for social media data." *Materials Today: Proceedings* (2021).

[22] Yaqub, Ussama. "Tweeting During the Covid-19 Pandemic: Sentiment Analysis of Twitter Messages by President Trump." *Digital Government: Research and Practice* 2.1 (2020): 1-7.

[23] Sahu, Kalyan, Yu Bai, and Yoonsuk Choi. "Supervised Sentiment Analysis of Twitter Handle of President Trump with Data Visualization Technique." *2020*

*10th Annual Computing and Communication Workshop and Conference (CCWC)*. IEEE, 2020.

[24] Asur, Sitaram, and Bernardo A. Huberman. "Predicting the future with social media." *2010 IEEE/WIC/ACM international conference on web intelligence and intelligent agent technology*. Vol. 1. IEEE, 2010.

[25] Kaggle Data science Company, "Datasets," *Datasets*. https://www.kaggle.com/austinreese/trump-tweets (accessed Nov.7, 2020).

[26] Ruz, Gonzalo A., Pablo A. Henríquez, and Aldo Mascareño. "Sentiment analysis of Twitter data during critical events through Bayesian networks classifiers." *Future Generation Computer Systems* 106 (2020): 92-104.

[27] Patro, V. M., and M. R. Patra. "A Novel Approach to Compute Confusion Matrix for Classification of N-Class Attributes with Feature Selection". *Transactions on Machine Learning and Artificial Intelligence*, Vol. 3, no. 2, May 2015, p. 52, doi:10.14738/tmlai.32.1108.

[28] Wang, Yidi, Zhibin Pan, and Yiwei Pan. "A Training Data Set Cleaning Method by Classification Ability Ranking for the $ k $-Nearest Neighbor Classifier." IEEE transactions on neural networks and learning systems 31.5 (2019): 1544-1556.

[29] Deshmukh, Kamalakshi V., and Sankirti S. Shiravale. "Ambiguity Resolution in English Language for Sentiment Analysis." *2018 IEEE Punecon*. IEEE.

[30] Verma, M. Tech Scholar Rajat. "Natural Language Processing (Nlp): A Comprehensive Study." (2018).

[31] Vasiliev, Yuli. *Natural Language Processing with Python and SpaCy: A Practical Introduction*. No Starch Press, 2020.

[32] Jakkula, Vikramaditya. "Tutorial on support vector machine (svm)." *School of EECS, Washington State University* 37 (2006).